Development and Application of New Platforms for Oligonucleotide and Protein Assays

by

Md Akteruzzaman

A dissertation submitted to the Graduate Faculty of
Auburn University
in partial fulfillment of the
requirements for the Degree of
Doctor of Philosophy

Auburn, Alabama
August 08, 2020

Keywords: Electrochemistry, Analytical Chemistry, Electrochemiluminescence

Approved by

Curtis Shannon, Chair, Professor of Chemistry and Biochemistry
Christopher J. Easley, Professor of Chemistry and Biochemistry
Wei Zhan, Associate Professor of Chemistry and Biochemistry
Byron H. Farnum, Assistant Professor of Chemistry and Biochemistry

Abstract

Sensitive and rapid detection of infectious disease is becoming very significant to improve human health. We have seen that the sensitive methods often required expensive, and sophisticated instruments. Biosensors are offering portable, cost-effective alternative to detect the clinically relevant biomarker, which also helps to design POC diagnosis. Several sensitive methods are being developed for biomarker detection. For POC systems required the methods which are inexpensive, sensitive, automated, and rapid that can serve to improve the health sector, especially in developing countries. One magnificent among these methods is the electrochemical biosensor. Electrochemiluminescence (ECL), the light-emitting process generated by electrochemical means, could transfer the electrochemical signal into light emission under specific applied potential. The ECL's main characteristics and advantages are its benefit for biological assays; its high specificity and sensitivity; and its least hardware requirements (i.e., voltage source, electrodes, and light sensor, all of which can be miniaturized). All the combinations make ECL an ideal analytical detection method. The primary goal of this dissertation work is to develop a DNA-based electrochemical method for quantification of small molecules and ECL based aptasensors for large proteins, which is suitable for dip-and-read and POC diagnoses. Chapter 1 exhibits a detailed literature review on electrochemical DNA-based biomarker detection methods. Furthermore, a brief insight into electrochemiluminescence (ECL) history, mechanism, and application in bio-analytical sensing. Chapter 2 focuses on the electrochemical proximity assay (ECPA) on the glassy carbon electrode as a transducer and its optimization. After optimization, the experimental condition of the ECPA model system was illustrated. This work evaluates DNA fabrication on the glassy carbon

electrodes, instrumentation issues, and illustrated to make ECPA DNA model measurement. Chapter 3 focuses on improving the redox moiety signal of methylene blue (MB) molecules by using catalytic molecules as $K_3[Fe(CN)_6]$. The electrochemical redox signal was increasing 30%, when the catalytic effect strategy was used. In Chapter 4 the large protein quantification approach is developed by exploiting the ECL, amplified ECL signal by using electroactive nanocomposites as Reduced graphene oxide-Tris(bipyridine)ruthenium (II) chloride composite (GO-$Ru(bpy)_3^{2+}$. This method, in the future, should provide a generalizable platform for quantifying multiple proteins, peptides, or small molecules by a dip-and-read workflow, and this should promote future real-time measurements. Chapter 5 summarizes the findings of the research. The recommended future work of projects is stated.

Acknowledgments

I would like to express my sincere gratitude to my major professor Dr. Curtis Shannon for his continuous supervision and untiring support throughout my Ph.D. study at Auburn University. I am grateful for getting the opportunity to work with a mentor like him. His penchant for electrochemistry and surface science has been such an inspiration and encouraged a productive environment for creative research. Beyond research and science, I learned the qualities of confidence from him. I am also grateful to my advisory committee members including Dr. Christopher J. Easley, Dr. Wei Zhan, and Dr. Byron H. Farnum in the direction of helpful insights and valuable suggestions for my research projects allows me to work at any time in their lab and for the preparation of this dissertation. I would like to give sincere thanks to Dr. Minseo Park, who is willing to be my university reader and participate in the process towards the final defense.

Professor Masoud Mehrgardi, thank you for always taking the time to answer my questions and teaching me the best ways to plan and execute experiments. Without your guidance and pipetting skills, I would not have accomplished this work. Not only by his insightful comments and encouragement but also for his numerous key advice that incented me to widen my research from various perspectives. I learned from him many experimental techniques and tips for research by his selfless and diligent instruction. His many thoughtful suggestions, both at the scientific and personal level, will always be remembered in my entire professional career. My colleagues in our research group have been very helpful at various stages of my study at Auburn, and I would like to thank each one of them, Apu Mazumder, Dr. Songyan Yu, Buhua Wang, Waliul Islam Khan, and Humaira Yeasmin.

Finally, I am also grateful to my family members, especially to my father Md. Rustom Ali and to my beloved brother Md. Kamruzzaman for their continuous support throughout my life. I would like to dedicate this dissertation to my beloved mother, Nasima Begum, and my beloved wife Sadia Afrin, for their inspiration, dedication, continuous mental and physical support as well as unconditional love to turn my day of hardship into a day of smiles.

Table of Contents

Abstract ii

Acknowledgments iv

List of Figures viii

List of Tables xi

CHAPTER 1 1

Review of Literature 1

1.1 Introduction 1

1.2 Electrochemical sensor and Bio-sensing 2

1.3 Biosensor recognition elements 8

1.4 Electrochemical detection techniques and Applications 11

1.5 Electrochemiluminescence (ECL) 17

1.6 Conclusions 21

CHAPTER 2 23

Carbon-based Electrochemical systems for Electrochemical Proximity Assay (ECPA) 23

2.1 Introduction 23

2.2 Materials and methods 29

2.3 Results and Discussion 34

2.4 Conclusions 51

CHAPTER 3 52

Electrocatalysis in ECPA Biosensors…… 52

3.1 Introduction.....52

3.2 Materials and methods.....56

3.3 Results and Disscussion.....58

3.4 Conclusions.....69

CHAPTER 4 70

Signal Amplification using Electroactive Nanocomposites: Reduced graphene oxide- Tris(bipyridine)ruthenium (II) chloride composite for Ultra-sensitive electrochemiluminescence aptasensing of thrombin …… 70

4.1 Introduction.....70

4.2 Materials and methods.....79

4.3 Results and discussion.....87

4.4 Conclusions.....101

CHAPTER 5 102

Conclusions and Future Directions.....102

REFERENCES 106

List of Figures

Figure 1.1 Scheme of Biosensor analyte detection. 2

Figure 1.2 Schematic representation of sandwich Enzyme-Linked Immunosorbent Assay (ELISA)..... 3

Figure 1.3 Schematic representation of the Proximity ligation assay. 5

Figure 1.4 Schematic representation of Ratio-metric electrochemical proximity assay. ... 7

Figure 1.5 Square wave voltammetry 13

Figure 1.6 Schematic representation of Electrocatalytic reporter system..... 14

Figure 1.7 Schematic illustration of ECL mechanism. 18

Figure 1.8 Generation of ECL mechanism in the presence of coregent. 20

Figure 2.1 Biosensors schematic representation. 24

Figure 2.2 The proximity effect. 25

Figure 2.3 Pictorial representation of complete complex of ECPA..... 26

Figure 2.4 Mechanical cleaning of electrodes. 30

Figure 2.5 SWV characterization of modified GCE. 36

Figure 2.6: SWV characterization of standard gold electrode immobilized. 37

Figure 2.7 SWV of 3-MPA/AuE modified after 1 µM A-DNA immobilization 38

Figure 2.8 Electrodeposition of 4-Amino Benzoic Acid (4-ABA) on the GCE. 39

Figure 2.9 Cyclic voltammograms for a (a) bare GCE and (b) 4-ABA/GCE..... 40

Figure 2.10 SWV characterization of modified GCE (deposition of ABA)..... 41

Figure 2.11 Cyclic voltammograms for in 2 µM MB intercalation. 42

Figure 2.12 SWV of MB intercalation at different modification of GCE. 43

Figure 2.13 SWV output and Schematic diagram of full match DNA hybridization. 46

Figure 2.14 SWV output of full match MB-DNA and Integrated signal vs Time(min)... 47

Figure 2.15 SWV output and calibration curve of different concentration of full match MB-DNA. 48

Figure 2.16 DNA based model for ECPA and SWV output for background and Signal.49

Figure 2.17 SWV output and calibration curve of DNA loop concentration 50

Figure 3.1 Schematic representation of the electrocatalytic reduction 54

Figure 3.2 CV and SWV of probe DNA in 5.0 mM $[Fe(CN)_6]^{4-/3-}$ solution 60

Figure 3.3 Chronocoulometric response curves for DNA probe density determination .. 62

Figure 3.4 SWV output without and with catalytic molecules 63

Figure 3.5 Catalytic efficiency on different concentrations of $K_3[Fe(CN)_6]$ 64

Figure 3.6 A microscopic image of a gold-coated QCM sensor before and after measurment 65

Figure 3.7 SWV output without and with $K_3[Fe(CN)_6]$ at different periods and A quantitative correlation between the peak height in SWV at different scan rates. 66

Figure 3.8 SWV characterization for signal amplification by electrolysis 67

Figure 3.9 The integrated signal of SWV at different DNA Loop concentrations without and with of $K_3[Fe(CN)_6]$. 68

Figure 4.1 Schematic illustration of ECL mechanism 71

Figure 4.2 Timeline of ECL experiment. 72

Figure 4.3 Illustration of various nanostructure materials or nanomaterials or metal nanocluster or nanocomposite being used for the fabrication of ECL nano biosensors... 74

Figure 4.4 Schematic illustration of the multiplexed ECL immunosensor for simultaneous detection of IFN-γ, TFN-a and IL-2 75

Figure 4.5 Schematic representation of aptasensors for Thrombin detection based on $[Ru(bpy)_3]^{2+}$-anchored GO amplification. 78

Figure 4.6 Characterization of Graphene Oxide 86

Figure 4.7 EIS and CV of the gold electrode at different stages in 5 mM $[Fe(CN)_6]^{4-/3-}$ 88

Figure 4.8 Chronocoulometric response curves for DNA probe density determination .. 91

Figure 4.9 ECL intensity at different pH 92

Figure 4.10 Effect of GO concentration in emission of ECL. 93

Figure 4.11Number based size distribution of GO in PBS-KCl buffer at room temperature 91

Figure 4.12 Intensity based size distribution of GO in PBS-KCl buffer at room temperature 92

Figure 4.13 Compare ECL intensity at different condition. 93

Figure 4.14 Confocal fluorescence images of sensor without and with target 97

Figure 4.15 AFM of sensor without and with target 97

Figure 4.16 ECL intensity vs time curves for different SH-TBA-thrombin complex electrode.. 99

Figure 4.17 The selectivity of TB aptasensor 100

List of Tables

Table 2.1 Sequences of DNA strands used in the experiments. 29

Table 3.1 Single-stranded DNA sequences used in the ECPA model systems. MB-DNA, and G7, were employed in the optimized detection system..... 56

Table 3.2ECPA signal amplification by $K_3[Fe(CN)_6]$..... 63

Table 3.3 ECPA signal amplification by $K_3[Fe(CN)_6]$ at different scan rate of SWV…. 66

Table 4.1 Sequences of DNA strands used in the experiments. 79

Table 4.2 Zeta potential of GO and its composite 94

Table 4.3 Comparison of % of ECL signal decrease 97

Table 4.4 Comparisn of fluorescence intensity without and with TB. 98

CHAPTER 1

Review of Literature

1.1 Introduction

In clinical applications, identification and quantification of protein biomarkers have gradually become crucial for areas such as clinical analysis, identification, and treatment of specific diseases, which can be associated with the changes of protein biomarker concentration in biological fluids. Nucleic acid, protein, and small molecules are involved in the biological and physiological activity of the cell and its regulating transmitting genetic information, and they can be used as a biomarker for clinical analysis[1]. The quantification protein biomarkers at low concentrations is a useful diagnostic tools for many diseases in biological samples[2]. By using different recognition elements (e.g., antibodies, aptamers) and different sensing principles and techniques (e.g., optical, electrochemical), several strategies have been studied to improve accurate and simple diagnosis methodologies for protein biomarkers. To develop suitable diagnostic tools for diseases is using resource-limited settings, the World Health Organization (WHO) has established a group of guidelines: Affordable, Sensitive, Specific, User-friendly, Robust and rapid, Equipment-free, and Delivery to those who need it, leading to the acronym *"*ASSURED*"*[3].

The substantially sensitive technique is being developed for biomarker detection. Enzyme-linked immunosorbent assay (ELISA) is usually used in the clinics to quantify protein biomarkers[4]. This quantification technique is expensive, laborious, required trained people to operate[4]. For point-of-care (POC) system should be inexpensive,

efficient, and automated, which can improve health care. Nucleic acid-based electrochemical biosensors for the detection of proteins offers high sensitivity, excellent signal stability, simple instrumentation, and ease of calibration, as well as this detection technique, has excellent compatibility with miniaturization technologies[5, 6]. Hence, the electrochemical sensors are considered as the ideal candidate in developing portable devices with high selectivity and sensitivity at reasonable cost.

1.2 Electrochemical sensor and Bio-sensing

An electrochemical biosensor is a chemical type sensor, detecting analytes by utilizing a biochemical recognition unit that undergoes a conformational change or reaction. A typical electrochemical sensor[5, 7, 8] consists of a) recognition elements that specifically bind to the analyte; b) a transducer where a specific reaction takes place on the interface with recognition elements and gives rise to a signal; c) an electronic system that converts an electric signal to a meaningful parameter describing a signal which is recorded by a signal processor (Figure 1.1)[9, 10]

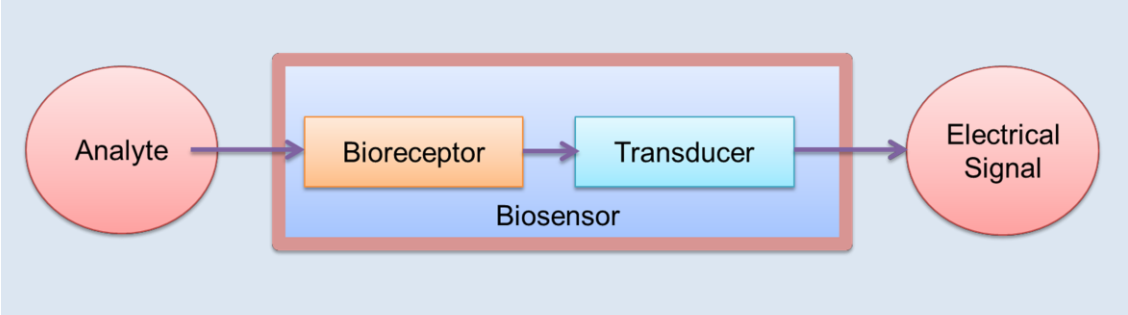

Figure 1.1 Scheme of Biosensor analyte detection.

Sensor converts the interaction of an analyte to an electrochemical signal, which is transduced to the signal processor.

For example, an electrochemical biosensor with biological recognition units immobilized on an electrode surface is exposed to an analyte, and recognition unit transfers electrons to the transducer like electrode which registers a current flow and generates a signal which is recorded by a signal processor (Figure 1.1)[9, 10]. Viral and bacterial infections can be diagnosed by analyzing the presence of their nucleic acids. Disease biomarkers usually consist of nucleic acids or proteins in biological matrices at low concentrations, requiring signal amplification to achieve adequate sensitivity. Two types of amplification are used in biosensors: target-based amplification or signal-based amplification. In target-based amplification, the target interacts with the sensor, starting a chain reaction of amplification of the target. Methods based on amplification with polymerase chain reaction (PCR) are an example of this type.

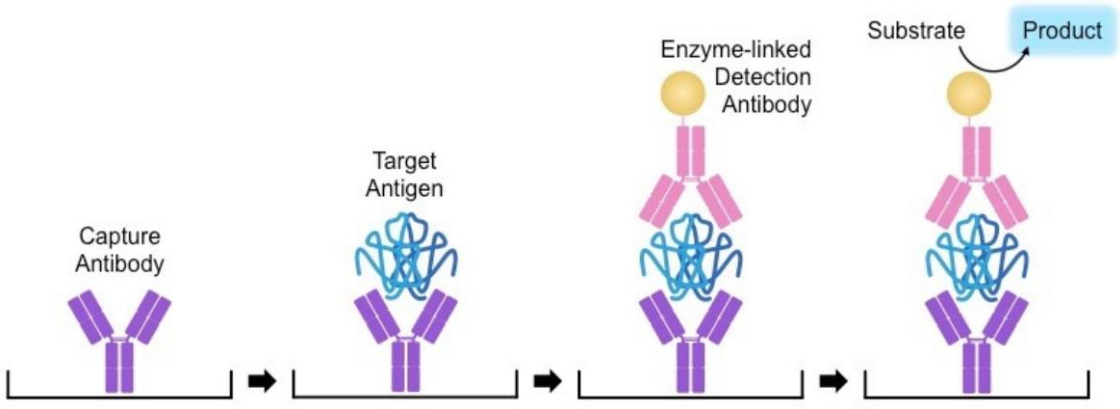

Figure 1.2 Schematic representation of sandwich Enzyme-Linked Immunosorbent Assay (ELISA).
Reprinted with permission. **Copyright ©**

https://ib.bioninja.com.au/options/untitled/b4-medicine/elisa.html

The signal-based amplification occurs from a single analyte binding event that is catalytically amplified. An example of a signal-based amplification is enzyme-linked immunosorbent assay (ELISA), a layer of antibodies is pre immobilized on a solid

substrate. When a testing solution containing antigens flows across the surface, analytes can be captured by the antibodies absorbed on the surface, and a secondary enzyme-linked antibody associated with a reporter or reporter generating molecule then amplifies and creates a detectable signal[11]. The utility of antibodies in molecular recognition offers excellent sensitivity, selectivity, and stability[12]. In addition, with the success of sandwich immunoassays, there exists an extensive, commercially available library of antibody pairs against many targets[13]. Traditionally, the result of immunoassays is displayed as a color change that is only suitable in a binary scenario indicating the presence or absence of analytes, such as a pregnancy test, but not for quantitative analysis. This quantification technique is expensive, laborious, required trained people to operate, and complicated testing procedures involving multiple washing steps. Enhancing the signal by the duel antibody recognition concept is productive and draws the attention of the researcher in the past few years[14-16].

Proximity immunoassays such as proximity ligation assay (PLA)[17] can solve some of the significant issues of traditional sandwich-type immunoassays. Fredriksson, et al. developed a method for macromolecules and *in vitro* protein detection called the proximity ligation assay (PLA) by exploiting the proximity effect between DNA and T4 DNA ligation[17, 18]. PLA is one of the most simple-to-use and sensitive assays for protein detection and analysis of other biological targets. It relies on simultaneous recognition of a target molecule by a pair of affinity probes inhomogeneous solutions, and measurements are currently highly dependent on fluorescence readout, which is not ideal for sensor development because of the high cost and drifting of experimental results.

In Figure 1.3 the schematic representation of aptamer-based PLA; when the target protein bind with the two aptamers, by proximity effect the binding of connector DNA (black) with these two aptamers becomes stronger. By binding, the connector DNA of the phosphorylated 5 end aptamer is come closer to the 3 ends and form double-stranded, which is effectively binding by the T4 DNA ligase enzyme. The Taqman probe (Green) binds strongly with T4 ligated DNA.

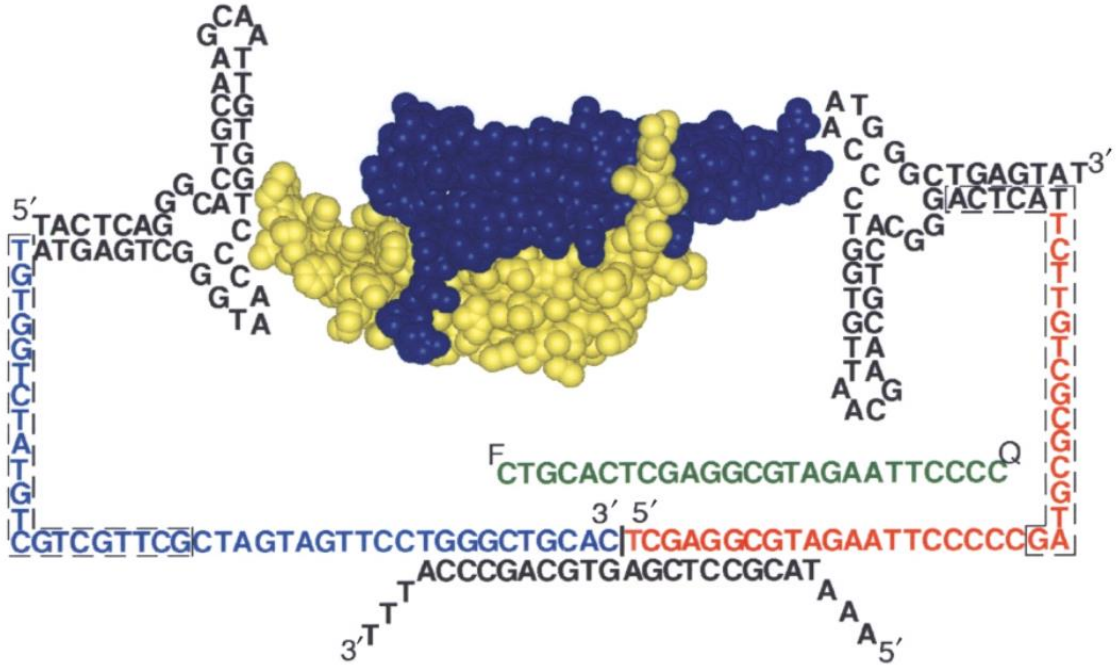

Figure 1.3 Schematic representation of the Proximity ligation assay.

The black DNA sequence represents the aptamer region when aptamers bind with the protein bring the tails to proximity, which can strongly bind with the connector. Upon enzymatic ligation, the tails act as a single DNA, which can be amplified by real-time PCR. The primers are shown in boxes, and taqman probe is shown in green[17].

The primer binding sites are represented in boxes. The DNA amplified by PCR, which enables to bind with more Taqman probe. Simultaneously, the DNA polymerase exonuclease activity digests the dsDNA while amplifying. The fluorescence signal increases by separating the fluorophore from the quencher. But small fluorescence signal was observed in the absence of protein due to weaker binding between the Taqman probe and the aptamers.

The proximity effect has also been used in electrochemical detection of protein. Easley, et al. developed an electrochemical detection method in which DNA assembly happens on the electrode surface in the presence of the target protein[13, 19]. As an improvement to this method, Ren, et al. developed a ratiometric electrochemical proximity assay shown in Figure: 1.4[20]. DNA tagged to antibody 1 is also tagged with methylene blue, an electrochemical redox molecule. This antibody–DNA complex is bounded to capture DNA on the electrode surface; this DNA is bound to the electrode covalently due to its thiol-modification. The other end of the surface-bound DNA is tagged with ferrocene, another electrochemical redox molecule. Initially, there will be a signal from methylene blue but not from ferrocene. When the target is introduced with antibody 2, due to the proximity effect, the antibody 1 is removed from the surface, the thiolated DNA forms a loop placing the ferrocene at the place of methylene blue. The target introduction results in an increase and decrease of ferrocene and methylene blue signals, respectively, making a ratiometric sensor. Zhang, et al. also used dual aptamers in a different configuration and quantified platelet-derived growth factor protein (PDGF) through electrochemical detection of the proximity-dependent complex on electrode surface[21, 22]. More details of electrochemical detection and sensor are presented in the following sections.

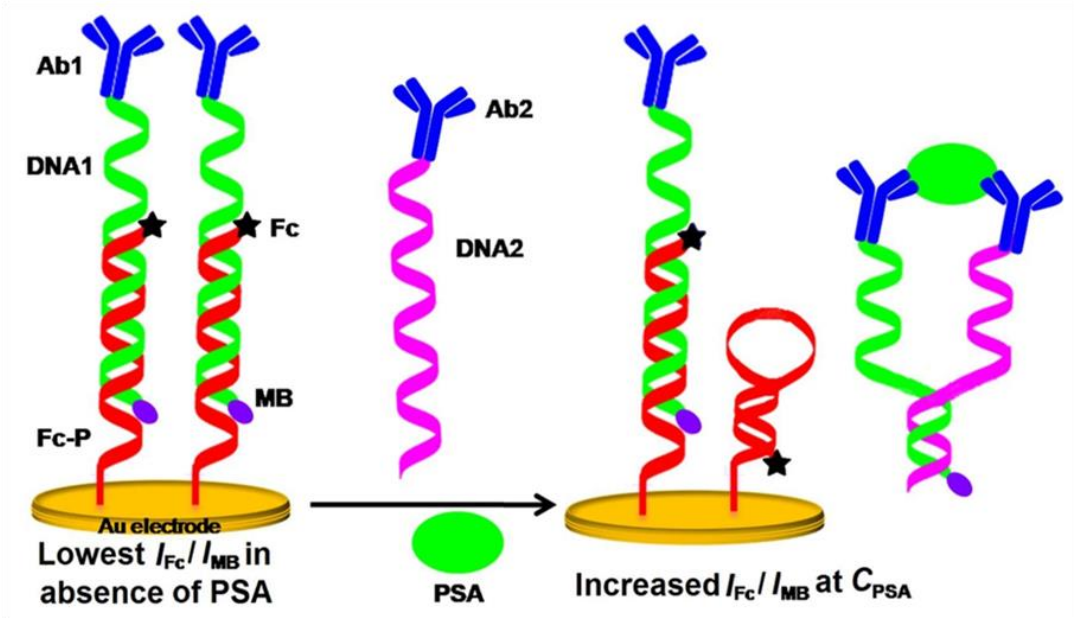

Figure 1.4 Schematic representation of Ratio-metric electrochemical proximity assay. Initially since methylene blue (MB) is closer to the surface and ferrocene (Fc) being far, the IFc /IMB is lower. On introducing the target, due to proximity effect the DNA tagged with MB is removed from surface and Fc is brought closer which increases IFc /IMB, by which protein can be quantified ratio-metrically[20].

Reprinted with permission [20] **Copyright © (2014) Nature Publishing Group.**

Electrochemical biosensor techniques have attracted much attention because of their potential in building the relatively compact device, capability of quantitation of analytes and ease of operation and result interpretation[23, 24]. However, there are two major drawbacks when incorporating antibodies onto electrode surfaces to build electrochemical sensors. Firstly, an electrochemically active label is necessary for generating electrical signal since most analytes cannot intrinsically act as redox partners in an electrochemical reaction. The labeling process for antibodies is inconvenient, expensive, and time-consuming;[12, 25] Secondly, Selectivity is the ability to detect a specific biomolecule within a complex mixture of possibly similar biomolecules. Generally,

biosensors exploit nature's machinery for high target specificity, such as enzymes' or antibodies' high binding and/or reaction specificities. Of course, such detection methods can sometimes suffer from nonspecific binding of proteins in the sample, increasing the baseline of the detection, and reducing selectivity.

The use of antibody-oligonucleotide conjugates[14, 18] can overcome these two limitations. Antibody-oligonucleotide conjugates can be simply prepared by coupling antibodies with short nucleic acids using an All-In-One Conjugation Kit from Solulink[13]. Compared with antibodies, nucleic acids can be easily modified with a variety of molecules (methylene blue, ferrocene). That allows the introduction of electrochemically active labels or functional groups (primary amine, thiol groups) that enable improved immobilization of conjugates on to electrodes at a reasonable cost[26]. Notably, the introduction of thiol groups to the probes allows the use of well- developed self -assembled monolayers (SAMs) technique that has been proven to avoid random orientations of biomolecules on the surface, protect the surface from nonspecific absorption, produce good surface coverage, and improve the overall quality of surface modification and sensor performance[27].

1.3 Biosensor recognition elements

The most widespread biosensor available commercially is the pregnancy test, followed by the glucose sensor, and sensors for lactate and glutamate[28]. These commercial biosensors rely on the conversion of target recognition into a measurable signal. The analyte is detected by a recognition element, which interacts with the transducer creating a signal, which is amplified and displayed. Successful biosensors require high sensitivity and specificity when interacting with the target molecule, and the output signal should be proportional to the concentration of the target analyte. These typically exploit

biological recognition elements such as nucleic acids or proteins (enzymes, antibodies). There are two main types of biosensors, biocatalytic devices or affinity sensors. Biocatalytic detection methods rely on recognition and downstream biochemical reactions, as in enzyme biosensors. Affinity sensors rely simply on the binding of the target to the recognition element, producing a signal such as an electrochemical current.

Sensitivity and selectivity are two other crucial aspects for the development of electrochemical sensors. Surface modification of electrodes by immobilizing recognition elements on the sensor substrates is a very efficient approach to reach enhanced current responses and obtain an interface with highly specific binding affinity to the desired molecule. The concept of surface modification of electrodes was introduced by Bard[29] and others[30-32] about thirty years ago for electrocatalysis purpose and has been highly developed over the years for applications in a wide range, such as energy storage[33], bioelectronics, and most importantly electrochemical sensors[5, 6, 34]. Enzymatic biosensors are amongst the most common and well-studied biosensors[28] and have very high selectivity in complex matrices.

However, many biochemical analytes are not conducive to enzymatic biosensors; either they are not commonly found in living systems, or there is no specific enzyme that will function with a sensor. Affinity biosensors combine a recognition element such as an antibody or aptamer, which actively and specifically binds to the target analyte by structural matching. Immunosensors are antibody-based sensors with low detection limits and high selectivity. The antibodies are created by introducing an antigen to a living animal and separating the antibody produced to recognize the antigen. After many years of commercial development, these days, a wide variety of analytes can be detected, including

bacteria, viruses, hormones, drugs, pesticides, etc. [1]. Nucleic acids are also used for detection, where short oligonucleotides selected specifically for a target are used to detect species of interest with very high selectivity and sensitivity[10].

One specific form of the nucleic acid biosensor is based on aptamers. In the early 1990s, nucleic acid aptamers were introduced as *in vitro* selected binding agents with high specificity. Aptamers are oligonucleotide segments which are selected against the target molecule of interest, forming complex structures of secondary or tertiary components. Aptamers act as a sort of chemically synthesized antibody, demonstrating several benefits such as selectivity against a library of chemicals or even cells. PCR can be performed on selected aptamers, they were allowing large amounts of a single aptamer to be synthesized, removing animal or cell line amplification from the process. The aptamer structure allows modification due to its simplicity and the advancement of nucleic acid synthesis and editing technologies. Specifically, the advantage of aptamers over antibody is like aptamers can be chosen in vitro for any given target, from small molecules to abundant proteins and even cells. The aptamers can be synthesized with high reproducibility and purity from commercial sources. The chemical stability of aptamers is very high, and the target approach to aptamers makes the significant conformational change. Finally, the size of aptamers is much smaller than that of antibodies, which helps to increase the density of aptamers on an electrode surface for the fabrication of electrochemical sensors[26]. However, the binding affinities of aptamers to targets are not as stable as antibodies, and the available number of aptamers is still much lower compare of antibodies.

The small molecule detection has already been successfully transitioning to the commercial market. For example, glucose, lactate, and glutamate can be detected with

enzyme-based biosensors. Diabetes is a growing epidemic amongst the US and other countries, and these patients rely heavily on glucose monitoring devices. The enzymatic glucose sensor is the most widely used electrochemical biosensor. Human blood contains typically between 4.0- and 5.9-mM glucose and a concentration above 6.9 mM after an 8 hour fast is considered a diabetic diagnosis. The main component of the glucose sensor is glucose oxidase (GOx) and proportionally generated H_2O_2 in the presence of glucose. The oxidization of H_2O_2 (facilitated by molecular O_2) at an electrode is a two-electron process and results in a current produce proportional to the concentration of glucose in solution. The basic principle of glucose sensing is commercially viable; however, sensors still required molecular oxygen and were sensitive to blood interferences. The second-generation GOx sensor relied on a mediator (non-physiological electron transfer mediator) operating at lower potentials to reduce electroactive interferences from being redox cycled in blood. Third generation GOx sensors strive to detect precursor cofactors directly and directly transfer electrons rather than rely on H_2O_2 detection. Commercially viable examples of both generation two and three exist and are used extensively. Both generations still rely on glucose oxidase, an enzyme, requiring storage at <44 ◦C and pH 2-8, which significantly limits storage conditions and therefore require expensive methods to attain long term storage[1, 10, 35].

1.4 Electrochemical detection techniques and Applications

Electrochemical biosensors offer cost-effective & user-friendly point-of-care diagnostic devices. This device provides fast diagnostic information. The electrochemical signals can be produced by potentiometry, amperometry, electrochemical impedance spectroscopy, anodic stripping voltammetry and conductometry[10, 35-37]. A small

volume of the analyte is sufficient for electrochemical measurements and observed very low detection limits like attomole to zeptomole range[10, 38]. An electrochemical cell is required to carry out an electrochemical analysis. The most common electrochemical cell consists of three electrodes: working, counter, and reference.

Electrochemical processes occur at the working electrode by precisely driving its potential/current and measuring the resulting signal output. The reference electrode maintains a stable and known potential without interfering with electrochemical reactions at the working electrode surface; an example is the silver/silver chloride reference. The counter electrode allows current to flow to the working without disturbing the reference electrode's stable potential, ensuring repeatability of measurements[35, 39, 40]. The working and counter electrodes are usually made of an inert metal such as the platinum group metals (gold, platinum, silver), where the electrode has minimal influence on the electrochemical reaction occurring at its surface. A reference electrode consists of a redox system generating a known potential to drive the working electrode's potential precisely. Other types of electrodes exist for specific applications, such as metal-coated glass, screen printed electrodes and microelectrodes[35, 39, 40]. Voltammetry is performed by varying the potential at the working electrode and recording the current response from the electrochemical cell, resulting in a peak or plateau, which is proportional to the concentration of the analyte.

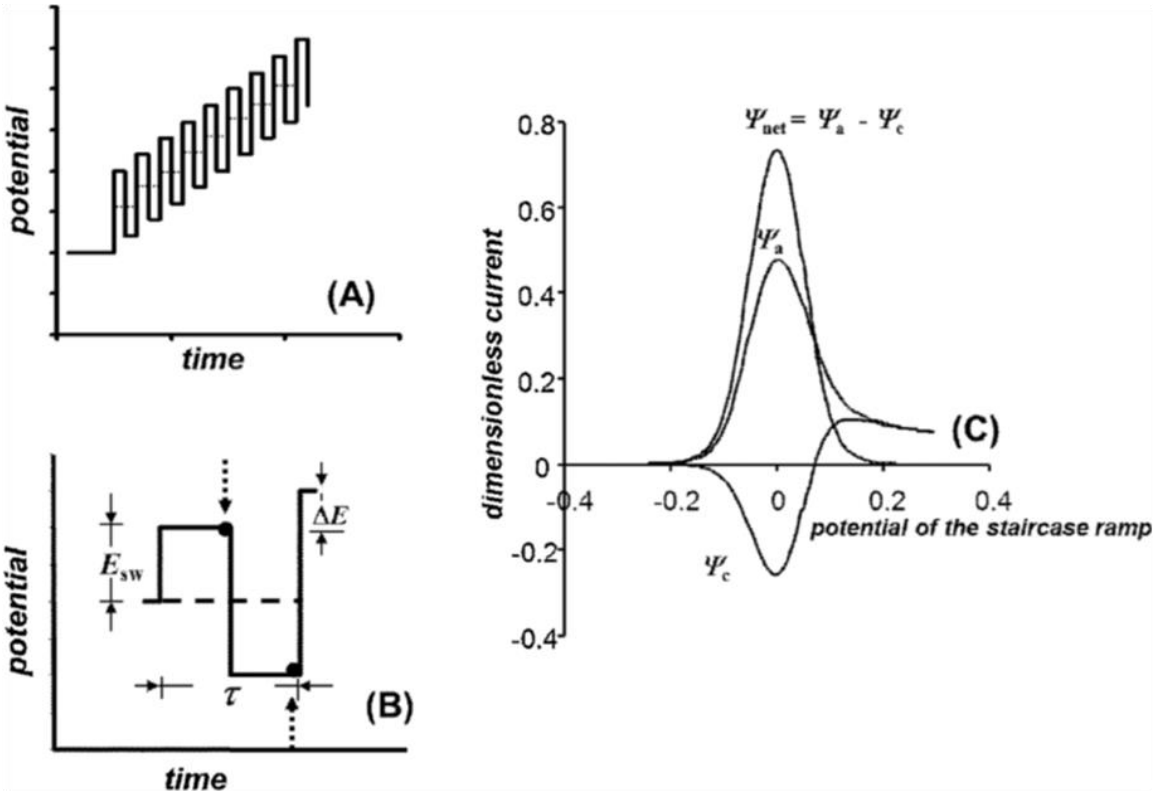

Figure 1.5 Square wave voltammetry

Potential waveform for square wave voltammetry,(B) Single square wave cycle,(C) Voltammogram in SWV where normalized currents Ψa, Ψc, and Ψnet corresponds to i_f, i_f, and Δi [41].

Reprinted with permission [41] **Copyright © (2013) Electrochimica Acta.**

Alternatively, in amperometry, a potential step is applied to the working electrode and held, and the current decay is recorded versus time[10, 35]. Multiple experiments can be formulated from the combination of parameters (current, potential, time, charge) present in both voltammetry and amperometry. One technique commonly employed in electrochemical biosensors is square wave voltammetry (SWV), a pulsed voltammetry technique[42]. The current response from the ECPA assay is quantified in AuE by square wave voltammetry (SWV). The SWV is a very sensitive technique, which reduced the

capacitance current as well as increased the signal by its differential output. Surface-confined reactions are observed by SWV due to decreasing background current followed by an increased signal as its differential output. The principle parameters & potential waveform describe in figure 1.5. SWV is defined by the combination of staircase waveform (ΔE) & square wave (E_{sw}). The τ is the time for one square wave cycle and square wave frequency(f) = $1/\tau$ in Hz. In every cycle, the current sample is taken two times, from the end of the first pulse for forwarding current (i_f) & end of the reverse pulse for reverse current (i_r). The voltammogram of SWV shows the difference current ($\Delta i = i_f - i_r$) vs. the potential on the corresponding staircase tread.

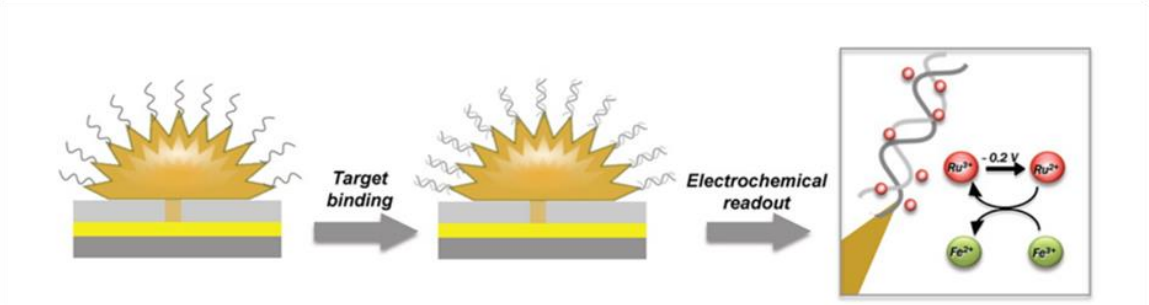

Figure 1.6 Schematic representation of Electrocatalytic reporter system

The $[Ru(NH3)_6]^{3+}$ molecules adsorbs on the negatively charged nucleic acid on surface. Ru^{3+} is electrochemically reduced, is been regenerated by Fe^{3+} ($[Fe(CN)_6]^{3-}$)[43].

To detect the different analytes in electrochemical quantification by the change in electron transfer kinetics. Notably, a structure switching aptamer is needed for this method development[44]. So, the exploration in using non-covalently (on the surface) attached redox reporters for bio-molecular quantification is done by the Kelley[45], Vallee-Belisle[46], and Shannon and Easley[47] groups. Lu, et al. detect thrombin protein by developing a signal off method. Firstly, the transducer was incubated in thrombin aptamer

solution hybridized with ferrocene tagged complementary sequence. When a thrombin approach to the aptamers by changing the aptamer conformation, ferrocene tagged complementary sequence displaced; as a result, signal off, and thrombin is quantified by measuring the amount of signal off[44]. Chen, et al. used anti-lysozyme DNA aptamers with which ruthenium hexamine ($[Ru(NH_3)_6]^{3+}$) was bound electrostatically[48]. The lysozyme pushed away from the $[Ru(NH_3)_6]^{3+}$, which was reflected in the signal for quantification. Das, et al., developed a new method by using a nanostructured gold electrode achieved ultrasensitive readout of CA-125 (cancer biomarker) in serum and whole blood[45]. In this method, antibodies upon interaction with protein blocked the redox molecules ($[Fe(CN)_6]^{3-/4-}$) from the bulk solution from reaching the electrode and signaling. Later, they developed an oligonucleotide quantifying sensor using the nanostructured gold electrode[43, 49-51]. In this method, $[Ru(NH_3)_6]^{3+}$ complex electrostatically adsorbed to the DNA, and the signal for this complex was amplified by an electrocatalytic reporter system in which $[Ru(NH_3)_6]^{3+}$ was regenerated by chemical oxidation of Ru(II) by Fe^{3+} of $[Fe(CN)_6]^{3-}$ in the bulk solution[43]. Figure 1.6 represent this electrochemical signal pattern. By using this method, the circulating tumor DNA was detected. The wild type was blocked using a DNA clutch probe, which made the sensor more sensitive to the mutant type[50].

White, et al. observed that the probe density on the transducer plays a vital role in the sensor sensitivity[52]. For every new sensor development strategy, should be optimized the probe density, as a higher probe density, leads to loss of sensitivity by steric hindrance. Mahshid, et al. developed a strategy of exploiting the steric hindrance for quantification[46]. This group used different molecules ranging from 0.2 to 150 kDa by

compared the SWV signal observed the steric hindrance effect. These molecules were tagged to DNA, which has a methylene blue tag on the other end. This DNA hybridized with the surface DNA via 16 bp. Since hybridization energy was the same, the drop in the signal as due to the effect of steric hindrance. With this knowledge, the indirect quantification of larger proteins was developed. The signaling DNA (which has redox moiety) is tagged to target recognizing unit (Biotin and digoxigenin for quantification of streptavidin and anti-digoxigenin, respectively). If the target molecule is present in the sample, the signaling DNA binds with the target, which, due to steric hindrance, is unable to bind with the capturing probe. In the absence of a target, the signal is generated due to a lack of hindrance. By this method, more abundant proteins can be indirectly quantified. This method was extended to indirectly quantifying small molecules[53]; then, the sensitivity was improved developed using nanostructured electrodes[54]. This strategy has recently been followed by an application of detecting signaling factors in stem cell cultures[55].

The exploit of high sensitivity and selectivity requires to maximize the redox signal and minimize the background. For that to reduce the background and maximally amplify the signal in the presence of the analyte[56], Gangli Wang and co-workers introduce a chemical reaction mechanism following electron transfer reaction[57], using a reductant tris(2-carboxyethyl) phosphine hydrochloride (TCEP) in the detection solution that will reduce the oxidized MB in situ at the electrical detection potential[58]. Thorp and co-workers reported the catalytic guanine oxidation with an exogenous inorganic ruthenium complex, $[Ru(bpy)_3]^{2+}$, as an oxidation catalyst. A two-step electrochemical oxidation of

$[Ru(bpy)_3]^{2+}$ to Ru(III) species, followed by the chemical oxidation of guanine in a redox reaction to regenerate the $[Ru(bpy)_3]^{2+}$ is suggested[59-62].

Barton et al. reported a new strategy to improve the sensitivity for the electrochemical detection of DNA hybridization by employing an exogenous electrocatalytic species for signal amplification[63]. Before the introduction of catalytic species, under the duplex formation, the original signal from the charge transport was through self-assembled monolayers of oligonucleotides between the intercalated indicator MB and the gold electrode surface. After the introduction of the solution- based mediator, potassium ferricyanide, the resulting voltammetric signal was significantly improved by the catalytic effect through the back-oxidation of MB. With a single base pair mismatch on the hybrids, the signal was dramatically lowered by the prevention of electron transfer through the hybrid. As a result, MB or other intercalated species, such as the grove binder, could be utilized to amplify the signal with its specific DNA design. On the other hand, the catalytic effect from a solution mediator with a suitable formal potential, such as ferricyanide in the case of MB label, is capable of further enhancing the electrochemical response under our DNA hybridization event. In this way, each MB molecule near the electrode surface, a consequence of recognizing a target molecule, will be cyclically oxidized electrochemically and reduced chemically by the reductant, a process that amplifies the redox signal[64-66].

1.5 Electrochemiluminescence (ECL)

Electrochemiluminescence (ECL) is an electrochemical technique in which electroactive molecules undergo electron-transfer reactions at electrode surfaces to form excited states that emit light (Figure-1.7).

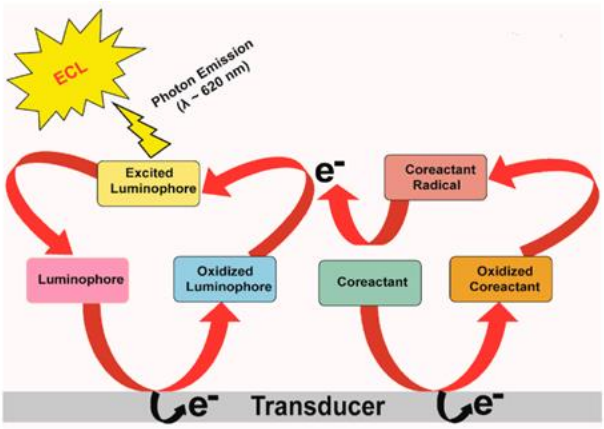

Figure 1.7 Schematic illustration of ECL mechanism.

Schematic illustration of ECL mechanism and its generation on the electrode surface in the presence of suitable luminophore and co-reactant. An ECL reagent (e.g., luminol, $Ru(bpy)_3^{2+}$, QD) is being oxidized at an electrode surface. The oxidized species (like $Ru(bpy)_3^{2+}$, QD, luminol) can undergo transfer into an exited, photon emitting state[67]. Reprinted with permission [67] **Copyright © (2018) Sensors.**

Therefore, the emitted light is identified upon ECL reaction at the initiation of an essential voltage. Highly sensitive photon identification is possible because of several existing high-performance detectors and current improvement to more sensitive and tiny sensor devices. The integration of ECL reactions with highly sensitive detectors to make this technique as highly sensitive analytical methods and tools[68-70]. Although fluorescence remains the predominant light-emission based detection method, ECL offers excellent benefits over fluorescence, resulting in the mechanism by which the excited photon is produced. In ECL mechanism, no need for the external light source, but in fluorescence need an external light source. ECL reach higher signal-to-noise ratios and reduce limits of detection due to background-free detection. The ECL reaction generates a signal by the certain applied voltage at the electrode surface, and this is a remarkably localized and time-triggered detection method. A co-reactant can participate in and promote the electron transfer processes into the ECL reagent's excited state and allow for a constant applied voltage.

When tracing the history of electrochemiluminescence (ECL), there was no co-reagent involved at the beginning time. In a conventional three-electrode system, the ECL is observed on the working electrode by the annihilation between cation radicals and anion radicals. The annihilation generates an excited state of the emission species, and then the emission is produced from the radiative decay of it. At the earliest stage, the cation radicals and anion radicals were generated by cyclic electrochemical steps such as a CV. The ECL biosensors based on $Ru(bpy)_3^{2+}$/TPrA system have been mostly studied due to their excellent stability and high luminescence efficiency. Notably, the ECL biosensors based on the enhancement of $Ru(bpy)_3^{2+}$/TPrA ECL system have been extensively investigated with improved performance.

$$A + e^- \rightarrow A^{-\bullet} \quad \text{(reduction at electrode)} \quad (1)$$

$$D - e^- \rightarrow D^{+\bullet} \quad \text{(oxidation at electrode)} \quad (2)$$

$$A^{-\bullet} + D^{+\bullet} \rightarrow {}^1A^* + D \quad \text{(excited state formation)} \quad (3)$$

$${}^1A^* \rightarrow A + h\nu \quad \text{(light emission)} \quad (4)$$

ECL of $Ru(bpy)_3^{2+}$ can be emitted through an annihilation procedure, requiring only $Ru(bpy)_3^{2+}$ in an electrolyte solution, and is addressed in more detail in several publications[71-73]. ECL is a highly developed and sensitive detection protocol that has been used for a variety of analytical applications[74, 75]. Moreover, because the ECL reactions only occur close to the surface of an electrode, the interrogated volume can be limited to a small value that is ideal for making portable and microdevices. A well-known ECL system uses $Ru(bpy)_3^{2+}$ as the light-emitting species and a co-reactant, such as tri-n-propylamine (TPrA). $Ru(bpy)_3^{2+}$ based ECL has been widely used in analytical purpose due to its excellent stability, good water solubility, and high sensitivity[75]. The mechanism of $Ru(bpy)_3^{2+}$ based ECL have been intensively studied and most of the

analytical applications are based on "oxidative-reductive" ECL[76]. Specifically, $Ru(bpy)_3^{2+}$ is first oxidized to $Ru(bpy)_3^{3+}$, which further reacts with the $TPrA^{\bullet}$ radical to generate $Ru(bpy)_3^{2+*}$, as shown in figure 1.8.

Catalytic route:	$Ru(bpy)_3^{2+} - e \longrightarrow Ru(bpy)_3^{3+}$
	$Ru(bpy)_3^{3+} + TPrA \longrightarrow Ru(bpy)_3^{2+} + TPrA^{\bullet+}$
Direct oxidation route:	$TPrA - e \longrightarrow TPrA^{\bullet+}$
Then	$TPrA^{\bullet+} \longrightarrow TPrA^{\bullet} + H^+$
Followed by either	$Ru(bpy)_3^{3+} + TPrA^{\bullet} \longrightarrow Ru(bpy)_3^{2+*} + P1$
Or	$Ru(bpy)_3^{2+} + TPrA^{\bullet} \longrightarrow Ru(bpy)_3^{+} + P1$
	$Ru(bpy)_3^{3+} + Ru(bpy)_3^{+} \longrightarrow Ru(bpy)_3^{2+*} + Ru(bpy)_3^{2+}$
	$Ru(bpy)_3^{2+*} \longrightarrow Ru(bpy)_3^{2+} + h\upsilon$

Where $TPrA^{\bullet+} = Pr_3N^{\bullet+}$, $TPrA^{\bullet} = Pr_2NC^{\bullet}HCH_2CH_3$, and $P1 = Pr_2NC^{+}HCH_2CH_3$

Figure 1.8 Generation of ECL mechanism in the presence of coregent.

Schematic representation of the generation of ECL mechanism in the presence of coregent[77].

When $Ru(bpy)_3^{2+*}$ decays to the ground state, a red light will emit. The intensity of the emitted light is used as an indicator for the sensing event. Specific DNA, Protein-based on the amplify ECL intensity has been reported for several times[78-80]. On the other hand, detection of analytes based on ECL quenching is also a very useful sensing strategy[74]. Although detection of analytes, such as DNA detection through hybridization using photoluminescence quenching, has been widely reported, the investigation of ECL quenching has been minimal. A variety of compounds, such as phenols[81],

hydroquinones[81],$Fe(CN)_6^{3-}$[82, 83], $Fe(CN)_6^{4-}$,[82, 83] and O^2,[84] have been reported for their excellent characteristics for photoluminescence quenching of $Ru(bpy)_3^{2+}$ via energy-transfer or charge-transfer mechanism. Most frequent, however, a co-reactant, such as tripropylamine (TPrA), is present during the ECL process, promoting the generation of the light-emitting excited photon state of $Ru(bpy)_3^{2+}$ and allowing for a continuously applied voltage. One significant advantage of $Ru(bpy)_3^{2+}$ and the reactant of ECL is that it can take place in aqueous solution, making it functional for a large variety of medical and biological applications and diagnostics.

1.6 Conclusions

Sensitive and rapid detection of infectious disease is becoming very significant to improve human health. We have seen that the sensitive methods often required expensive, and sophisticated instruments. Biosensors are offering portable, cost-effective alternative to detect the clinically relevant biomarker, which also helps to design POC diagnosis. Several sensitive methods are being developed for biomarker detection. For POC systems required the methods which are inexpensive, sensitive, automated, and rapid that can serve to improve the health sector, especially in developing countries. One magnificent among these methods is the electrochemical biosensor. Electrochemiluminescence (ECL), the light-emitting process generated by electrochemical means, could transfer the electrochemical signal into light emission under specific applied potential. The ECL's main characteristics and advantages are its benefit for biological assays; its high specificity and sensitivity; and its least hardware requirements (i.e., voltage source, electrodes, and light sensor, all of which can be miniaturized). All the combinations make ECL an ideal analytical detection method. The ECL detection method provides advantages like high

sensitivity and high signal to noise ratio for no-background. The primary goal of this dissertation work is to develop a DNA-based electrochemical method for quantification of small molecules and ECL based aptasensors for large proteins, which is suitable for dip-and-read and POC diagnoses. Chapter 2 focuses on the electrochemical proximity assay (ECPA) on the glassy carbon electrode as a transducer and its optimization. After optimization, the experimental condition of the ECPA model system was illustrated. This work evaluates DNA fabrication on the glassy carbon electrodes, instrumentation issues, and illustrated to make ECPA DNA model measurement. Chapter 3 focuses on improving the redox moiety signal of methylene blue (MB) molecules by using catalytic molecules as $K_3[Fe\ (CN)_6]$. In Chapter 4 the large protein quantification approach is developed by exploiting the ECL, amplified ECL signal by using electroactive nanocomposites as Reduced graphene oxide- Tris(bipyridine)ruthenium (II) chloride composite (GO-$Ru(bpy)_3^{2+}$. This method, in the future, should provide a generalizable platform for quantifying multiple proteins, peptides, or small molecules by a dip-and-read workflow, and this should promote future real-time measurements. Chapter 5 summarizes the findings of the research. The recommended future work of projects is stated.

CHAPTER 2

Carbon-based Electrochemical systems for Electrochemical Proximity Assay (ECPA)

2.1 Introduction

The clinically relevant biomolecule diagnosis is one of the most significant steps in health care and medical treatment[85]. The multiparameter measurements of the blood approach to analysis and therapeutic of disease[86]. This clinical analysis includes detecting small molecules like glucose, ATP to the large biomarker, which determine the biological function of the cell. The three-subdivision group of clinically relevant molecules is proteins, nucleic acids, and small molecules, which is made by Kelly et al. The respiratory insufficiency, diabetes, cardiovascular, metabolic and neurological disorders, and liver diseases are diagnosed by small molecules, and myocardial infarction, inflammatory diseases, and screening and diagnosis of tumor and cancer are diagnosed by large biomarker like protein[1]. In recent decades, lots of protein detection techniques are developing; which is sensitive & specific enough for Nano- & micro-materials[87], enzyme-labeled beads[88] used with electrochemical readout.

In recent decades, lots of protein detection techniques are developing; which is sensitive & specific enough for Nano- & micro-materials[87], enzyme-labeled beads[88] used with electrochemical readout. All the techniques are promising to detect protein biomarker, but a challenge is remaining cost effectiveness & user-friendly for point of care (POC). Electrochemical biosensors offer cost-effective & user-friendly point-of-care diagnostic devices. This device provides fast diagnostic information.

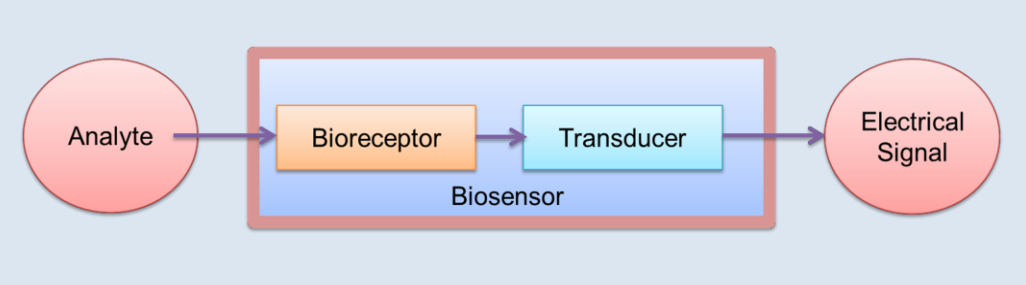

Figure 2.1 Biosensors schematic representation.

Usually, the electrochemical biosensor is working three significant steps, a) a bio-receptor analyte binding b) a signal transducer and c) Signal readout system. In the past decade, the target-induced DNA assembly and affinity binding is called the proximity effect, accomplished nano sensors and ultrasensitive for protein detection[89-91]. The ultrasensitive protein detection achieves by assembling DNA through affinity binding[92], which explained the proximity effect by a change in local DNA concentration and comparison of inter and intramolecular DNA hybridization.

Figure 2.2 A shows that the target molecule stabilizes the weak DNA hybridization. When a weak DNA pair (6 base pair) tagged to two antibodies which specifically binds to a target in separate epitope is diluted in the same buffer to 1 nM, without and with a target distance, the volume between two DNA will be 1500 nm, 1.7 fL, and 20 nm, 4.2 zL respectively. Local concentration is increased 400,000-fold to the presence of the target compared to the absence of the target. Figure 2.2 B shows stability by comparing the melt temperature (Tm) of intra- and inter-molecular hybridization. The intermolecular Tm of the 6 bp DNA at 1 nM (in 1 mM Mg^{2+} and 50 mM Na) is only 10 ^{o}C (calculated using IDT Oligo Analyzer). If the same 6 bp is in the ends of a single strand making an intramolecular hairpin DNA binding, the Tm is much higher at 53 ^{o}C. Theoretically, the presence and

absence of a target are responsible for intra-and inter-molecular binding respectively, through the proximity effect.

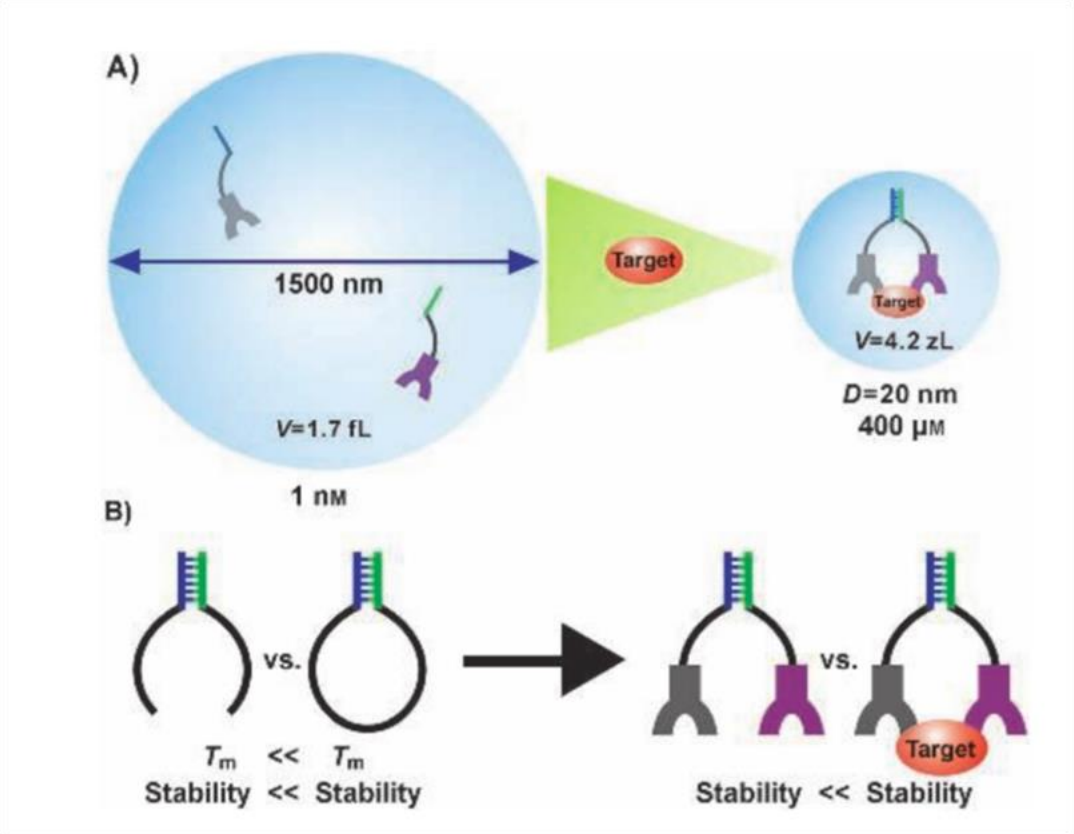

Figure 2.2 The proximity effect.

A) When two antibodies conjugated with weakly hybridizing complementary DNA is in a solution with 1 nM concentration, the distance between them will be 1500 nm and 1.7 fL as a local volume. On introduction of the target, the distance drops to 20 nm making local volume as 4.2 zL and 400 µM as local concentration. B) Proximity hybridization in the presence and absence of target can be seen as intra and inter DNA hybridization, with intra being very strong than inter[92].

During the last decades, many electrochemical sensors have been developed to detect protein by using the proximity effect. For example, Ren, et al. developed a ratiometric electrochemical proximity assay for selective and sensitive protein detection[20]. Initially since methylene blue (MB) is closer to the surface and ferrocene (Fc) being far, the ratio of IFc /IMB is lower. On introducing the target due to proximity effect, the DNA tagged with MB is removed from the surface, and Fc is brought closer which increases the ratio of IFc /IMB, by which protein can be quantified ratio-metrically[20]. Zhang et al. also develop electrochemical aptasensor based reusable, sensitive protein assay by proximity effect on the surface[21, 22]. In this method used dual aptamers in a different configuration and quantified platelet-derived growth factor protein (PDGF) through electrochemical detection of proximity dependent complex on electrode surface[21, 22].

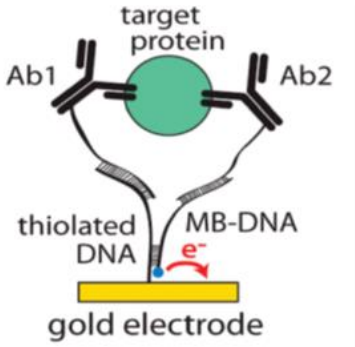

Figure 2.3 Pictorial representation of complete complex of ECPA which has six component including target.

Reprinted with permission from [47]. **Copyright © (2012) American Chemical Society.**

The Shannon and Easley groups developed a generalizable protein assay, marriage between the concepts of the sandwich ELISA within an electrochemical detection platform that exploits the proximity effect, termed the Electrochemical Proximity Assay (ECPA)[47]. ECPA is also flexible and can be extended to any protein target with two

antibody or aptamer probes, like sandwich ELISA. Figure 2.3 shows a cartoon depiction of ECPA, where the protein target has two antibodies targeting different epitopes. The hybridization between methylene blue tagged DNA, and thiolated DNA is made stronger in the presence of the target protein by the proximity effect. The electrochemical signal from the methylene blue is thus proportional to the concentration of target protein[47]. In gold-thiol SAM the gold-thiol bond can only endure reasonably mild potentials since alkanethiols are prone to thermal desorption and oxidative damage[93]. SAMs might not be stable and are readily oxidized in the air[94, 95] resulting in a gradual reduction in DNA immobilization. Additionally, the gold electrode potential window is limited by hydrogen evolution. In ECPA, the reduction of MB molecule (around -250 mV) is quite close to the H_2 evolution at -400 mV in neutral solution. If the potential is kept at a low value to avoid H_2 evolution, it may not be enough to trigger an enough MB reduction across the transducer under a small driving force.

In contrast, carbon electrodes are free of this problem by their broader potential window range. The appearance of H^+ reduction is shifted more negatively because of its slow kinetics. Also, the oxidation potential of carbon is more positive than Au. More fundamentally, the linkage between DNA and the carbon surface is often a stronger covalent bond compared to the weak thiol-Au bond. In ECPA model, by using EDC and NHS cross-linking reaction on the carboxylate-terminated 4-aminobenzoic acid (4-ABA) monolayer modified glassy carbon electrode (GCE)[96] to detect a broad range of biomolecules with square wave voltammetry (SWV), which has shown promising performance on the proof-of-concept stage. The presence of the non-faradaic charging current imposed to the faradaic current from the target analyte is the inadequacy of SWV

characterization. Nevertheless, the signal of the charging current can be downcast by selecting an appropriate sampling time point which is usually larger than five times the cell time constant, it would also sample the analyte signal in an attenuated value, especially for limited electro-active species in the monolayer-level. Whereas the ECL sensing, even though with a low quantum efficiency, is capable of excluding all the charging effect by only producing the ECL emission corresponding to the faradaic reaction. In electrochemistry, the carbon electrode has been widely used with their low cost, relatively inert electrochemistry, broader potential window, and electrocatalytic activity for a variety of redox reactions. According to the behavior of carbon for electrochemical sensing, carbon is a promising substrate to perform as a transducer material, which provides direct readout and is adequate for point-of-care detection. The present chapter and the following chapters will be helpful in understanding various factor influencing electrochemical, DNA-based protein and small molecule sensors. This information should be useful not only in optimizing ECPA but also with many DNA-based electrochemical platforms for detecting clinically relevant molecules.

2.2 Materials and methods

All solutions are prepared with deionized, ultra-filtered water (Fisher Scientific). The following reagents were used as received: sodium percholorate ($NaClO_4$) and *4-(2*-hydroxyethyl)-1-piperazineethanesulfonic acid (HEPES) (99.5%) from Alfa Aeser, tris-(2-carboxyethyl) phosphine hydrochloride (TCEP), 6-mercapto-1-hexanol (MCH), Potassium ferricyanide (III) and Potassium ferrocyanide (II) (99%), N-(3-Dimethylaminopropyl)-N′-ethylcarbodiimide hydrochloride (EDC), N-Hydroxysuccinimide (NHS), Thioctic acid, 3-Mercaptopropionic acid, 4-aminobenzoic acid (4-ABA) and Lithium perchlorate($LiClO_4$) from Sigma-Aldrich St. Louis, MO., Potassium Nitrate (KNO_3) (Fisher Scientific), Methylene blue-conjugated DNA (MB-DNA) was purchased from Biosearch Technologies (Novato, CA), purified by RP-HPLC. All other oligonucleotides were obtained from Integrated DNA Technologies (IDT; Coralville, Iowa). All measurements were performed using Reference with a Differential Potentiostat and a bipotentiostat/galvanostat (WaveDriver 20, Pine) with standard three-electrode configuration.

Table 2.1 Sequences of DNA strands used in the experiments.

Name	Abbreviation	DNA sequence, list from 5' to 3'
Amino-DNA	A-DNA	/5AmMC6/ GCA TGG TAT TTT TCG TTC GTT AGG GTT CAA ATC CGC G
Methylene blue-DNA (7 base pair match)	MB-DNA	CCA CCC TCC TCC TTT TCC TAT CTC TCC CTC GTC ACC ATG C /MB-C7/
Methylene blue-DNA (Full match)	MB-DNA (Full match)	CGC GGA TTT GAA CCC TAA CGA ACG AAA AAT GTC ACC ATG C /MB-C7/
Methylene blue-DNA-10	MB-DNA (10 bp)	CCA CCC TCC TCC TTT TCC TAT CTC TCC CTC GTC ACC ATG C/MB-C7/
ECPA-Loop	Loop	TAG GAA AAG GAG GAG GGT GGC CCA CTT AAA CCT CAA TCC ACC CAC TTA AAC CTC AAT CCA CGC GGA TTT GAA CCC TAA CG

Abbreviations: /MB-C7/ = methylene blue modification, /5AmMC6/ = Amino bond flanked by six-carbon spacers.

Preparation of Glassy Carbon Electrode, gold Electrode and DNA Monolayer Assembly The ECPA and all other experiments were done with commercially glassy carbon electrode (GCE; CH Instruments, diameter = 3 mm) and gold electrodes (AuE; CH Instruments, diameter = 2 mm) were used to optimize the condition of ECPA for Glassy Carbon Electrode. The Au electrode was modified by thioctic acid and 3-mercapto propanoic acid. As the first step in sensor fabrication, the GCE and AuE were cleaned and polished. Both the glassy carbon electrode (GCE) and the gold electrode (AuE) careful polishing to a mirror-like surface with deagglomerated alumina suspension (0.05 micrometer: Allied High-Tech Products, Inc. Rancho Dominguez, CA). The suspension had been dropped on a polishing mat Micro Floc (Buehler, Lake Bluff, IL), and the electrode was held perpendicularly while a spinning motion was made as shown in Figure 2.4 for 10 minutes.

[A] [B]

Figure 2.4 Mechanical cleaning of electrodes.

[A] Polish with 1.0,0.3 and 0.05 µm alumina sequential polish. [B] shows the procedure for mechanical cleaning, where the electrode is holed perpendicular and polished by pattering the motion as 8.

Then the GCE and AuE electrode were rinsed and sonicated in an ethanol and water mixture (1:1) for five minutes to remove alumina particles effectively. Then the GCE electrodes were finally rinsed with deionized water and dried under flowing nitrogen. After that, the gold electrode was further cleaned electrochemically by 20 cycles of cyclic voltammetry (CV) in 0.5 M H_2SO_4 with a three-electrode system (Ag/AgCl as Reference, platinum as counter). The CV scans were from -0.35 to +1.5 V at a scan rate of 0.1 V s^{-1}. The electrochemically cleaned Au electrode was finally rinsed with deionized water and dried under flowing nitrogen. The clean GCE and Au electrode were ready for the introduction of the self-assembled monolayer (SAM).

Amino-DNA monolayer assembly on pretreated on glassy carbon electrode After cleaning the surface of GCE, the glassy carbon electrode was oxidized at 0.5 V for 1 min in PBS solution (pH 7.4) to form a functional group like carboxylic acid, and it was rinsed. The generated carboxylic acid groups on the surface of GCE were activated by immersing in a solution containing 5 mM EDC and 8 mM NHS in 1X PBS buffer for 1 h[97]. The Amino-DNA was covalently attached to the activated carboxylic groups via carbodiimide bond to form DNA monolayer on the GCE. The shipped Amino-DNA is used to make the stock solution of the Amino-DNA (A-DNA) with HEPES buffer (10 mM HEPES buffer and 0.5 M $NaClO_4$, pH 7.0) at a concentration of 100 µM. The solution was then diluted with HEPES buffer (10 mM HEPES buffer and 0.5 M $NaClO_4$, pH 7.0) to a concentration of 1.0 µM[98] and a volume of 200 µL for an electrode in a 2 mL PCR tube. The GCE electrode was dipped in this solution and incubated at room temperature for 1 hour in the dark. Once this incubation was done, the electrode was rinsed with HEPES and transferred

to the HEPES buffer. This SAM electrode was ready to be used and could be stored at 4 ◦C for about a week.

Thioctic acid and 3-Mercaptopropionic acid assembly on the clean gold electrode

To optimize the activation condition of the functional group like carboxylic acid on thioctic acid or 3-Mercaptopropionic acid-modified AuE surface by using EDC and NHS to form carbodiimide bond. Thioctic acid has disulfides; thus, they required chemical reduction by dithiothreitol or TCEP. We used TCEP for reduction, where 1 µL of 200 µM thioctic acid and 3 µL of 10 mM TCEP were mixed in a 200 µL PCR tube and placed in the dark for 1 hour at room temperature. The thioctic acid or stock solution of 3-Mercaptopropionic acid was diluted with HEPES buffer (10 mM HEPES buffer and 0.5 M $NaClO_4$, pH 7.0) to a concentration of 1.0 µM[98] and a volume of 200 µL for an electrode in a 2 mL PCR tube. The Au electrodes were dipped in thioctic acid or 3-Mercaptopropionic acid and incubated at room temperature for 1 hour in the dark. Then the electrode was dipped into 200 µL of 3 mM MCH for 1 hour in the dark at room temperature. The MCH solution should be freshly prepared, and since MCH has a foul smell, it is suggested to do all these processes in a fume hood. MCH acts as a spacer molecule between covalently bounded thiol molecules, which is helpful in reducing the capacitance current in electrochemical measurements. Additionally, it also helps to remove non-specific binding between thiol molecules and the gold surface, and it contributes toward the effective orientation of the thiol molecules on the gold surface. Once this incubation was done, the electrode was rinsed with HEPES and transferred to the HEPES buffer. This SAM of thioctic acid or 3 Mercaptopropionic acids of the Au electrode was ready to be used and could be stored at 4 ◦C for about a week.

GCE modified by 4-Amino Benzoic Acid (ABA) and DNA Monolayer Assembly The clean surface of GCE modification was performed by the procedure reported in the following Reference[95]. Briefly, the electrochemical modification of the clean GCE was carried out by 4-ABA via C-N covalent bond in an absolute ethanol solution containing 3 mM 4-ABA and 0.1 M $LiClO_4$ by cyclic scanning between 0.0 and +1.40 V versus SCE for 20 cycles at a scan rate of 10 mVs^{-1}. The mechanism of the oxidation of 4-ABA was as reported in[95]. The carboxylic acid groups of 4-ABA on the surface of GCE were activated by immersing in a solution containing 5 mM EDC and 8 mM NHS in 1X PBS buffer for 1 h[97]. The Amino-DNA was covalently attached to the activated carboxylic groups to form DNA monolayer on the GCE. The modified GCE was rinsed with 10 mM HEPES buffer (pH 7.0) to wash off the excess EDC and NHS.

Electrochemical Measurements All electrochemical measurements were performed using Reference with a Differential Potentiostat and a bipotentiostat/galvanostat (WaveDriver 20, Pine) with standard three-electrode configuration. It consisted of Ag/AgCl(s)|NaCl (3M) reference electrode (BASi), a platinum wire counter electrode (CH Instrument, Inc.), and a standard glassy carbon and gold working electrode (CH Instrument, Inc.). All potentials are measured relative to the saturated Ag|AgCl reference electrode. The Electrochemical measurements were performed by using square wave voltammetry (SWV) with a 25-mV amplitude signal at a period of 10 ms, over the range from -0.45 V to 0.00V versus Ag|AgCl reference in HEPES/NaClO4 buffer. The characteristic voltammetric peak of the MB molecule was detected by SWV at -210 mV (vs. Ag/AgCl Reference). MB molecule was chosen as the redox tag because its excellent shelf life and

robust electrochemical behavior in serum compared to other redox tags, such as ferrocene[98, 99].

2.3 Results and Discussion

There are several quantitative and qualitative methods used to analyze clinically relevant molecules. Even with the developments of detection techniques, there remains a need for improved quantification techniques from the perspectives of cost, sensitivity, and POC detection. Most of the methods address the issue of sensitivity. However, due to instrument sophistication and the need for expert technicians, there is still a need for better technology to address the other two issues. To address these, some point-of-care methods have been developed for selected analytes, those that are highly specialized to a target molecule[100, 101]. For future point-of-care testing, in addition to high sensitivity and do-it-yourself workflows, more flexible methods are needed that can function with a variety of targets using the same platform. The Shannon and Easley groups developed a generalizable protein assay, marriage between the concepts of the sandwich ELISA within an electrochemical detection platform that exploits the proximity effect, termed the Electrochemical Proximity Assay (ECPA)[47]. ECPA is also flexible and can be extended to any protein target with two antibody or aptamer probes, like sandwich ELISA.

In gold-thiol SAM the gold-thiol bond can only endure reasonably mild potentials since alkanethiols are prone to thermal desorption and oxidative damage[93]. SAMs might not be stable and are readily oxidized in the air[94, 95] resulting in a gradual reduction in DNA immobilization. Additionally, the gold electrode potential window is limited by hydrogen evolution. In ECPA, the reduction of MB molecule (around -250 mV) is quite close to the H_2 evolution at -400 mV in neutral solution. If the potential is kept at a low

value to avoid H_2 evolution, it may not be enough to trigger an enough MB reduction a small driving force. In contrast, carbon electrodes are free of this problem by their broader potential window range. The appearance of H^+ reduction is shifted more negatively because of its slow kinetics. Also, the oxidation potential of carbon is more positive than Au. More fundamentally, the linkage between DNA and the carbon surface is often a stronger covalent bond compared to the weak thiol-Au bond.

In ECPA model, by using EDC and NHS cross-linking reaction on the carboxylate-terminated 4-aminobenzoic acid (4-ABA) monolayer modified glassy carbon electrode (GCE)[96] to detect a broad range of biomolecules with square wave voltammetry (SWV), which has shown promising performance. For that, modified GCEs as the substrate in making biosensor towards DNA monolayer and ECPA study. Several modification methods have been tried by directly oxidizing the surface to carboxylic groups on GCEs, followed by EDC and NHS cross-linking reaction. The carboxylic acid functionalized GCE surface was activated by EDC and NHS, followed by incubated in Amino-DNA solution for forming amide bond. Then the GCE was incubated in MB-DNA (40) solution and characterized by square wave voltammetry (SWV). The glassy carbon electrode was oxidized at 0.5 V for 1 min in PBS solution (pH 7.4) to form a functional group like carboxylic acid, and it was rinsed. The generated carboxylic acid groups on the surface of GCE were activated by immersing in a solution containing 5 mM EDC and 8 mM NHS in 1X PBS buffer for 2 h[97]. The 1 μM Amino-DNA was covalently attached to the activated carboxylic groups via carbodiimide bond to form DNA monolayer on the GCE. Then the GCE was incubated in 1 μM full match MB-DNA solution for the hybridization.

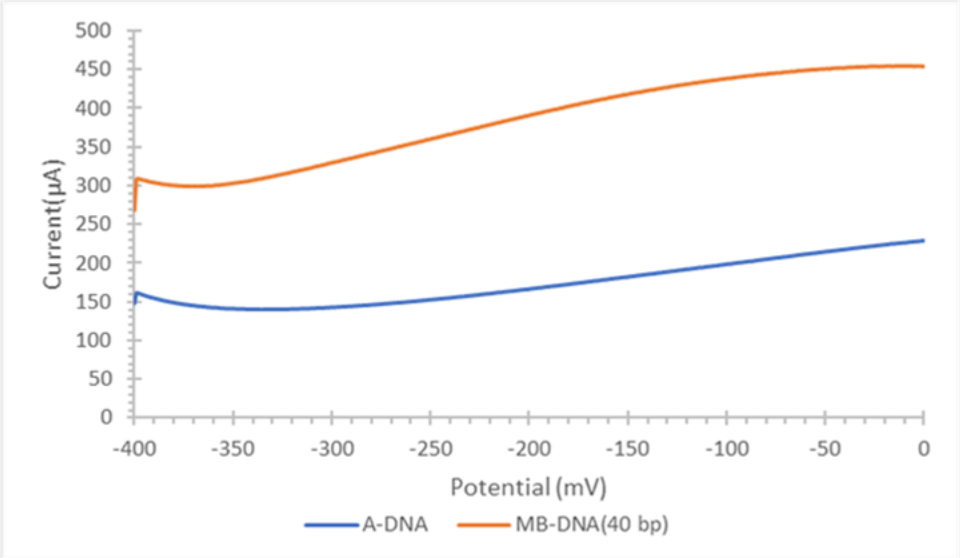

Figure 2.5 SWV characterization of modified GCE.

SWV characterization of modified GCE (anodization: in 0.5 V for 1 min in PBS solution pH 7.4) immobilized with amino-DNA (blue) and full match MB-DNA (brown).

However, as shown in Figure 2.5, in the SWV, there is no difference before/after the hybridization of full match MB-DNA (40); a Similar results were also obtained from the anodization in 0.1 M KNO_3[102] and acetate buffer as well[103] due to the high capacitance current[102]. In Figure 2.5 The capacitance current was observed in SWV 150 µA after A-DNA immobilization and capacitance current was increased (such as 300 µA) after hybridization with full match MB-DNA (40). This large capacitance current would necessarily conceal the faradic current from the redox molecule for detection. As a result, the expected electrochemical response was absent. The failure in the fabrication of the sensor may lie in two reasons. First, the surface oxidation to carboxylic groups was not well-achieved. Second, the activation of carboxylic groups by EDC and NHS process was not successful.

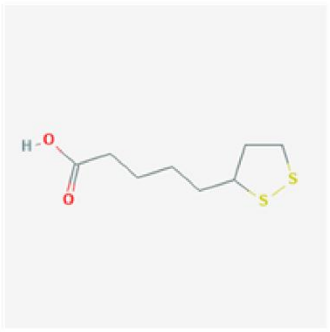

[A] Thioctic acid

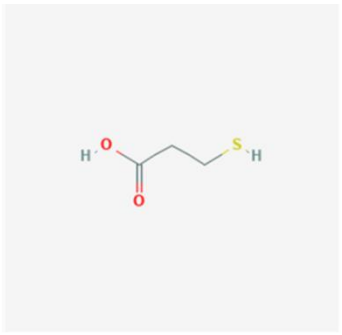

[B] 3-Mercaptopropionic acid

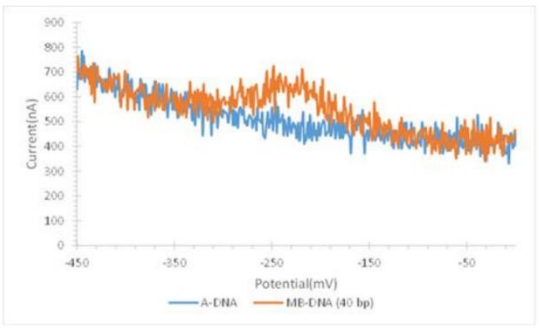

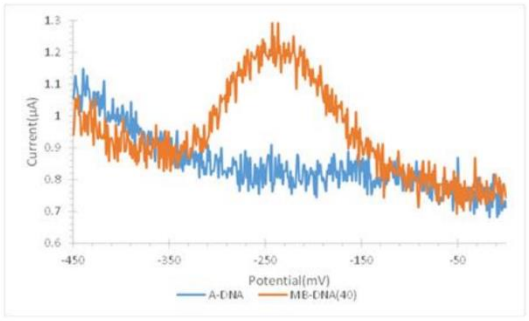

Figure 2.6: SWV characterization of standard gold electrode immobilized.

SWV characterization of standard gold electrode immobilized with [A] Thioctic acid and [B] 3-mercaptopropionic acid after amino-DNA coupling and MB-DNA hybridization.

The EDC and NHS coupling were tested by immobilizing various of SAMs on the standard gold electrode surface such as L-cysteine[104, 105], thioctic acid or 3-mercaptopropionic acid[106-112]. For example, standard gold electrodes were modified by Thioctic acid or 3-mercaptopropionic acid to form SAM on AuE surface with carboxylic acid group containing. Those acid groups were activated by EDC and NHS to form amide bond with A-DNA. The oxidation peak of MB is appeared at -240 mV after hybridization between A-DNA and full match MB-DNA. For 3-mercaptopropionic acid the MB oxidation response is more compare to the thioctic acid modified Au electrode due to 3-mercaptopropionic acid is sorter length compared to thioctic acid.

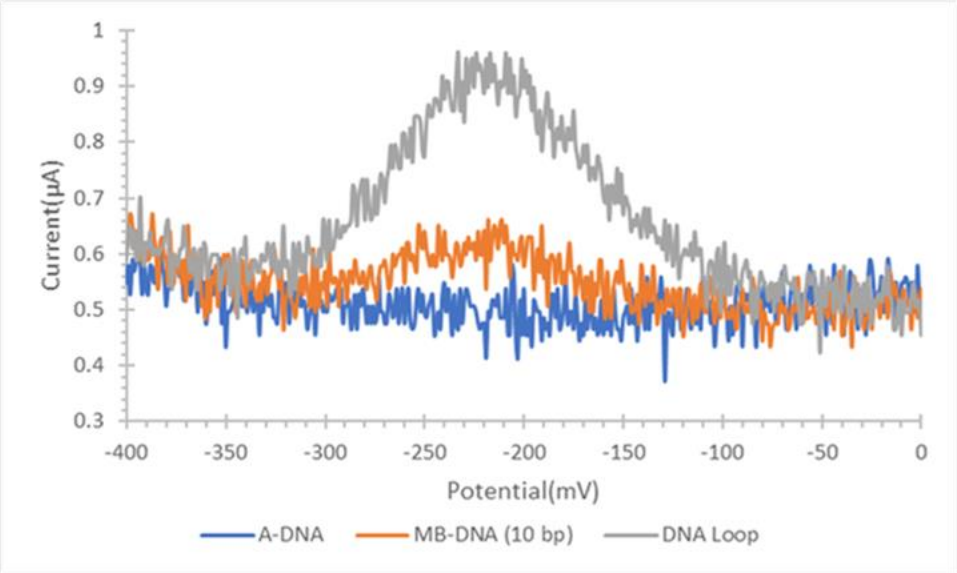

Figure 2.7 SWV of 3-MPA/AuE modified after 1 μM A-DNA immobilization, 1 μM MB-DNA (7 bp) and 1 μM DNA-Loop in HEPES/$NaClO_4$ buffer (pH 7.0).

The 3-mercaptopropionic acid modified Au electrodes also investigated for DNA-based model in ECPA. The 80-nucleotide containing the DNA loop mimics the formation of the ECPA complex, bringing MB near to the gold surface and increasing redox current. The background was modeled using only the Amino DNA and MB-DNA. All the experimental evidence indicating the successful coupling of carboxylic groups SAMs to the amino groups on the probe DNA. As a result, the absence of expected electrochemical response is referred to the lack of carboxylic groups after oxidization treatment. The carboxylic groups produced by direct oxidation generally has a low surface coverage (<10%)[113] and is unstable toward acidic or basic media. Besides, this type of modification often results in strong surface/adsorbate bonds. Other than this low coverage, the capacitive current from the carbon electrode in Figure 2.5 is more than 150 μA, which is much larger than that from the gold electrode in Figure 2.6 about only a few hundred nA to several μA. This large capacitance would necessarily conceal the faradaic current from the redox tag for

detection. After this, a series of experiments using different carbon sources such as carbon paste and screen printed carbon electrode were tested using different modification methods including adsorptive accumulation, bulk modification of carbon paste, yet with unsatisfied results with unobserved signal and large capacitance. As a result, a new approach is modified glassy carbon electrode (GCE) by the carboxylate-terminated 4-aminobenzoic acid (4-ABA) which contains more functional groups for probe immobilization and reducing the capacitance of carbon electrode.

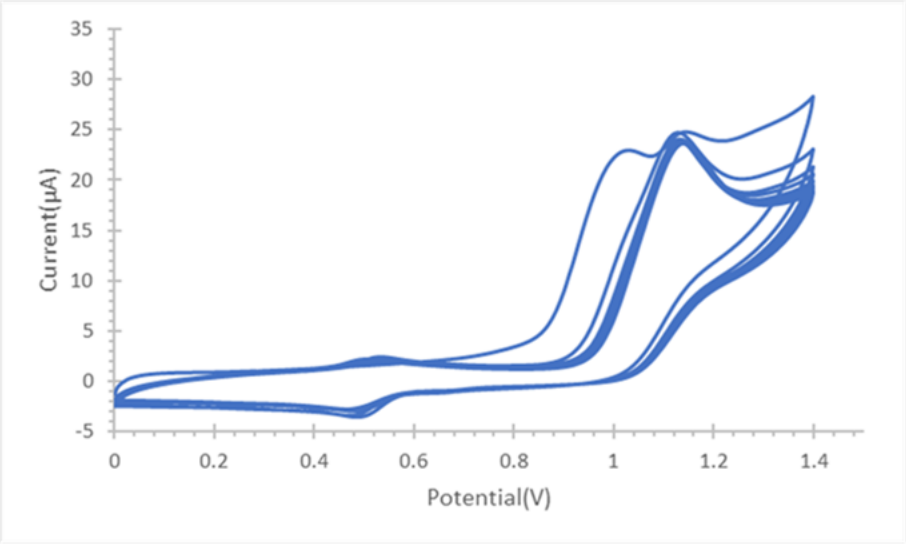

Figure 2.8 Electrodeposition of 4-Amino Benzoic Acid (4-ABA) on the GCE.

Electrodeposition of 4-Amino Benzoic Acid (4-ABA) on the GCE in 0.1 M $LiClO_4$ by cyclic scanning between 0.0 and +1.40 V versus SCE for 20 cycles at a scan rate of 10 mVs^{-1}.

The electrochemical modification of the clean GCE was carried out by 4-ABA via C-N covalent bond in an absolute ethanol solution containing 3 mM 4-ABA and 0.1 M $LiClO_4$ by cyclic scanning between 0.0 and +1.40 V versus SCE for 20 cycles at a scan rate of 10 mVs^{-1}. 4-ABA was deposited by layer by layer with the scan of CV. The mechanism of the oxidation of 4-ABA was as reported in[95].

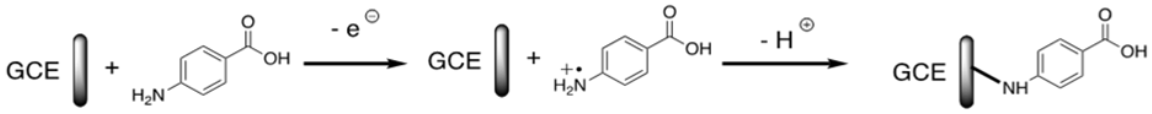

4-Aminobenzoic acid (4-ABA)

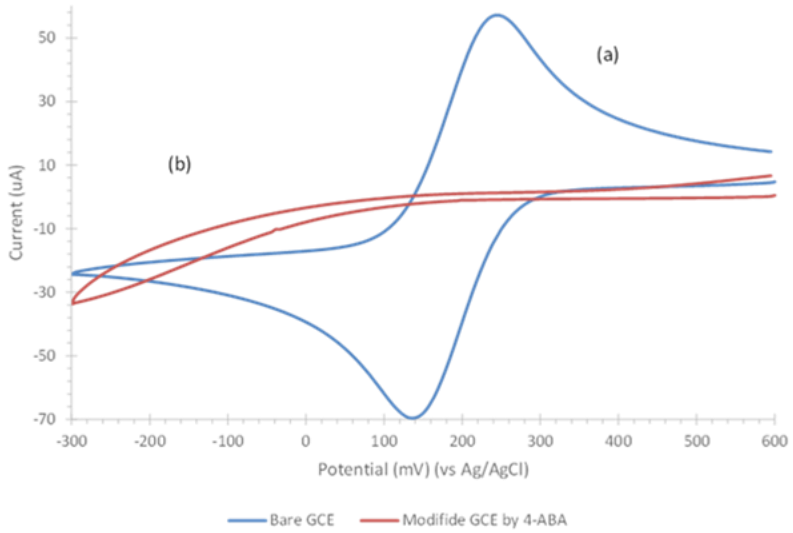

Figure 2.9 Cyclic voltammograms for a (a) bare GCE and (b) 4-ABA/GCE.

Cyclic voltammograms for a (a) bare GCE and (b) 4-ABA/GCE for 5 mM $[Fe(CN)_6]^{3-}$ in 10 mM HEPES/$NaClO_4$ buffer solution (pH 7.0) and scan rate of 100 mV s^{-1}.

The deposition of 4-ABA on GCE was confirmed by sweeping the bare GCE and modified 4-ABA/GCE electrode in 5 mM $[Fe(CN)_6]^{3-}$ in 10 mM HEPES/$NaClO_4$ buffer solution (pH 7.0) and scan rate of 100 mV s^{-1}. In figure 2.9 the reduction and oxidation peak of $[Fe(CN)_6]^{3-}$ were appear at 110 mV and 220 mV respectively in bare GCE. After deposition of 4-ABA on GCE, those reduction and oxidation peaks were disappeared, which indicate the perfect deposition of 4-ABA on GCE.

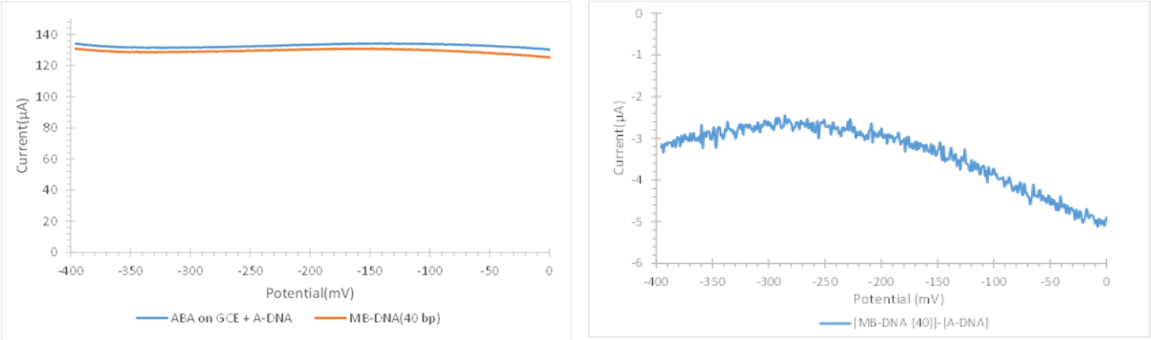

[A] [B]

Figure 2.10 [A] SWV characterization of modified GCE (deposition of ABA) and [B] SWV output (baseline corrected) of full match MB-DNA.

SWV characterization of modified GCE (deposition of ABA) immobilized with amino-DNA (blue) and full match MB-DNA (40) (brown), in HEPES/$NaClO_4$ buffer solution (pH 7.0).

The deposition of ABA on GCE modification contains carboxylic acid functional groups which activated by immersing in a solution containing 5 mM EDC and 8 mM NHS in 1X PBS buffer for 2 h[97]. The 1 μM Amino-DNA was covalently attached to the activated carboxylic groups via carbodiimide bond to form DNA monolayer on the GCE. Then the GCE was incubated in 1 μM full match MB-DNA solution for the hybridization. However, as shown in Figure 2.10 [A], in the SWV, there is no difference before/after the hybridization of full match MB-DNA and Figure 2.10 [B] shows the SWV output by subtracting A-DNA signal from full match MB-DNA. The capacitive current from the carbon electrode in Figure 2.10 is more than 130 μA, which is much larger compare with the gold electrode. This large capacitance would necessarily conceal the faradaic current from the redox tag for detection.

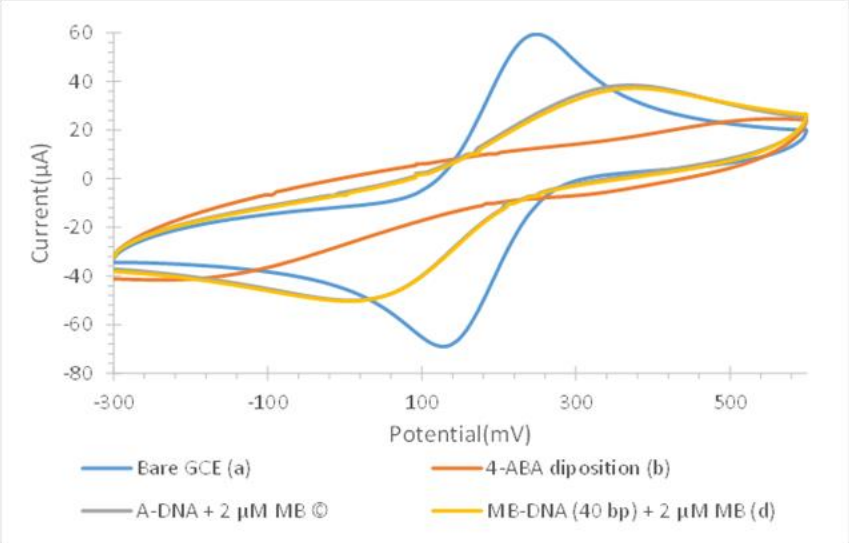

Figure 2.11 Cyclic voltammograms for in 2 µM MB intercalation.

Cyclic voltammograms for in 2 µM MB intercalation a (a) bare GCE; (b) 4-ABA/GCE; (c) A-DNA/4-ABA/GCE; and (d) MB-DNA (40 bp)/ A-DNA/4-ABA/GCE for 5 mM $[Fe(CN)_6]^{3-}$ in 10 mM HEPES/$NaClO_4$ buffer solution (pH 7.0) and scan rate of 100 mV s^{-1}.

To overcome the capacitance current interference for detect MB signal, we can amplify the electrochemical response of MB by increasing the no of MB molecules in the model system, which called the MB intercalation. Methylene blue (MB) is an organic dye that belongs to the phenothiazine family. Nevertheless, MB serves as an intercalation indicator toward double-stranded DNA. In particular, the cationic charge of MB would improve the DNA binding affinity by the electrostatic interaction with the phosphate backbone. Figure 2.11 shows cyclic voltammograms of the different modified glassy carbon electrode in 5 mM $[Fe(CN)_6]^{3-}$ in 10 mM HEPES/$NaClO_4$ buffer solution (pH 7.0); [A] The reduction and oxidation peak of $[Fe(CN)_6]^{3-}$ were appear at 120 mV and 220 mV respectively in bare GCE with 60 µA peak current; [B] After deposition of 4-ABA on GCE, those reduction and oxidation peaks were disappeared, which indicate the perfect

deposition of 4-ABA on GCE; [C] The ABA deposited GCE was activated by immersing in a solution containing 5 mM EDC and 8 mM NHS. Then immobilized A-DNA on activated GCE and intercalate in MB solution; The reduction and oxidation peak of [Fe $(CN)_6]^{3-}$ were appear at 20 mV and 300 mV respectively in A-DNA modified GCE with 40 µA peak current. The ABA deposited GCE pinhole was open by activation and washing step. As a result, [Fe $(CN)_6]^{3-}$ can penetrate to the modified GCE surface and appear the oxidation and reduction peak. [D] The immobilized single-strand A-DNA hybridized with full match MB-DNA and intercalate in MB solution. The reduction and oxidation peak of [Fe $(CN)_6]^{3-}$ were appear same as A-DNA modified GCE due to the same reasons.

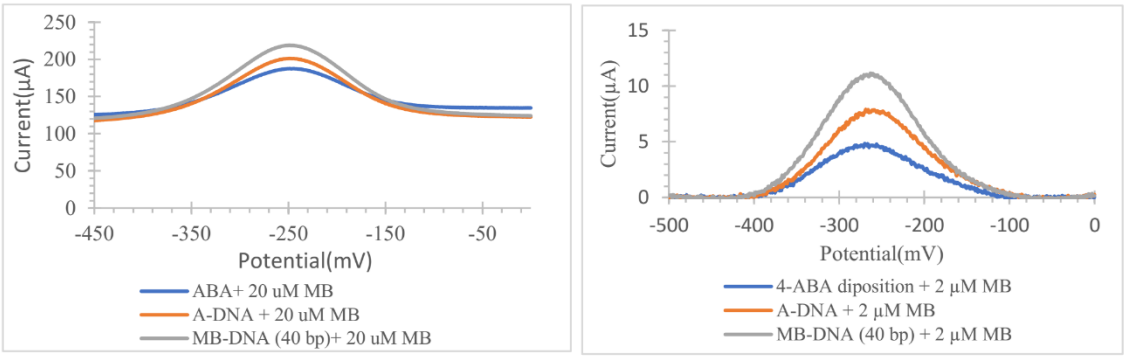

[A] [B]

Figure 2.12[A] SWV of 20 µM MB intercalation at different modification of GCE and [B] SWV output (baseline corrected) of 2 µM MB intercalation at different modification of GCE.

Yang proved that there was a specific interaction of MB with guanine bases on the DNA when using carbon paste electrode[114]. Rohs et al. reported a modeling study for MB binding to DNA with alternating guanine-cytosine base sequence. Kelley first studied the intercalation of MB into a thiol terminated self-assembled monolayer of oligonucleotides on gold employing chronocoulometry, cyclic voltammetry and ellipsometry[63]. Tani et al. stated that there was a shift in the peak potentials of the square

wave voltammetric signals of MB from this condition[115]. In Figure 2.12 [A] Methylene blue (MB) was accumulated onto the surface of hybrid modified GCE by immersing the electrode into 20 µM MB containing HEPES/$NaClO_4$ buffer for 10 mins. After accumulation of MB, the electrode was rinsed with 10 mM HEPES buffer for 2 min to remove the nonspecifically bound MB. After intercalation of MB check SWV in every step modification was done. Even though capacitance current ware also high but we observed characteristic MB oxidation signal at -250 mV due to more MB molecules accumulate in every step. Enlighted by the method of intercalation, we applied it to our DNA assembly on the 4-ABA/GCE surface in order to amplify the electrochemical response. The existing DNA sequence was studied at this time considering the cost performance and time efficiency. The presence of some nonspecific adsorption of MB to the 4-ABA/GCE was observed using square wave voltammetry (SWV) on the bare electrode. After the A-DNA assembling, we performed the intercalation by incubating modified GCE in 20 µM MB in HEPES/$NaClO_4$ solution for 10 min. The modified GCE was rinsed with HEPES buffer for 2 min before SWV characterization. From a brief calculation, there are 10 guanines bases (Gs) on the Amino-DNA (7) and 8 G on the full match MB-DNA. The MB molecules intercalated on the Gs in ss-DNA are driven away by duplex formation due to a weak interaction between the MB and ds-DNA. After a second MB intercalation, a current signal higher than that of the first intercalation shows up. Though there is 8 G in the full match MB-DNA, the covalent attached MB label which is close to the electrode surface with fast electron transfer contributes to increase the signal. The current response from the ECPA assay is quantified in GCE by square wave voltammetry (SWV), which measures in differential potentiostat (DiffStat)[116], it is built up by Dr. Easley lab. The differential

potentiostat (DiffStat) is constructed to utilize two working electrodes, where one electrode provides a signal and the second electrode provides a background, which is subtracted from the first[116]. In Figure 2.12 [B] Methylene blue (MB) was accumulated onto the surface of hybrid modified GCE by immersing the electrode into 2 μM MB containing HEPES/$NaClO_4$ buffer for 10 mins. Same observation was observed like figure 2.12 [A] but in experiment 2.12 [B] signal current is smaller than experiment 2.12 [A] due to in experiment 2.12 [B] use small amount of MB intercalation in the experiment 2.12 [B].

The differential potentiostat was used to remove non-Faradaic current by on-board analog subtraction of two working electrodes where one is exposed to target and the other is background[116]. With the significant reduction of non-Faradaic current, larger surface area electrodes producing larger Faradaic current can potentially be leveraged in surface confined electrochemical nucleic acid bioassays. The background subtraction is performed concurrently, during data collection from both electrodes by a differential operational amplifier configuration. SWV is a very sensitive technique, which reduced the capacitance current as well as increased the signal by its differential output. Surface-confined reactions are observed by SWV due to decreasing background current followed by an increase signal as its differential output. ECPA is a generalizable assay; here we utilized a DNA loop as a model system of ECPA on GCE. The preliminary experiments show that ECPA is also responsive to GCE by using the differential potentiostat[116].

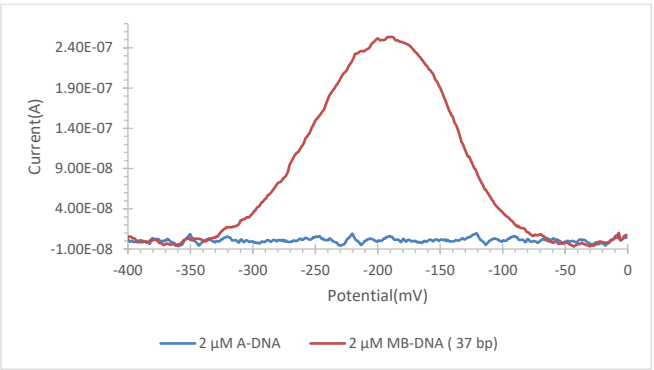

[A] [B]

Figure 2.13[A] SWV output (baseline corrected) of full match MB-DNA. [B] Schematic diagram of full match DNA hybridization.

In these experiments, Amino-DNA (A-DNA) SAMs were prepared by using EDC and NHS cross-linking reaction on the carboxylate-terminated 4-aminobenzoic acid (4-ABA) monolayer modified on the GCE. After the assembly of A-DNA (2 µM) onto the GCE surface, we incubated the GCE in 2 uM of MB-DNA (full match) for 1 h. Figure 2.13 [A] shows the baseline corrected SWV output of MB-DNA signal. In the background ECPA using standard glassy carbon electrode, the concentration of MB-DNA (full match) was contrilled at 2 µM in an aliquot with a volume of 100 µL. The calculated total MB-DNA amount was about 1.2×10^{14} molecules in the incubation solution. According to the literature, the theoretical surface coverage of hybridized DNA with 100% efficiency was roughly 4×10^{12} molecules/cm^2[132].

Figure 2.14 A and B shows the current increasing and integrated signal response with respect to the time for full match MB-DNA hybridization, respectivly. It is obvious that initially current is increasing faster with time, after 30 min current increasing begans slowdown and at 60 min incubation in full match MB-DNA showes saturation point.

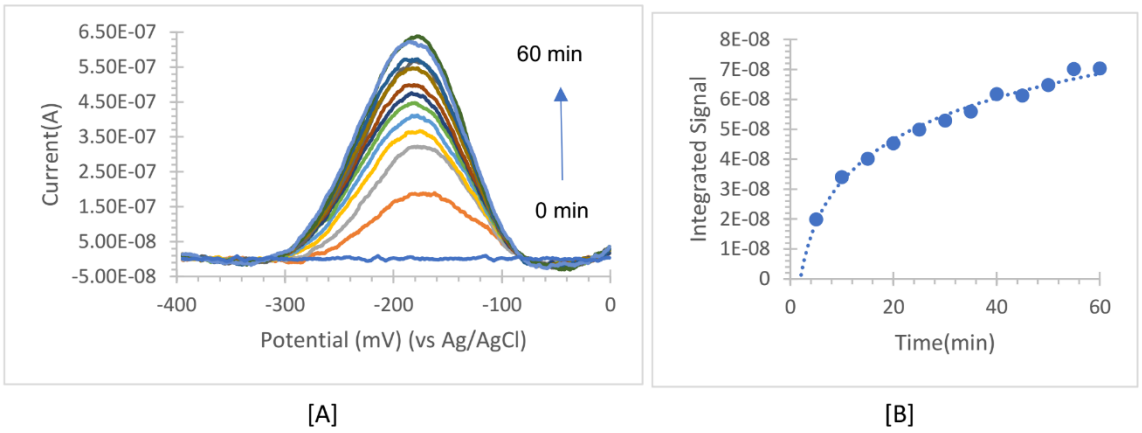

Figure 2.14 [A] SWV output (baseline corrected) full match 500 nM MB-DNA for kinetic study and; [B] Integrated signal vs Time(min).

This observation indicating that, initially 4-ABA modified glassy carbon has maximum free single strand A-DNA, which hybridized with full match MB-DNA very easily. As a result, redox current increase faster. After 30 min increasing the redox current was slowdown. In 4-ABA modified glassy carbon has unreactive -COOH group and after hybridization starting DNA population was increasing, which also contribute to repel the coming hybridized MB-DNA. Here, we used 40 bp DNA, which is longer compare to different thiol molecules; for that kinetics is slow compare to thiol molecules[117].

The DNA probe density on the surface of the electrode plays a crucial role in electrochemical DNA based sensors[52]. The kinetics of DNA hybridization, protein, and small-molecule binding to a DNA/aptamer on the surface of the electrode depends on probe density[118]. Lower probe density can result in weaker signal due to lack of capture probes, and more significant probe density can result in steric hindrance[46].

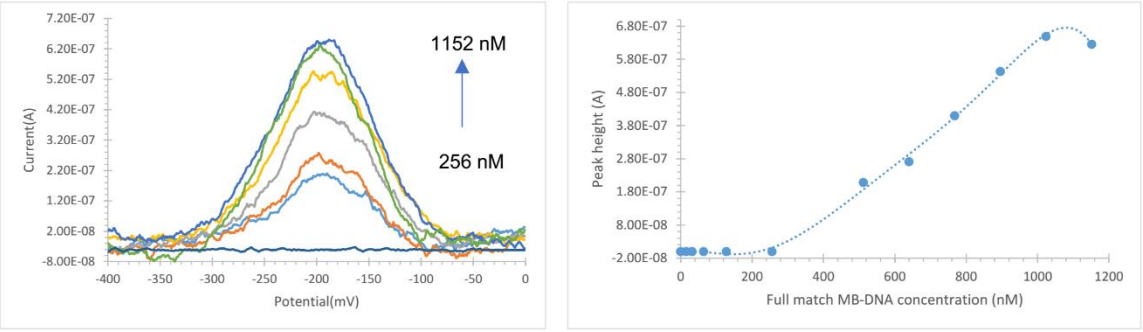

[A] [B]

Figure 2.15 [A] SWV output (baseline corrected) of different concentration of full match MB-DNA. [B] Calibration curve of different concentration of full match MB-DNA.

Plaxco, et al. compared their cocaine and thrombin aptamer sensors and the effect of the changing thiolated-DNA concentration, which resulted in differences in capture probe packing density. Besides, they conducted a kinetic study in both these cases, concluded that lower packing density is optimal for cocaine, while for thrombin, the intermediate density is preferred[52]. Thus, it can be found that optimizing probe density is an essential step in improving assay performance. In this experiment we used 1 µM concentration of A-DNA probe immobilization[47]. Optimum probe density helps to give better redox signal, which we observed Figure 2.14 and 2.15; this observation also coordinates with previous report. In figure 2.15 the 1 uM A-DNA SAMs modified GCE incubated in (0 to 1152 nM) MB-DNA (full match) for 30 min. After every 30 minutes check SWV and increasing full match MB-DNA concentration up to 1152 nM. We first observe MB-DNA signal at 512 nM and increasing current is proportional to MB-DNA concentration and 1152 nM MB-DNA concentration gives a saturation point. Though capacitance is higher in GCE, so up to 512 nM we did not observed redox signal of MB-DNA.

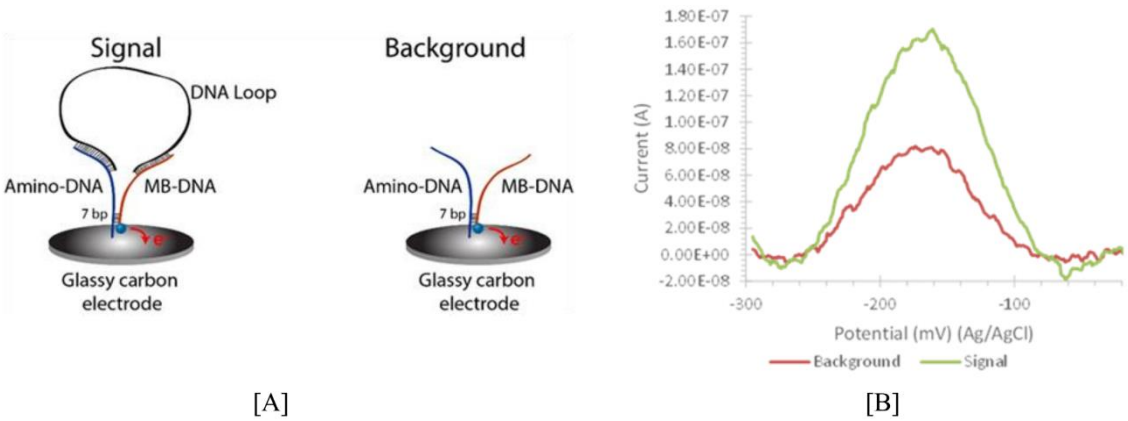

[A] [B]

Figure 2.16[A] Schematic diagram of DNA based model for ECPA. [B] SWV output (baseline corrected) for background (MB-DNA) and Signal (100 nM loop and 100 nM MB-DNA).

Schematic diagram of DNA based model for ECPA. The continuous DNA loop is used to model the Signal complex shown in Figure 2.16 [A]. The background is modeled by simply adding MB-DNA without the loop. [B] SWV output (baseline corrected) for background (MB-DNA) and Signal (100 nM loop and 100 nM MB-DNA).

For modeling signal for loop, the sensor was immersed in 100 nM DNA-loop and 100 nM MB-DNA sequences in 3 mL HEPES/$NaClO_4$ buffer solution. For modeling the background of ECPA, the sensor was immersed in 100 nM MB conjugated DNA in 3 mL HEPES/$NaClO_4$ buffer solution. Both signal and background currents were measured at the 30-min time point. Figure 2.16 [B] shows an apparent enhancement of the signal over background in ECPA based on the proximity effect. Furthermore, in DNA-ECPA model, compared to the background peak current of glassy carbon electrode is 80 nA with G7 (7 bp), but in Au electrode background current was reported at 30 nA with G7 (7 bp)[47]. The signal peak current of of GCE is 170 nA with G7 (7 bp) and in Au electrode signal peak current was reported at 70 nA with G7 (7 bp)[47]. The signal and background current is higher in GCE compare with standerd Au electrode due to GCE has the 16 times higher

surface area than standard Au electrode and DNA loop, MB-DNA concentration is also higher.

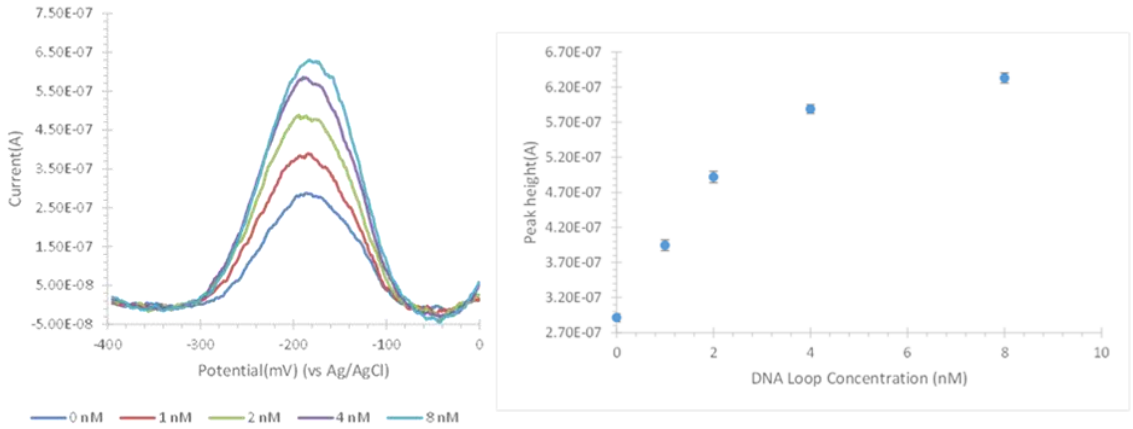

[A] [B]

Figure 2.17 SWV output (baseline corrected) of the different concentration of DNA loop; (B) Calibration curve of different concentration of the DNA loop.

In Figure 2.17 [A] shows the baseline corrected SWV output of DNA loop ECPA. A clear increase in current with DNA loop concentration was observed. Figure 2.17 [B] shows the calibration curve of DNA loop ECPA, in which current (A) peak height is plotted against the concentration of DNA Loop. The current (A) peak height has a non-linear response to the concentration, as expected. This result shows a new transducer like GCE also suitable for additional application of ECPA. The redox signal has dependence on distance between electrode surface and redox molecules. The DNA loop detection dynamic range is small due to the ABA is large molecules deposited on GCE to form A-DNA monolayer, which forbidden MB-DNA come close to the GCE surface. In saturation point of GCE-ECPA at loop concentration 8 nM produced 650 nM peak current, similar peak current also observed in full match DNA for GCE (Figure 2.14).

2.4 Conclusions

We describe the development of the electrochemical proximity assay (ECPA) based on glassy carbon electrode where proximity dependent DNA hybridization to move a redox active molecule near glassy carbon electrode. Optimize the condition to form DNA monolayer by amide bond. The differential potentiostat was used to remove non-Faradaic current by on-board analog subtraction of two working electrodes where one is exposed to target as DNA loop (Faradaic current) and the other is background like MB-DNA (non-Faradaic current). The 80-nucleotide containing DNA loop formation of the ECPA complex, bring MB near the glassy carbon electrode surface and increase redox current with DNA loop concentration. This detection system is flexible, capable of detecting a wide variety of analytes at different concentration range, and protein quantification via the MB electrochemical redox signal, showing great promise in numerous analytical applications.

CHAPTER 3

Electrocatalysis in ECPA Biosensors

3.1 Introduction

The accurate diagnosis of disease is the first step in proper prevention and treatment of human health[85, 119, 120]. For early identity of disease-associated biomarkers is needed accurate and sensitive detection techniques[4, 121, 122]. The clinical analysis includes detecting small molecules like glucose, ATP to the large biomarker, which determine the biological function of the cell. The three-subdivision group of clinically relevant molecules is proteins, nucleic acids, and small molecules, which is made by Kelly. The respiratory insufficiency, diabetes, cardiovascular, metabolic, and neurological disorders, and liver diseases are diagnosed by small molecules, and myocardial infarction, inflammatory diseases, and screening and diagnosis of tumor and cancer are diagnosed by large biomarker like protein [1]. Conventionally detection technique has been accomplished through optical measurements during melting curve analysis of a polymerase-chain-reaction (PCR) amplified oligonucleotide, where single-base mismatches can be resolved[123]. While several other specialized techniques exist, electrochemical measurement is an appealing alternative due to its small instrument size, low cost, and ease of handling[123, 124]. In one standard format for electrochemical oligonucleotide detection, a DNA/RNA capture probe which has a redox moiety like ferrocene or methylene blue (MB) is immobilized onto an electrode surface. Introducing

the target, which has a complementary sequence to the capture DNA, results in a conformational change that affects the distance between the redox moiety and the surface and effectively alters the electron transfer rate to the electrode[125-131]. In these protocols, the percentage change in the signal is proportional to the target concentration. Similarly, there are methods in which the target brings a redox moiety to the surface from a bulk solution[50, 132], which makes the signal proportional to the target concentration.

With the development of biosensing techniques, the DNA based electrochemical sensors become more and more promising towards a point of care applications because they are rapid, low-cost, suitable for miniaturized devices, and ideal for use in chemically complex environments such as blood serum[133, 134]. Types of designs that are deployed include electrochemical DNA (E-DNA), traditional sandwich/super sandwich assays, competition-type assays, electrochemical aptamer-based sensors (E-AB), double antibody sandwich assay, an aptamer-based sandwich assays[98, 135-139]. Generally, DNA based electrochemical sensors are developed by attaching an electro-active reporter to one position of the DNA sequence, which transfers electrons from or to the electrode surface, thus effecting electrochemical signal change at a detector. The principle can be based on analyte-induced conformational changes, target-induced strand displacement mechanisms, or combinations with a sandwich and competitive assays, by forcing redox-labeled DNA into proximity with the electrode surface[98]. Motivated by the point of care applications the first generation of standard electrochemical proximity assay (ECPA) was successfully developed. Even with these developments, there remains a need for improved quantification techniques from the perspectives of cost, sensitivity, and POC detection. Most of the methods address the issue of sensitivity, but due to instrument sophistication

and the need for expert technicians, there is still a need for better technology. Resolving this issue, some point-of-care methods have been developed for selected analytes, those that are highly specialized to a target molecule[100, 101]. For future point-of-care testing, in addition to high sensitivity and do-it-yourself workflows, more flexible methods are needed that can function with a variety of targets of amplify the signal by using the same platform.

The exploit of high sensitivity and selectivity requires to maximize the redox signal and minimize the background. For that to reduce the background and maximally amplify the signal in the presence of the analyte, Gangli Wang and co-workers introduce a chemical reaction mechanism following electron transfer reaction[57], using a reductant tris(2-carboxyethyl) phosphine hydrochloride (TCEP) in the detection solution that will reduce the oxidized MB *in situ* at the detection electrical potential[58].

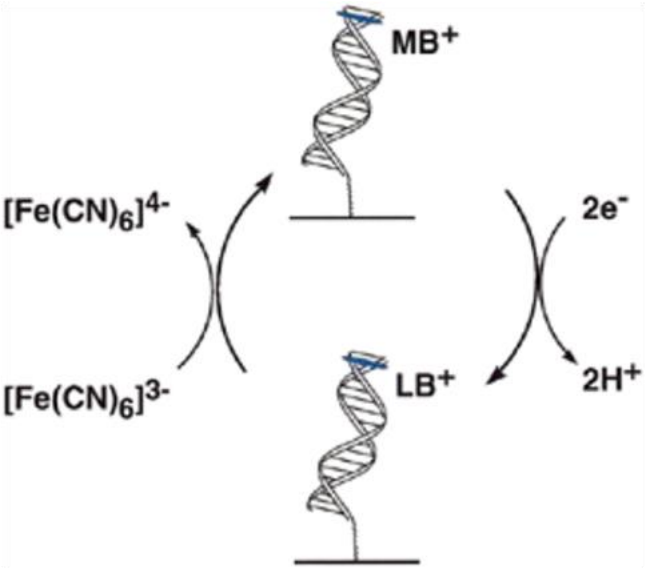

Figure 3.1 Schematic representation of the electrocatalytic reduction of $[Fe(CN)_6]^{3-}$ by MB at a DNA-modified electrode. LB+ is leucomethylene blue, the product of the electrochemical reduction.

Reprinted with permission[63] **Copyright © (1999) Nucleic Acids Research.**

Thorp and co-workers reported the catalytic guanine oxidation with an exogenous inorganic ruthenium complex, $[Ru(bpy)_3]^{2+}$, as an oxidation catalyst. A two-step electrochemical oxidation of $[Ru(bpy)_3]^{2+}$ to Ru(III) species, followed by the chemical oxidation of guanine in a redox reaction to regenerate the $[Ru(bpy)_3]^{2+}$ is suggested[59-62]. Barton et al. reported a new strategy to improve the sensitivity for the electrochemical detection of DNA hybridization by employing an exogenous electrocatalytic species for signal amplification[63]. Before the introduction of catalytic species, under the duplex formation, the original signal from the charge transport was through self-assembled monolayers of oligonucleotides between the intercalated indicator MB and the gold electrode surface. After the introduction of the solution- based mediator, potassium ferricyanide, the resulting voltammetric signal was significantly improved by the catalytic effect through the back-oxidation of MB. With a single base pair mismatch on the hybrids, the signal was dramatically lowered by the prevention of electron transfer through the hybrid.

As a result, MB or other intercalated species, such as the grove binder, could be utilized to amplify the signal with its specific DNA design. On the other hand, the catalytic effect from a solution mediator with a suitable formal potential, such as ferricyanide in the case of MB label, is capable of further enhancing the electrochemical response under our DNA hybridization event. In this way, each MB molecule near the electrode surface, a consequence of recognizing a target molecule, will be cyclically oxidized electrochemically and reduced chemically by the reductant, a process that amplifies the signal[64-66]. Moreover, with a multistep surface modification procedure, the interference signal caused by nonspecific adsorption and surface-bound redox signal probe is reduced

to a negligible level, which has been a well-known technical barrier for sensor development.

3.2 Materials and methods

All solutions are prepared with deionized, ultra-filtered water (Fisher Scientific). All of the following reagents were used as received: *sodium percholorate ($NaClO_4$) and* 4-(2-hydroxyethyl)-1-piperazineethanesulfonic acid (HEPES) (99.5%) from Alfa Aeser, tris-(2-carboxyethyl) phosphine hydrochloride (TCEP), 6-mercapto-1-hexanol (MCH), Potassium ferricyanide (III) and Potassium ferrocyanide (II) (99%), Methylene blue-conjugated DNA (MB-DNA) was purchased from Biosearch Technologies (Novato, CA), purified by RP-HPLC. All other oligonucleotides were obtained from Integrated DNA Technologies (IDT; Coralville, Iowa).

Table 3.1 Single-stranded DNA sequences used in the ECPA model systems. MB-DNA, and G7, were employed in the optimized detection system.

Name	Abbreviation	DNA sequence, list from 5' to 3'
Thiolated -DNA	Th-DNA (G7)	/5ThioMC6-D/ GCA TGG TAT TTT TCG TTC GTT AGG GTT CAA ATC CGC G
Methylene blue-DNA (7 base pair match)	MB-DNA	CCA CCC TCC TCC TTT TCC TAT CTC TCC CTC GTC ACC ATG C /MB-C7/
Methylene blue-DNA (Full match)	MB-DNA (Full match)	CGC GGA TTT GAA CCC TAA CGA ACG AAA AAT GTC ACC ATG C /MB-C7/
Methylene blue-DNA-10	MB-DNA (10 bp)	CCA CCC TCC TCC TTT TCC TAT CTC TCC CTC GTC ACC ATG C/MB-C7/
ECPA-Loop	Loop	TAG GAA AAG GAG GAG GGT GGC CCA CTT AAA CCT CAA TCC ACC CAC TTA AAC CTC AAT CCA CGC GGA TTT GAA CCC TAA CG

Abbreviations: /MB-C7/ = methylene blue modification, /5ThioMC6-D/ = disulfide bond flanked by two six-carbon spacers (IDT).

Preparation of the Au Electrode and DNA Monolayer Assembly ECPA sensors for the model system were fabricated using a gold working electrode (Bioanalytical Systems Inc., r = 0.75 mm). The gold electrode was polished precisely to a mirror surface with an aqueous slurry of 1 µm, 0.3 µm and 0.05 µm diameter alumina particles respectively and then successively washed by D.I water and ultrasonic in 50:50 D.I H_2O and ethanol mixture. Then the electrode was then immersed into fresh piranha solution (H_2SO_4/H_2O_2, 3:1) for 5 minutes, rinsed with D. I. water, and dried under a stream of nitrogen gas. At last, the gold electrode was electrochemically polished by scanning the potential from -0.50 to 1.50 V in 0.1 M H_2SO_4 at a scan rate of 0.1 V s^{-1} for 50 cycles. This cleaned gold electrode was thoroughly washed by D. I. water and ethanol and dried under a stream of nitrogen gas. Before modification of the cleaned Au electrode, 1 µL of 200 µM thiolated-DNA mixed with 3 µL of 10 mM TCEP in one 2 mL PCR tubes. The tube was incubated for 60 min at room temperature (21 °C) for the reduction of disulfide bonds in the thiolated-DNA. The solution was then diluted to make a total volume of 200 µL in HEPES/$NaClO_4$ buffer solution (10 mM HEPES and 0.5 M $NaClO_4$, pH 7.0)[98] to a final concentration of Th-DNA was 300 nM. The pH was 7.0 of the HEPES buffer solutions, which was used in all the experiments. For immobilization, the Prior cleaned gold electrode was transferred directly to the diluted and reduced thiolated-DNA solution and incubated for 1h in the dark at room temperature. Following the formation of a self-assembled monolayer (SAM), the excess thiolated-DNA physically adsorbed on the electrode surface was removed by a room temperature-deionized water rinse (~ 20 s).

Instrumentation All measurements were performed using reference with a bipotentiostat/galvanostat (WaveDriver 20, Pine) with standard three-electrode configuration. It consisted of an Ag/AgCl(s)|NaCl 3M) reference electrode (BASi), a platinum wire counter electrode (CH Instrument, Inc.), and a standard gold working electrode (CH Instrument, Inc.). Electrochemical measurements were carried out in HEPES/$NaClO_4$ buffer using square wave voltammetry (SWV) with a 50-mV amplitude signal at a frequency of 10 Hz, over the range from -450 mV to 0.0 mV versus Ag|AgCl reference electrode.

The characteristic voltammetric peak of the MB molecule was detected by SWV at -210 mV (vs. Ag/AgCl). The MB was chosen as the redox tag because of its excellent shelf life and strong electrochemical response in serum solution compared to other redox tags, such as ferrocene[98, 99]. The electrochemical measurements were performed in HEPES/$NaClO_4$ buffer using cyclic voltammetry (CV) with a frequency of 10 Hz, over the range from 500 mV to -100 mV versus Ag|AgCl reference. The characteristic ferricyanide redox peak was observed in a cyclic voltammogram.

3.3 Results and Disscussion

The DNA probe density on the surface of the electrode plays a crucial role in electrochemical DNA based sensors[52]. The kinetics of DNA hybridization, protein, and small-molecule binding to a DNA/aptamer on the surface of the electrode depends on probe density[118]. Lower probe density can result in weaker signal due to lack of capture probes, and more significant probe density can result in steric hindrance[46]. Plaxco, et al. compared their cocaine and thrombin aptamer sensors and the effect of the changing thiolated-DNA concentration, which resulted in differences in capture probe packing

density. Besides, they conducted a kinetic study in both these cases, concluded that lower packing density is optimal for cocaine, while for thrombin, the intermediate density is preferred[52]. Thus, it can be found that optimizing probe density is an essential step in improving assay performance.

The changes in the characteristics of the surface of AuE by electrochemical oxidation could be monitored using both CV and SWV. Figure 3.2 shows the voltammograms of 5 mM $[Fe(CN)_6]^{4-/3-}$ ion on the bare AuE at 30 nM, 100 nM, 300 nM and 1000 nM concentration of thiolated probe DNA (7 bp). According to the increase of the concentration of thiolated probe DNA (Th-DNA) on AuE surface, the peak-to-peak separation increases, and a substantial decrease in the peak current is also observed. The self-assembly of the Th-DNA on the electrode surface generates a negatively charged interface that repels negatively charged $[Fe(CN)_6]^{4-/3-}$ anions. This repulsion is anticipated to retard the interfacial electron-transfer kinetics of the redox probe at the electrode interface. When complementary DNA hybridized with Th-DNA, the SWV redox current was increased due to the DNA double-strand was aligned more efficiently on AuE surface and make more pinholes spaces, and the redox probe is sufficiently small to penetrate through these pinholes freely[140]. Figure 3.2 C, D shows the SWV for the assay under same conditions. In Figure 3.2 [C] we observed signal response of $K_3[Fe(CN)_6]$ with probe density on 300 nM and 1000 nM almost same peak current; comparatively 300 nM probe shows higher response. Though probe density is crucial parameter, So we was used 300 nM thiolated-DNA solution to make thiolated probe on Au electrode.

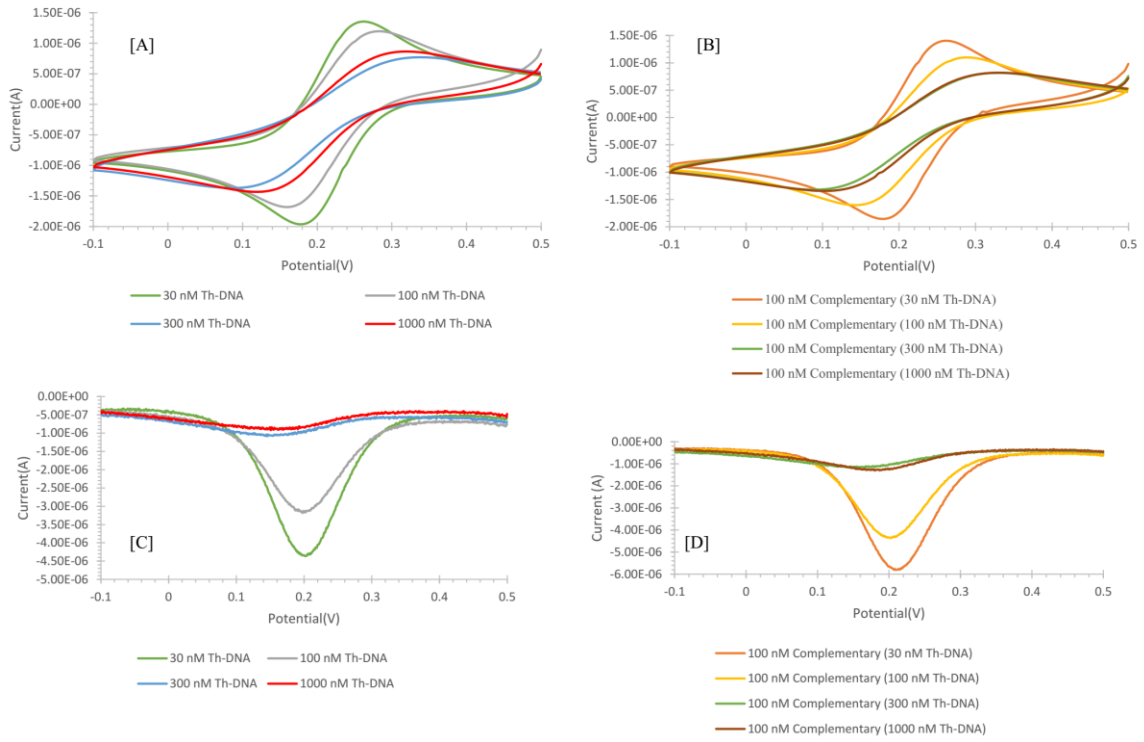

Figure 3.2 CV and SWV of Th-DNA in 5.0 mM $[Fe(CN)_6]^{4-/3-}$ - 10 mM HEPES buffer solution.

Cyclic voltammograms and square wave voltammograms of 5.0 mM $[Fe(CN)_6]^{4-/3-}$ probe in 10 mM HEPES buffer solution of pH 7.0 at scan rate of 10 mV/s for Au/30 nM Th-DNA (7 bp)-modified electrode [A], Au/100 nM Th-DNA (7 bp)-modified electrode [B], Au/300 nM Th-DNA (7 bp)-modified electrode [C], Au/1000 nM Th-DNA (7 bp)-modified electrode [D].

The surface coverage of the Th-DNA modified Au electrode was determined by a protocol previously reported by Steel et al[141]. Briefly, the surface coverage of the SH-TBA on modified Au electrode surface was calculated from the number of cationic redox molecules such as, ruthenium hexamine trichloride electrostatically associated with the anionic SH-TBA backbone. The chronocoulometric signals of the modified AuE were followed in the presence and absence of a cationic redox reporter, ruthenium hexamine

trichloride, that is electrostatically bound to the negatively charged DNA backbone. After the immobilization of probes on the electrode surface, the probe-modified electrode was subjected to ruthenium-hexamine. Then, the amount of ruthenium-hexamine was measured by the integrated current, or charge *Q*, as a function of the square root of time ($t^{1/2}$) in a chronocoulometric experiment is given by the integrated the Cottrell equation.

$$Q = \frac{2nFAD_0^{1/2}C_0^*}{\pi^{1/2}} t^{1/2} + Q_{dl} + nFA\Gamma_0$$

Where, *n* represent the number of electrons per molecule for reduction, *F* is the Faraday constant (C/equiv), *A* is the electrode area (cm^2), D_o is the diffusion coefficient (cm^2/s), C_o* is the bulk concentration (mol/cm^2), Q_{dl} is the capacitive charge (C), and $nFA\Gamma_o$ is the charge from the reduction of Γ_o (mol/cm^2) of adsorbed redox marker. The term Γ_o indicates the surface excess and represents the amount of redox marker (RuHex) confined near the electrode surface. The intercept of chronocoulometric at t=0 is the surface excess terms and the sum of the double-layer charging. The surface excess redox marker is calculated from the difference in chronocoulometric intercepts for the identical potential step experiment in the presence and absence of redox marker. DNA surface density was obtained using the following equation:

$$\Gamma_{DNA} = \Gamma_0 \left(\frac{z}{m}\right) N_A$$

Where Γ_{DNA} is the probe surface density in molecules per cm^2, m is the number of bases in probe DNA, z is the charge of ruthenium-hexamine, and N_A is the Avogadro's number. The

obtained surface density of the probe Th-DNA is equal to (4.0 ± 0.5) *10^{12} molecules per cm^2. According to the literature, the theoretical surface coverage of hybridized DNA with 100% efficiency was roughly 4×10^{12} molecules/cm^2[132].

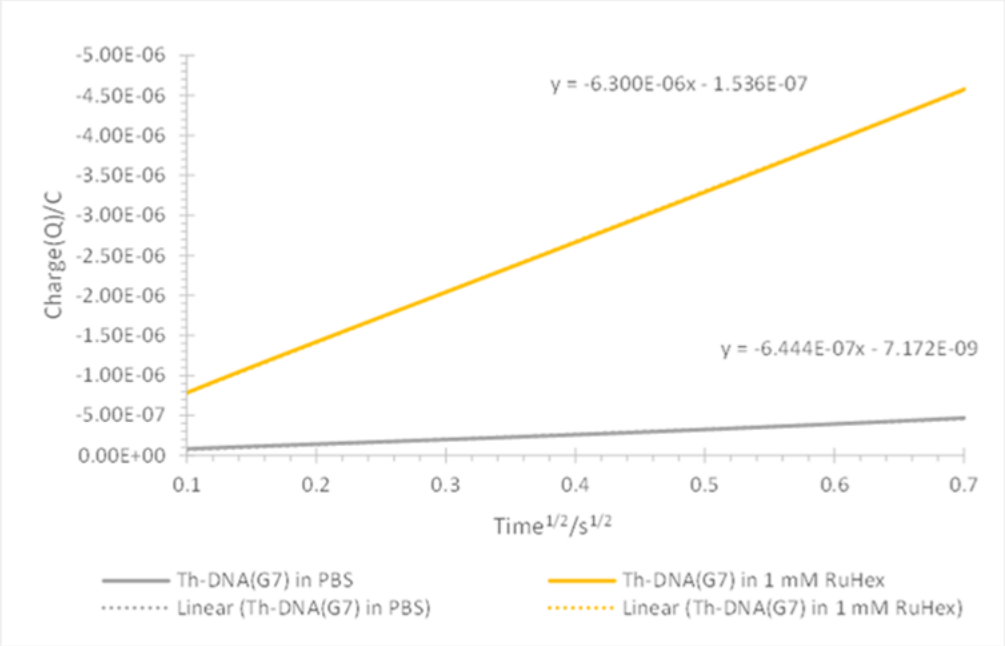

Figure 3.3 Chronocoulometric response curves for SH-TBA/MCH (in PBS; gray) and SH-TBA/MCH (in 50 µM ruthenium-hexamine; yellow) modified electrodes.

Amplify ECPA signal of DNA model by using electrocatalysis Generally, DNA based electrochemical sensors are modified by attaching an electro-active reporter to one position of the DNA sequence which transfers electrons to or from the transducer surface, thus inducing electrochemical redox signal change at the detector. The principle can be based on analyte-induced conformational changes, target-induced strand displacement mechanisms, or combinations with a sandwich and competitive assays, by forcing redox-labeled DNA into proximity with the electrode surface[98]. Motivated by the point of care application's the first generation of standard electrochemical proximity assay (ECPA) was successfully developed[47] [13]. The sensor used the proximity effect[17, 142] to move an

electrochemically active redox label, like methylene blue (MB), closer to a gold electrode upon connecting of two probes to a protein target with high sensitivity and selectivity.

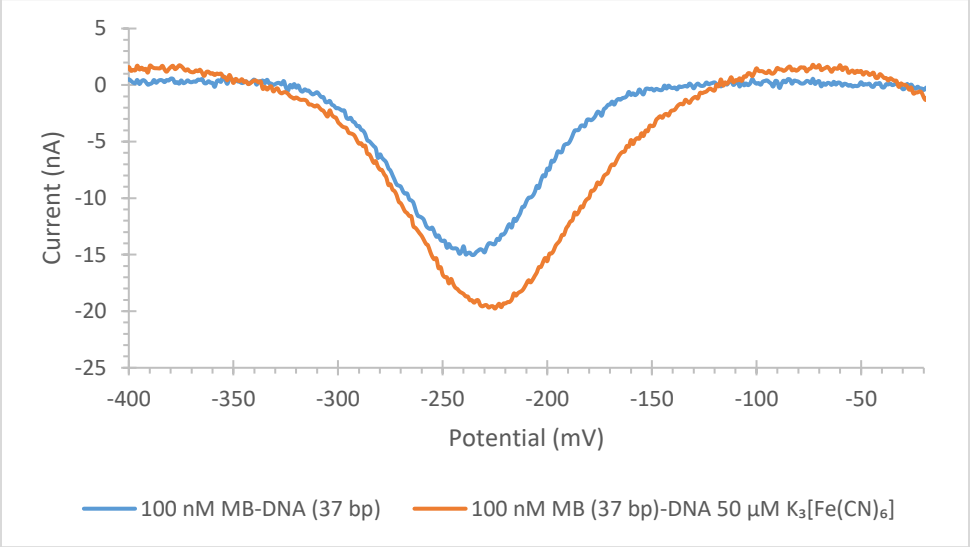

Figure 3.4 SWV output (baseline corrected) without (blue) and with (brown) catalytic molecules.

SWV (scan rate=10 Hz) at a gold electrode modified with 300 nM Th-DNA 100 nM MB-DNA (37 bp) (Blue), and 300 nM Th-DNA 100 nM MB-DNA (37 bp) & 50 µM K_3[Fe $(CN)_6$] (orange).

Table 3.2ECPA signal amplification by K_3[Fe $(CN)_6$]

Name	Peak height	% of signal amplification
100 nM MB-DNA (37 bp)	15	0
100 nM MB-DNA and 50 µM K_3[Fe $(CN)_6$]	20	33

The absolute electrochemical redox signals are limited by the surface concentration of the redox molecules. In order to increase the inherent sensitivity of this assay, we have coupled the direct electron transfer to an electrocatalytic process involving a species freely diffusing in solution. This effectively amplifies the redox molecule like the MB signal of the ECPA

DNA model system. Methylene blue was chosen as the redox molecule catalyst, with potassium ferricyanide as the solution substrate. Specifically, this signal comes at the reduction potential of MB. The chemically oxidized MB is again available for electrochemical reduction, and the catalytic cycle continues as long as the potential of the gold electrode is sufficiently negative to reduce MB. The % of MB reduction of ECPA DNA model signal increasing by $K_3[Fe(CN)_6]$ catalysis.

Optimization of Ferricyanide concentration The efficiency of the catalytic effect investigated using the electrocatalytic assay quantitation was sensitive to the amount of K3[Fe (CN)6]. Increasing the % of MB redox signal depends on the concentration of K3[Fe (CN)6]. Increasing the % of MB redox signal depends on the concentration of K3[Fe (CN)6]. The increasing amount of K3[Fe (CN)6] catalyzes more MB in the DNA hybridization up to 1000 nM K3[Fe (CN)6]. The full match MB-DNA catalyze by 1000 nM $K_3[Fe(CN)_6]$ gives 70 nA redox current. But at 2000 nM $K_3[Fe(CN)_6]$ provides 60 nA redox current due to a higher concentration of $K_3[Fe(CN)_6]$ etching the Au surface and destroy the Th-DNA monolayer. In the presence of $K_3[Fe(CN)_6]$ gold electrode being etched in the presence of CN^-[143].

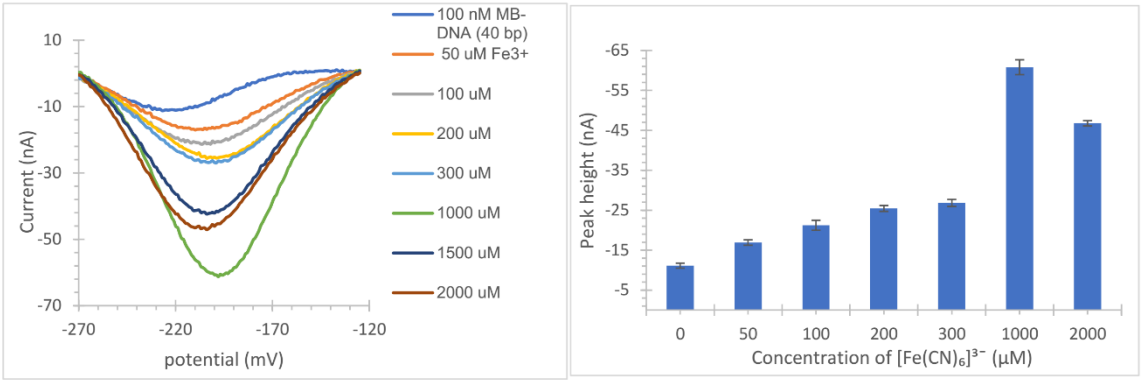

[A] [B]

Figure 3.5 Dependence of catalytic efficiency on different concentrations of $K_3[Fe(CN)_6]$.

Gold electrode being etched in the presence of CN^-[143] which is released from ferricyanide. This may happen via a mechanism in which CN^- is first adsorbed at the Au surface before a gold complex is formed, which will then be released from the surface[110, 143]. Since the gold electrode could be etched from CN^- formed by partial degradation of the redox couple[108, 110, 144, 145]. The optimized experimental condition for limiting the etching effect of the AuE surface, the concentration of $K_3[Fe(CN)_6]$ was chosen at 34 µM for later catalytic measurements.

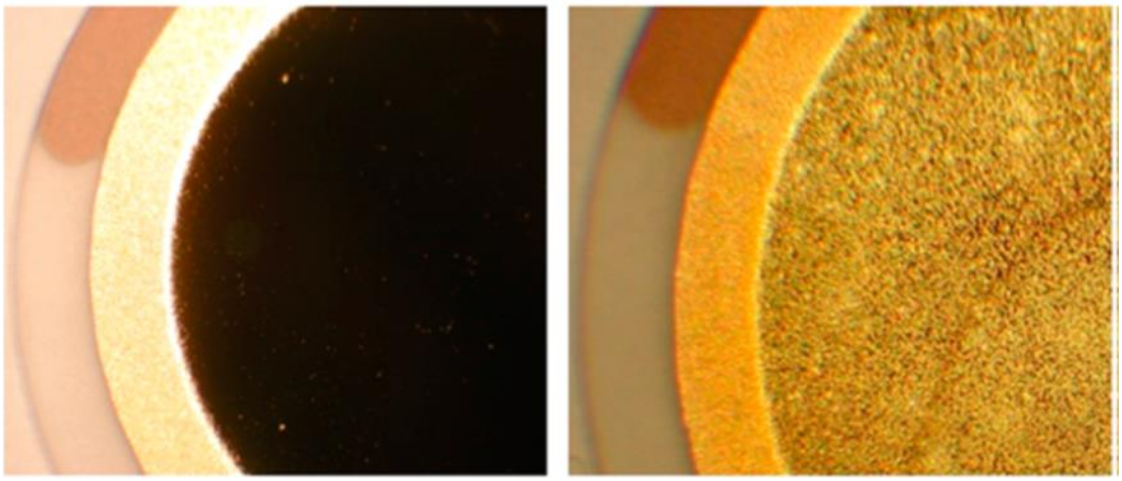

Figure 3.6 A microscopic image of a fresh gold-coated QCM sensor (left) and the QCM-D sensor chip after 26 h of combined EIS/QCM measurement (right) is shown [146].

In the electrochemical detection system, each MB molecule near the electrode surface, a consequence of recognizing a target DNA loop, will be cyclically oxidized at the electrode and reduced by the reductant, thus greatly amplifying the signal during the detection period. In analogy, the surface-bound probes can be considered to function as the Gate (with each MB molecule as a "tunnel") while the reductant in solution and the electrode were the Sources and Drain in the electron tunneling or field-effect transistors,

respectively. Many efforts have been imposed into the development of electrocatalytic strategies for DNA sensors[64-66].

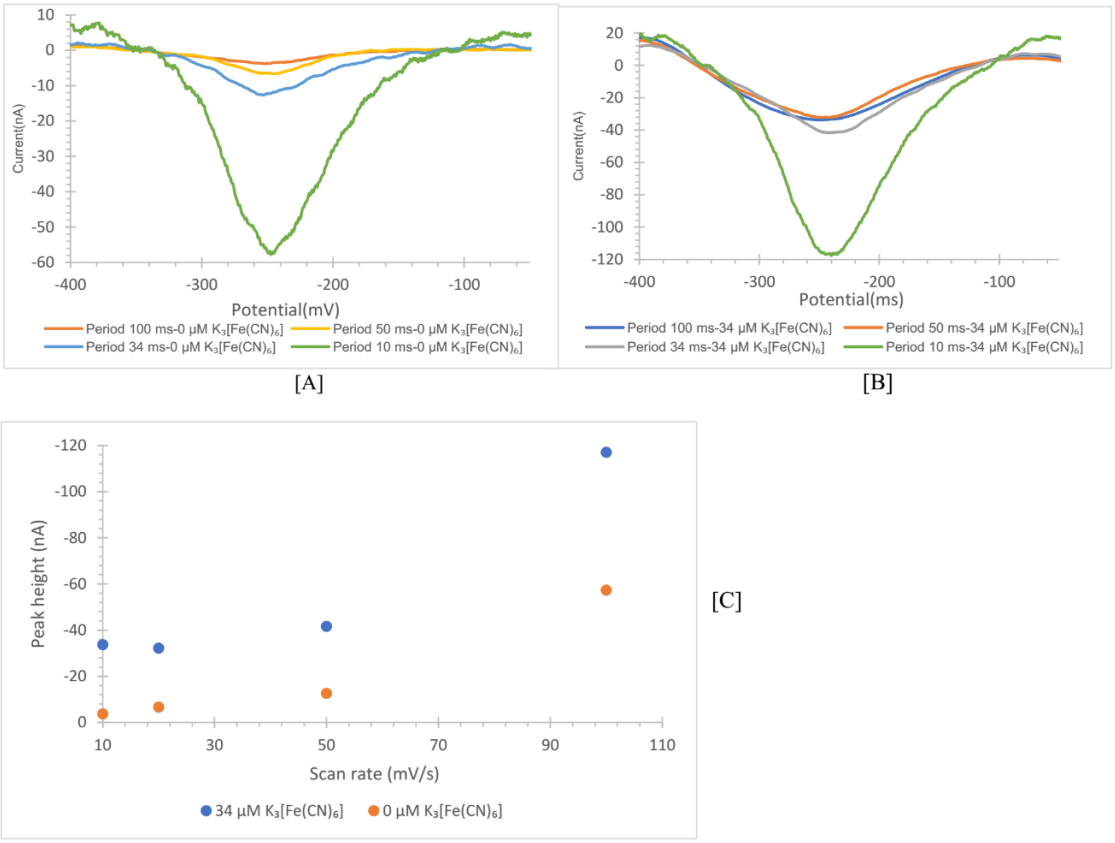

Figure 3.7 SWVs at different periods (scan rates) [A] without $K_3[Fe(CN)_6]$ and [B] with 34 μM $K_3[Fe(CN)_6]$. [C] A quantitative correlation between the peak height in SWV at different scan rates.

Table 3.3 ECPA signal amplification by $K_3[Fe(CN)_6]$ at different scan rate of SWV.

Scan rate (Hz)	0 μM K_3 [Fe $(CN)_6$]	34 μM K_3 [Fe $(CN)_6$]	% of Signal amplification
10	4	34	750
20	7	32	357
50	13	41	215
100	57	117	105

The observed SWV features at different scan rates are characteristic of electrodes. It is essential to define that the current signal is enabled through the surface-bound MB

molecule on the electrode. The baseline adjusted SWVs at varied frequencies further affirm the analysis (Figure 3.7 A & B). Because the capacitive charging current is substantially subtracted in SWVs, the current peak is better determined. At higher frequencies, the % of peak current amplification decreases which is coherent with earlier reports that SWV peak current could decrease at the higher frequency ranges at the DNA sensors[147]. At scan rate 10 Hz MB redox signal amplification by $K_3[Fe(CN)_6]$ was around 750 times, but at 100 Hz MB redox signal amplification was approximately 100 times. The frequency of 10 Hz was used in later SWV measurements and the uncertainty of charging current in different solution conditions as well as possible effects by different kinetic processes in signal production at a higher frequency.

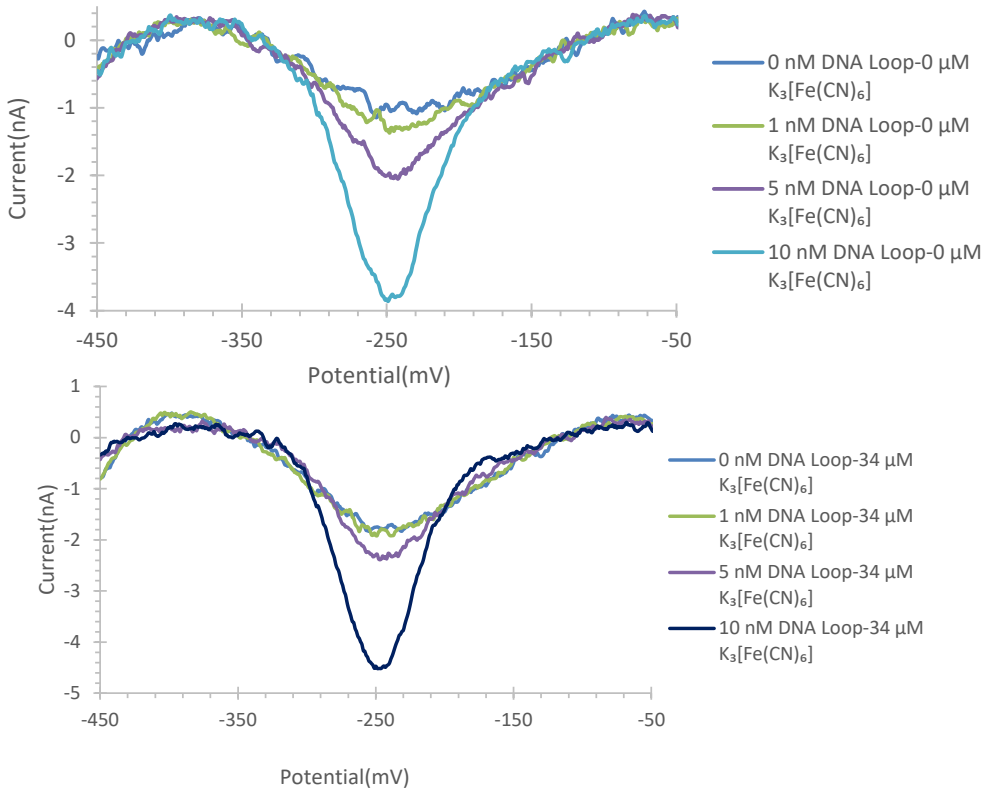

Figure 3.8 SWV characterization for DNA loop-based model for ECPA without [A] 0 µM $K_3[Fe(CN)_6]$ and with [B] 34 µM $K_3[Fe(CN)_6]$ catalytic effect for signal amplification.

However, it is known that the signal generation by SWV is highly dependent on the measurement parameters, such as the frequency, due to its sensitive nature to electrode reaction rates[147]. DNA based ECPA model, an 80-nucleotide DNA loop, mimics the formation of the ECPA complex, moving MB-conjugated oligonucleotide close to the gold surface. Thus, electrical current is increased in proportional to the loop concentration. In the ECPA using a standard gold electrode, the concentration of MB-DNA (10 bp) was controlled at 15 nM in an aliquot with a volume of 200 µL. Figure 3.9 (Blue) shows the calibration curve for ECPA DNA loop model at different loop concentrations. As catalytic, reagent $K_3[Fe(CN)_6]$ was used for the same condition in ECPA DNA model. Figure 3.9 (Brown) shows the calibration curve for ECPA DNA loop model at different loop concentrations with amplifying redox signal by the catalytic effect. This result indicates an additional application of ECPA.

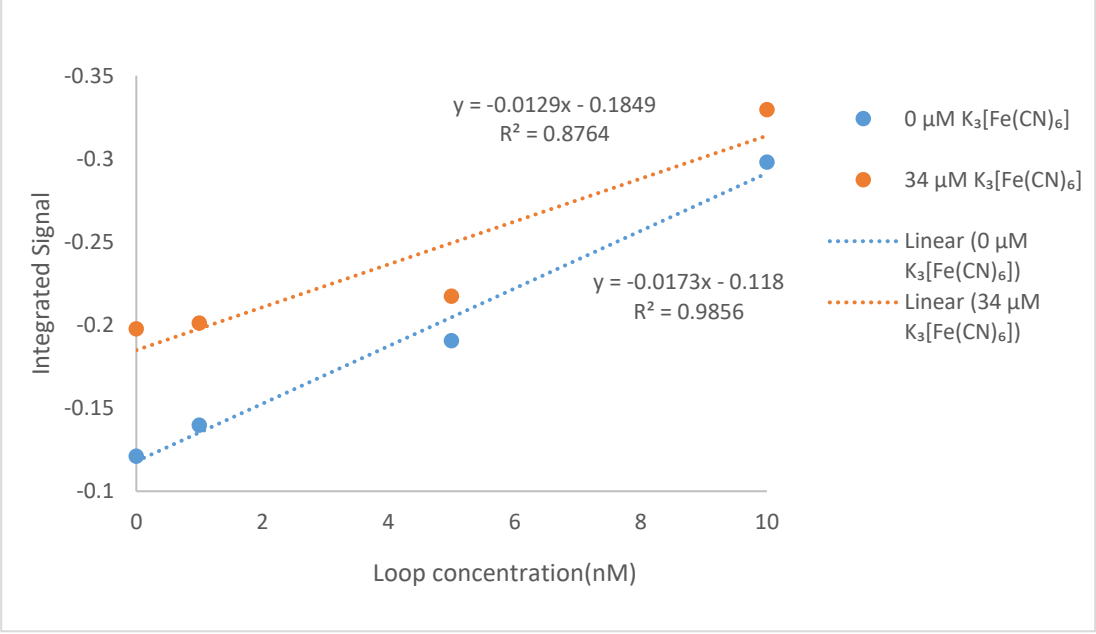

Figure 3.9 A quantitative correlation between the integrated signal in SWV and different concentrations of DNA Loop for ECPA DNA model without (Blue) and with (Brown) of $K_3[Fe(CN)_6]$.

The catalysis of the redox molecule depends on its position; in ECPA model, MB molecule is present in ECPA complex, it is located at underneath of the ECPA-DNA complex structure and close to Au surface. So, the accessibility of $K_3[Fe(CN)_6]$ was hindered by complex DNA structure. Barton et al. reported to improve the sensitivity for the electrochemical detection of DNA hybridization by employing an exogenous electrocatalytic species for signal amplification [34]. The DNA loop detection dynamic range is small due to ECPA complex structure forbidden to penetrate of catalytic molecule $K_3[Fe(CN)_6]$ to MB redox molecule.

3.4 Conclusions

Electrochemical signal amplification is employed in the development of the DNA loop based ECPA sensors. We used a common reductant $K_3[Fe(CN)_6]$ and as target DNA loop in the model ECPA system to demonstrate the sensor efficiency evaluated by pulsed SWV techniques. Benefitting from the multistep surface modification method, background current was minimized to the baseline level. Easily accessible catalytic molecules to redox molecules like MB by the redesign of ECPA model will help to amplify the redox signal more significantly. The significant advantages such as significant sensitivity, and low cost, make it an up-and-coming sensing platform of various redox-active species and biomolecules such as DNA and proteins.

CHAPTER 4

Signal Amplification using Electroactive Nanocomposites: Reduced graphene oxide-Tris(bipyridine)ruthenium (II) chloride composite for Ultra-sensitive electrochemiluminescence aptasensing of thrombin

4.1 Introduction

The early Electrochemiluminescence (ECL) is an electrochemical process in which electro-active molecules undergo electron-transfer reactions at electrode surfaces to form excited states that emit light. (Figure 4.1). Therefore, the emitted light is detected upon ECL reaction at the initiation of an essential voltage. Highly sensitive photon identification is possible because of several existing high-performance detectors and current improvement to more sensitive and tiny sensor devices. The integration of ECL reactions with highly sensitive detectors to make this technique as highly sensitive analytical methods and tools[68-70].

Although fluorescence remains the predominant light-emission based detection method, ECL offers excellent benefits over fluorescence, resulting from the mechanism by which the excited photon is produced. In ECL mechanism, no need for the external light source, but in fluorescence need an external light source. ECL reach higher signal-to-noise ratios and reduce limits of detection due to background-free detection. The ECL reaction generates a signal by the certain applied voltage at the electrode surface, and this is a remarkably localized and time-triggered detection method.

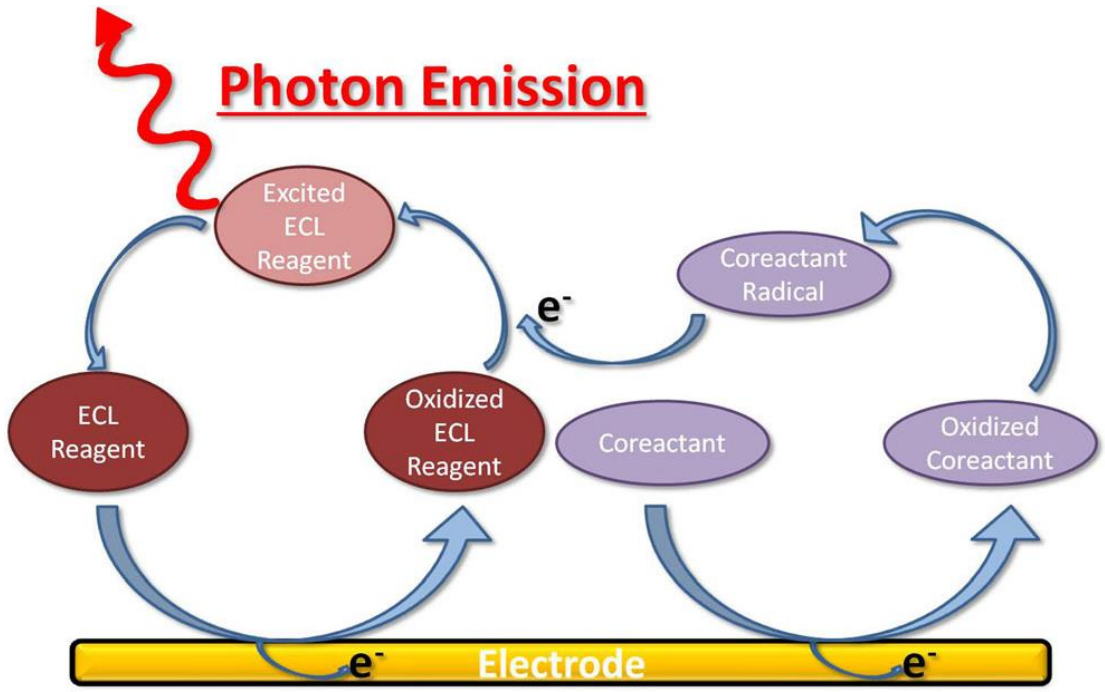

Figure 4.1 Schematic illustration of ECL mechanism

Reprinted with permission[148] **Copyright © (2015) Analytical and Bioanalytical Chemistry.**

A co-reactant can participate in and promote the electron transfer processes into the ECL reagent's excited state and allow for a constant applied voltage. ECL generation on the electrode surface in the presence of suitable luminophore and co-reactant. An ECL reagent (e.g., luminol, $Ru(bpy)_3^{2+}$, QD) is being oxidized at an electrode surface. The oxidized species (like $Ru(bpy)_3^{2+}$, QD, luminol) can undergo transfer into an exited, photon emitting state. When tracing the history of electrochemiluminescence (ECL), there was no co-reagent involved early studies (Figure 4.2). In a conventional three-electrode system, the ECL is observed on the working electrode by the annihilation between cation and anion. The annihilation generates an excited state of the emission species, and then the emission is produced from the radiative decay of it. At the earliest stage, the cation radicals and anion radicals were generated by cyclic electrochemical steps.

Transient Potential Step ECL Experiment

$$A + e^- \rightarrow A^{-\bullet} \quad \text{(reduction at electrode)} \quad (1)$$

$$D - e^- \rightarrow D^{+\bullet} \quad \text{(oxidation at electrode)} \quad (2)$$

$$A^{-\bullet} + D^{+\bullet} \rightarrow {}^1A^* + D \quad \text{(excited state formation)} \quad (3)$$

$${}^1A^* \rightarrow A + h\nu \quad \text{(light emission)} \quad (4)$$

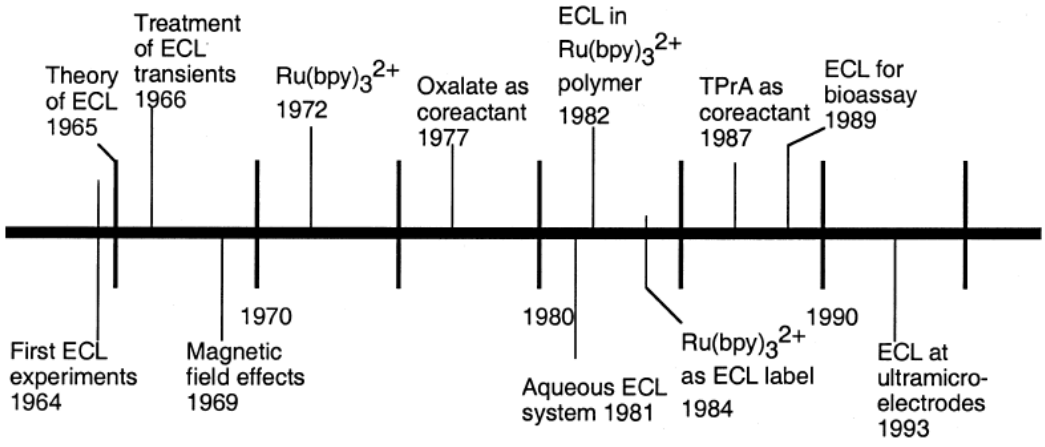

Figure 4.2 Timeline of ECL experiment.

Reprinted with permission[40]. **Copyright © (2004) CRC PRESS LLC.**

The ECL biosensors based on $Ru(bpy)_3^{2+}$/TPrA system have been mostly studied due to their excellent stability and high luminescence efficiency. Notably, the ECL biosensors based on the enhancement of $Ru(bpy)_3^{2+}$/TPrA ECL system have been extensively investigated with improved performance. ECL of $Ru(bpy)_3^{2+}$ can be emitted through an annihilation procedure, requiring only $Ru(bpy)_3^{2+}$ in an electrolyte solution, and is addressed in more detail in several publications[71-73]. Most frequent, however, a co-reactant, such as tripropylamine (TPrA), is present during the ECL process, promoting the generation of the light-emitting excited photon state of $Ru(bpy)_3^{2+}$ and allowing for a continuously applied voltage.

One significant advantage of $Ru(bpy)_3^{2+}$ and the reactant of ECL is that it can take place in aqueous solution, making it functional for a large variety of medical and biological applications and diagnostics. The ECL's main characteristics and advantages are its benefit for biological assays; its high specificity and sensitivity; and its least hardware requirements (i.e., voltage source, electrodes, and light sensor, all of which can be miniaturized). All the combinations make ECL an ideal analytical detection method. The ECL detection method provides advantages like high sensitivity and high signal to noise ratio for no-background. The primary approach to improve the analysis sensitivity is to reduce the noise and enhance the signal. Signal amplification techniques focus on constructing a functionalized interface and designing novel trace tags. The integration of two or more signal amplification strategies has also been developed to achieve higher sensitivity and lower detection limits of biomolecules[149, 150].

The ECL is a low background signal technique; to increase sensitivity, the best approach is to enhance the number of emitted photons at the ECL system throughout the assay taking place. The number of molecules existing in an excited state at any given time is impacted by numerous factors, such as the presence of molecules promoting the shift of the ECL molecule into the excited state, the quantity of ECL molecules in the solution, diffusion effects on electrodes, including quenching. Particularly the first two factors can enhance the ECL signal substantially. The first can be proficient by employing new ECL reagents with modifications of the chemical environment or larger quantum yields, or the electrodes promoting the ECL reagent oxidation. The second appearance, increasing the quantity of ECL molecules in solution, can be accomplished by an accumulation of ECL reagents via another molecule conduct multiple binding sites. Both approaches have shown

excellent capability across the literature to enhance the sensitivity of ECL detection. Throughout literature, the most commonly used ECL reagents are luminol and $Ru(bpy)_3^{2+}$, though other alternatives are known, and more comprehensive lists can be found, like in reviews by Miao[71] and Richter[72]. In the past few years, nanomaterials such as quantum dots (QDs), carbon-based nanomaterials, metal nanoparticles and composite materials have also been studied as ECL reagents[151].

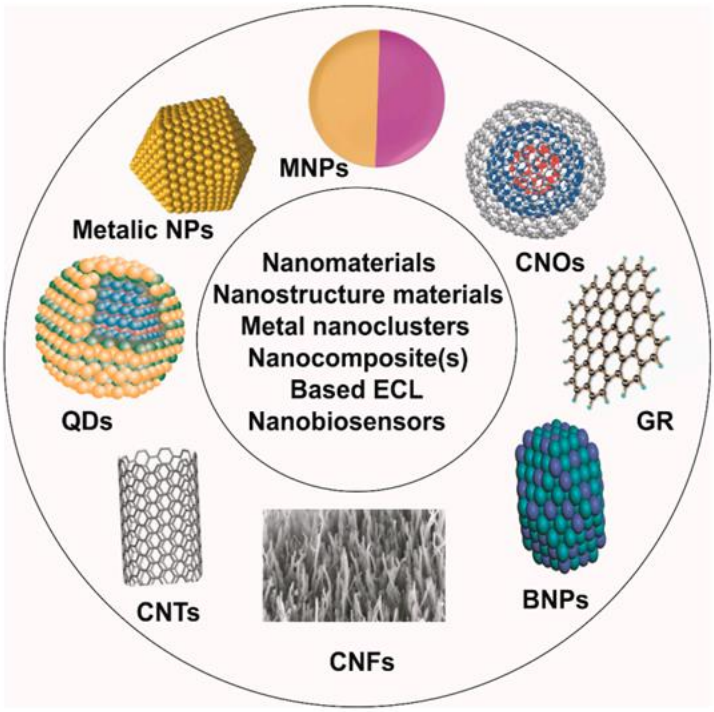

Figure 4.3 Illustration of various nanostructure materials or nanomaterials or metal nanocluster or nanocomposite being used for the fabrication of ECL nano biosensors. Reprinted with permission[67]. **Copyright © (2018) Sensors.**

The use of nanomaterial as amplifiers has attracted special interest in ECL biosensor designing such as Magnetic nanoparticles, Carbon nano-onions, Graphene, Bimetallic nanoparticles, Carbon nanofiber, Carbon nanotubes, Quantum dots, Nanoparticles, and nanocomposites, etc. NMs can enhance biosensor sensitivity by either

improving the conductivity of the sensor platform or providing increased surface area for recognition elements due to their unique physical and chemical properties[152]. The use of nanomaterials in designing sensors is the most direct and simple strategy for signal amplification, because of their remarkable biocompatibility, conductivity, and the high loading of signal molecules for synergistic amplification of the target response[13, 47, 153, 154].

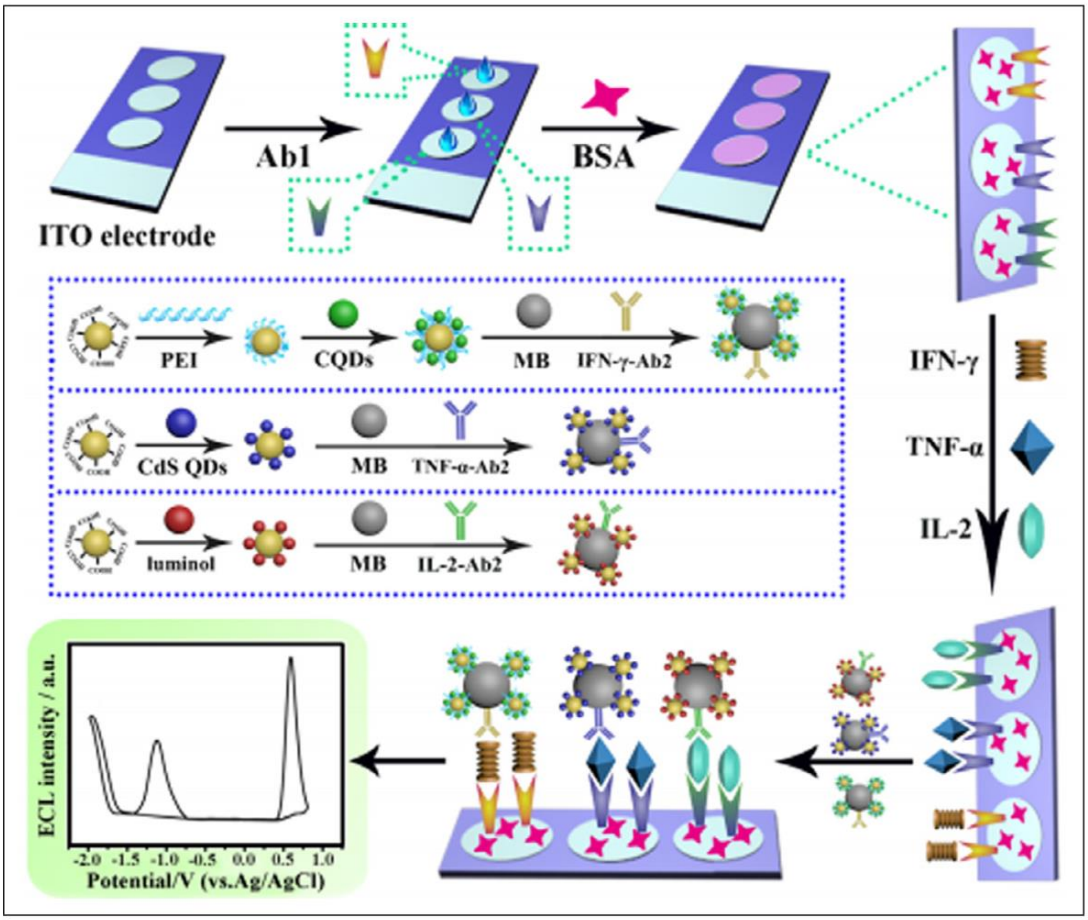

Figure 4.4 Schematic illustration of the multiplexed ECL immunosensor for simultaneous detection of IFN-γ. TFN-a and IL-2

Reprinted with permission[155]. **Copyright © (2017) ACS Applied Materials & Interfaces.**

One effective strategy is based on the functionalized nanomaterials as carriers with unique electronic, optical, and catalytic features[155-160]. For ECL signal enhance to prepare multifunctional luminal AuNPs@Mo_2C nanocomposite, where ECL probe nanocarriers are Mo_2C[156]. The ECL results indicated that luminol-AuNPs in the hybrid exhibited enhanced ECL performance as compared to individual luminol-AuNPs because of the facilitated electron transfer process in the nanocomposite. To develop a novel $Ru(bpy)_3^{2+}$-based ECL immunosensor utilizing palladium nanoparticle-functionalized graphene-aerogel supported Fe_3O_4 for the analysis of prostate-specific antigen in real-sample[157]. The development of multiplexed immunoassays for simultaneous identifying more markers has become an urgent need for the advantages of an improved sample, shortened assay time, and enhanced analysis accuracy, and the essential question for the successful fabrication of the multiplexed ECL immunosensor is the preparation of ECL probes with different potential signals. Furthermore, to develop a novel ECL immunosensor for the simultaneous determination of three biomolecules by nanomaterials. In this work, luminol, carbon quantum dots, and CdS quantum dots were integrated onto AuNPs and magnetic beads to fabricate potential-resolved ECL nanoprobes with signal amplification[155].

Additionally, using dendrimers for surface modification facilitated an ECL reaction. The glassy carbon electrode was modified with a poly(amidoamine) dendrimer with titanate nanotubes shows enhance ECL intensity for luminol compare with unmodified glassy carbon electrode[161]. The using dendrimers on ITO electrode also facilitated ECL signal. The regular combination of $Ru(bpy)_3^{2+}$ with TPrA co-reactent usually shows a low ECL efficiency on ITO electrode due to their slow electron transfer

process[162]. But when ITO electrode surface modified with amine- terminated dendrimers coating Au and Pt nanoparticles, the ECL intensity increase 213-fold compare to the bare ITO electrode.

Graphene (G), an allotrope of carbon in the form of a densely packed honeycomb two-dimensional lattice, has generated tremendous interest since its discovery in 2004[163]. Graphene compounds are used in a wide variety of applications in the fields of photoelectric devices, fuel cells, sensors, and biosensors owing to their unique properties, such as high mechanical strength, excellent biocompatibility, high surface area, fast electron transfer rate, and potentially low manufacturing cost[164]. Recently, the use of reduced graphene oxide (RGO) in the construction of biosensors has been extensively studied[165]. Peng et al. indicated that nanocomposite RGO enhanced electrochemiluminescence of peroxydisulfate and provided a novel sensing strategy for biomolecules[166]. Zhou et al. fabricated graphene-Fe_3O_4 composite-modified indium tin oxide (ITO) electrodes to construct H_2O_2 biosensors[167]. These results indicate that RGO shows great potential as an amplification material in the fabrication of ECL biosensors.

To date, ECL biosensing based on signal amplification strategies has been widely developed. The goal is a practical application rather than research. In short, while there is still a long way to go, we expect that signal amplification based ECL biosensors will eventually become a real-world tool that could meet challenges that would otherwise be impossible with currently available technologies.

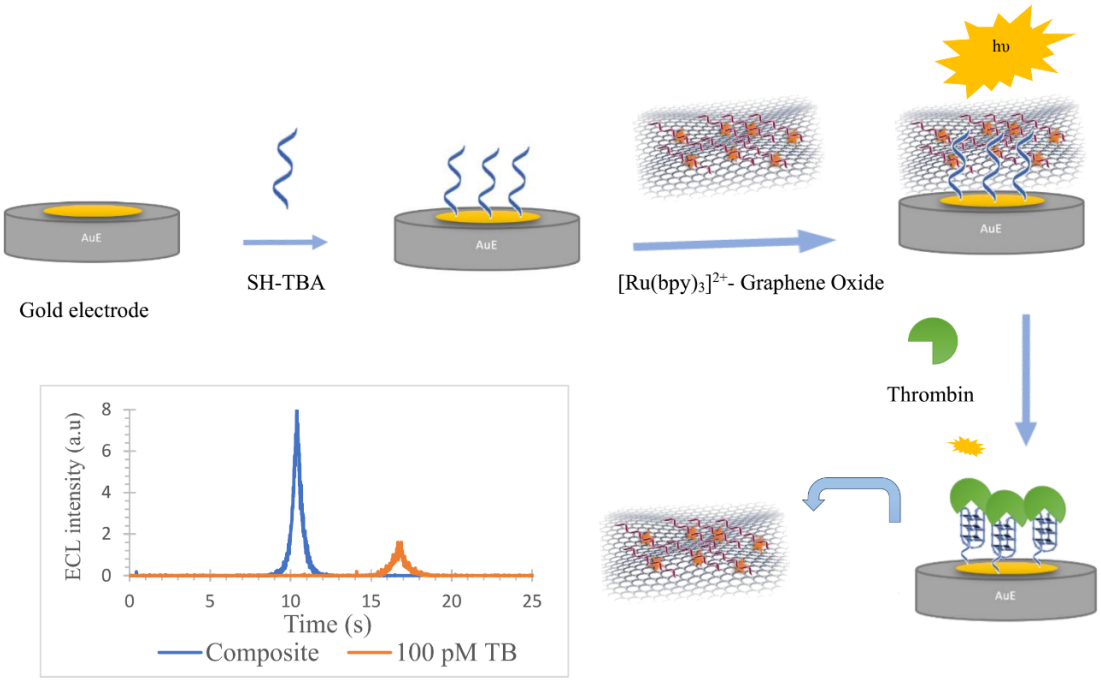

Figure 4.5 Schematic representation of aptasensors for Thrombin detection based on $[Ru(bpy)_3]^{2+}$-anchored GO amplification.

Herein, one simple probe-label-free electrochemical signal enhancement protocols was designed for specific and sensitive detection of thrombin (TB). A thiolated modified thrombin binding aptamer (TBA) was self-assembled on a gold electrode by gold–sulfur affinity. Then based on the strong electrostatic interactions between GO and $Ru(bpy)_3^{2+}$ fabricating GO-Ru composite, where abundant $Ru(bpy)_3^{2+}$ molecules were adsorbed and anchored by GO first. Then the pre-bound ssDNA of the aptamer electrode incubates in GO-$Ru(bpy)_3^{2+}$ composite solution and leading to a strong ECL signal in the absence of target. When TB is present, the formation of an aptamer–TB G-quadruplex structure prohibits π-π stacking interactions between TBA and GO, and consequently draws GO together with plenty of $Ru(bpy)_3^{2+}$ far away from the electrode, resulting in a sharply decreased ECL signal of $Ru(bpy)_3^{2+}$.Target is detected by monitoring the change of the ECL signal before and after analyte binding.

4.2 Materials and methods

Tris(2,2′-bipyridyl) dichlororuthenium (II) hexahydrate ($Ru(bpy)_3Cl_2 \cdot 6H_2O$) (99.95%, Sigma-Aldrich), Graphite powder (MCB), 6-Mercaptan hexanol (Sigma-Aldrich), Potassium persulfate (*(*$K_2S_2O_8$) (Sigma-Aldrich), Phosphorus pentoxide (P_2O_5) (Sigma-Aldrich), Sulfuric acid (*(*H_2SO_4) (Fisher Scientific), Potassium phosphate monobasic (KH_2PO_4), Dipotassium hydrogen phosphate (K_2HPO_4) (Fisher Scientific), Potassium chloride (VWR), Potassium ferricyanide (III) and Potassium ferrocyanide (II) (99%) (Sigma-Aldrich), Bovine serum albumin (BSA, 98%; EMD Chemicals Inc.) Tris(2-carboxyethyl) phosphine hydrochloride (TCEP) (Sigma-Aldrich, St. Louis, MO), and Insulin (Sigma-Aldrich) and Human thrombin, (EMD Millipore Corp.).

All solutions were prepared using deionized, ultra-filtered water generated from the milli-Q Gradient water purification system (Millipore). Without further purification to use all reagent as received. Thiolated-Thrombin Aptemar-15, Thiolated-Random DNA-15 and DNA loop were obtained from Integrated DNA Technologies (IDT; Coralville, Iowa), with purity and yield confirmed by standard desalting.

Table 4.1 Sequences of DNA strands used in the experiments.

Name	Abbreviation	DNA sequence, list from 5' to 3'
Thiolated-Thrombin Aptemar-15	SH-TBA-15	/5ThioMC6-D/GGTTGGTGTGGTTGG
Thiolated-Random DNA-15	Random SH-DNA-15	/5ThioMC6-D/TGA ATT TTC GTTCGT
DNA Loop	Loop	TAG GAA AAG GAG GAG GGT GGC CCA CTT AAA CCT CAA TCC ACC CAC TTA AAC CTC AAT CCA CGC GGA TTT GAA CCC TAA CG

Abbreviations: /5ThioMC6-D/=disulfide bond flanked by two six-carbon spacers (IDT).

Preparation of GO Graphene oxide (GO) was synthesized by using modified Hummers method by reported procedure[168]. For pretreating, 3 g of pure graphite flakes was added into 12 mL concentrated H_2SO_4 (80 °C), 2.5 g $K_2S_2O_8$, and 2.5 g P_2O_5 for 4.5 h. For remove any residual acid the mixture was filtered and washed with DI water. Pretreated 3g graphite flakes were added into 120 mL cold concentrated H_2SO_4 by using ice bath and stirred vigorously by magnetic stirring bar. Then, 15 g $KMnO_4$ was added slowly under stirring (700 rpm) at 10° C temperature (using ice bath). After 20 min of adding $KMnO_4$ then take out ice bath and followed by increase temperature 80°C for 30 min, then keep staring 300 rpm overnight at room temperature.

Then the solution was diluted to 700 mL by adding D.I. H_2O. Afterwards, 20 mL of 30% H_2O_2 was added into the mixture and changed the mixture color to brilliant yellow. Then that mixture was filtered and washed by 1: 10 HCl aqueous solution (1 L) to remove metal ions followed by a gentle wash to remove the acid. To get small GO centrifuge GO solution at 25k RPM for 30 min, collect the supernatant of GO solution, which was used in ECL experiment. The synthesized GO dried by fridge dryer (Labconco Fridge dryer, Marshall scientific).

Preparation of reduced graphene oxide (rGO)- ruthenium (Ru) composite Synthesized GO was placed in a vial and microwaved (Panasonic microwave oven, 1000 W) for 1-2 s[169]. Then exfoliation was carried out by sonicating a 0.1 mg/mL GO dispersion under ambient conditions for 30 min to prepare stock solutions. To make the 1 mM stock solution of $Ru(bpy)_3^{2+}$ a small (6.5 mg) amount of $Ru(bpy)_3^{2+}$ was dissolved in 10 mL PBS-KCl buffer. Then the stock solution of GO ultrasonicate for 15 min. 70 µg of GO and 1 µM DNA loop were added in 1 mL PBS buffer. After 15 min $Ru(bpy)_3^{2+}$ was

added which final concentration was 1 μM. Degassing this composite for 5 min by N_2 gas. Then the coregent TPrA was added to make the final concentration was 4 mM.

Preparation of thiolate-thrombin aptamer (SH-TBA-15) Biosensor on Au electrode

The gold electrode (2 mm in diameter) is polishing for 3 min with a micro cloth coated by a suspension of 0.05 mm Alumina (Buehler). Then that gold electrode sonicates for 5 min in water/absolute ethanol for removing any remaining polishing agent. For electrochemical cleaning of gold electrode via oxidation and reduction in basic conditions (sweep rate 2000 mV/s; in 0.5 M NaOH) over the potential rang -350 mV to -1350 mV (versus an Ag/AgCl reference electrode saturated with 3 M NaCl). The scan is repeated (typically 500–1,000 scans) until the scans are constant and no further changes in peak height or shape are observed. In acidic conditions (in 0.5 M H_2SO_4) to perform further oxidation and reduction scans over the potential – 350 mV to +1500 mV (segment 30; sweep rate 100 mV/s)[170]. Washed with D.I. water and dried the gold electrode by nitrogen flow. Before to the modification of the gold electrode, 1 μL of 200 μM Thioleted-TBA-15 (SH-TBA-15) was mixed with 3 μL of 10 mM TCEP in one 200-μL PCR tubes. The tube was incubated for 60 min at room temperature (21 °C) for reduction of disulfide bonds in the SH-TBA-15. Then the solution was diluted to a total volume of 200 μL in PBS-KCl buffer (200 μL in 0.1 M PBS buffer-0.1 M KCl, pH 7.4)[98]. to a final concentration of 300 nM. All solutions were made in the experiments to follow were carried out at pH 7.4. The formerly cleaned gold electrode was transferred directly to the diluted and reduced SH-TBA-15 solution for immobilization and incubated for 1 h at room temperature in the dark place. Following the forming of a self-assembled monolayer (SAM), excess SH-TBA-15 physically adsorbed on the electrode surface was removed via a room temperature PBS-KCl buffer rinse (~ 200

uL). Then the electrode was dipped into 100 µL of 1 mM MCH for 1 hour in the dark at room temperature. The MCH solution should be freshly prepared, and since MCH has a foul smell, it is advised to do all these processes in a fume hood. MCH acts as a spacer molecule between covalently bounded SH-TBA-15, which is helpful in reducing the capacitance current in electrochemical measurements. As well as, it also helps to remove non-specific binding between SH-TBA-DNA or proteins and the gold surface, and it contributes toward effective orientation of the SH-TBA-15 on the gold surface. Once this incubation was done, the electrode was rinsed with buffer and transferred to PBS buffer. This SAM electrode was ready to be used and could be stored at 4 ◦C for about a week.

Electrogenerated chemiluminescence detection The ECL measurements were performed at room temperature in a 10 mL homemade quartz cell. A three-electrode system was used with the modified Au electrode (2 mm in diameter) as the working electrode, an Ag/AgCl (sat.) as the reference electrode and a platinum wire as the counter electrode. Cyclic voltammetry mode with continuous potential scanning from 0.0 to 950 mV and scanning rate of 50 mVs^{-1} was applied to achieve ECL signal in 100 mM PBS-100 mM KCl containing 5 uM $Ru(bpy)_3^{2+}$ and 4.0 mM TPrA-rGO and DNA loop (pH 7.4). A high voltage of -800 V was supplied to the photomultiplier for luminescence intensity determination. The ECL and CV curves were recorded simultaneously.

Instrumentation A range of characterization techniques were employed to study GO and GO-$Ru(bpy)_3^{2+}$ composite. Cyclic voltammetry (CV) experiments were performed with a bipotentiostat/galvanostat (WaveDriver 20, Pine) with standard three-electrode configuration. It consisted of a Ag/AgCl(s)|NaCl 3M) reference electrode (BASi), a

platinum wire counter electrode (CH Instrument, Inc.), and a standard gold working electrode (CH Instrument, Inc.).

Electrochemical impedance spectroscopy (EIS) and voltammetric measurements were performed using with a Gamry 1010E potentiostat. Data were collected using a three-electrode setup, where the working electrode was the standard gold electrode (CH Instrument, Inc.), the counter electrode was Pt wire, and the reference was an aqueous Ag/AgCl electrode (saturated NaCl). Electrochemical impedance spectroscopy (EIS) was performed in a solution containing mixture of the $K_3[Fe(CN)_6]$–$K_4[Fe(CN)_6$ (1: 1, 0.5 mM) and KCl (0.1 M). EIS measurements were performed by applying an AC potential with a signal amplitude of 5 mV and a frequency range of 10 kHz to 0.1 Hz at open circuit potential (OCP).

Absorbance (UV−vis−near-IR transmittance and reflectance spectra) was measured using a Cary 5000 spectrophotometer with an integrating sphere accessory. Kubelka−Munk analysis was performed directly with the Cary Win-UV software. Attenuated total reflectance Fourier transform infrared spectroscopy (ATR-IR) was performed using a Nicolet iS-50 spectrometer with a built-in ATR and surface Raman spectra were collected on a Renishaw Raman spectrometer system by using 785 nm output from a wavelength stabilized high power laser diode system (model SDL-8530, SDL Inc.).

Dynamic light scattering and Zeta potential measurements The dynamic light scattering method was used for investigating particle size and particle size distribution of graphene oxide particles in PBS-KCl buffer. The DLS measurements were performed using the Malvern Zetasizer ZS instrument (Nano-ZS, Malvern Instruments, Worcestershire, United Kingdom) equipped with an He–Ne laser operated at $\lambda = 633$

nm[171]. To take advantage of the back-scattering mode by setting detector at 173^{o} angle. To select the Automatic position of the attenuator to achieve the optimum laser intensity based on the sample concentration. The GO-Ru(bpy)$_3^{2+}$ composite size was collected in two modes: intensity PSD, and number PSD. The intensity based particle size distribution was acquired from fitting the recorded data to a single or multi-exponential correlation function, measuring the mean size (z-average diameter), and estimating the width of the distribution (polydispersity index) according to the International Standard ISO13321, Methods for Determination of Particle Size Distribution.

Zeta potential of the different step of composite solutions was also measured by the Malvern Zetasizer ZS instrument. The incident laser beam passed through the center of the cuvette and illuminated the particles inside the sample. The scattered light was detected at an angle of 13° by the detector. When the electrical field was applied to the cell, any moving particles inside the sample caused a fluctuation of the light detected proportional to the particle speed. The zeta potential (ζ) was calculated from electrophoretic mobility (EM) of particles using the Henry equation by considering the Smoluchowski approximation (Malvern, 2005). Typically, three replicates of each sample were taken, and an average value reported.

TEM image of GO In TEM the morphology of GO, consisting of thin stacked flakes of shapes and having well defined multilayered structure at the edge, can be clearly seen in TEM image. TEM characterization of graphene Oxide (GO) was carried out using by Zeiss EM10 Transmission EM.

Fluorescence Microscopy Fluorescence images were captured by a Nikon A1+/MP confocal scanning laser microscope (Nikon Instruments, Inc., Melville, NY) with 10x

objectives. Laser beam at 561 nm was used to excite red-emitting GO-$Ru(bpy)_3^{2+}$ composites assemblies formed on semi-transparent gold-coated glass slides, and the corresponding emission signals were filtered at 595±25 nm.

Atomic Force Microscopy (AFM) AFM characterization of graphene Oxide (GO) was carried out using a Bruker MultiMode 8 atomic force microscope (Bruker, USA) in air and at room temperature. The silicon nitride probes (Model: ScanAsyst AIR, Bruker) was used in these measurements have a 0.4 N/m force constant, a resonant frequency of 70 kHz, and a 2 nm nominal tip radius and are operated in Scanasyst Air mode with a 1 Hz scan rate and a resolution of 512 × 512 pixels. The substrates were used are semitransparent gold-coated microscope slides, on which SH-TBA-15 SAMs were first formed as described above. Followed by that biosensor challenge by 1 nM Thrombin. Thus, untreated and treated SAMs were thoroughly rinsed with PBS-KCl buffer and then dried under N_2 flow before AFM scanning. All the AFM images presented in this work are original with no graphical touchup.

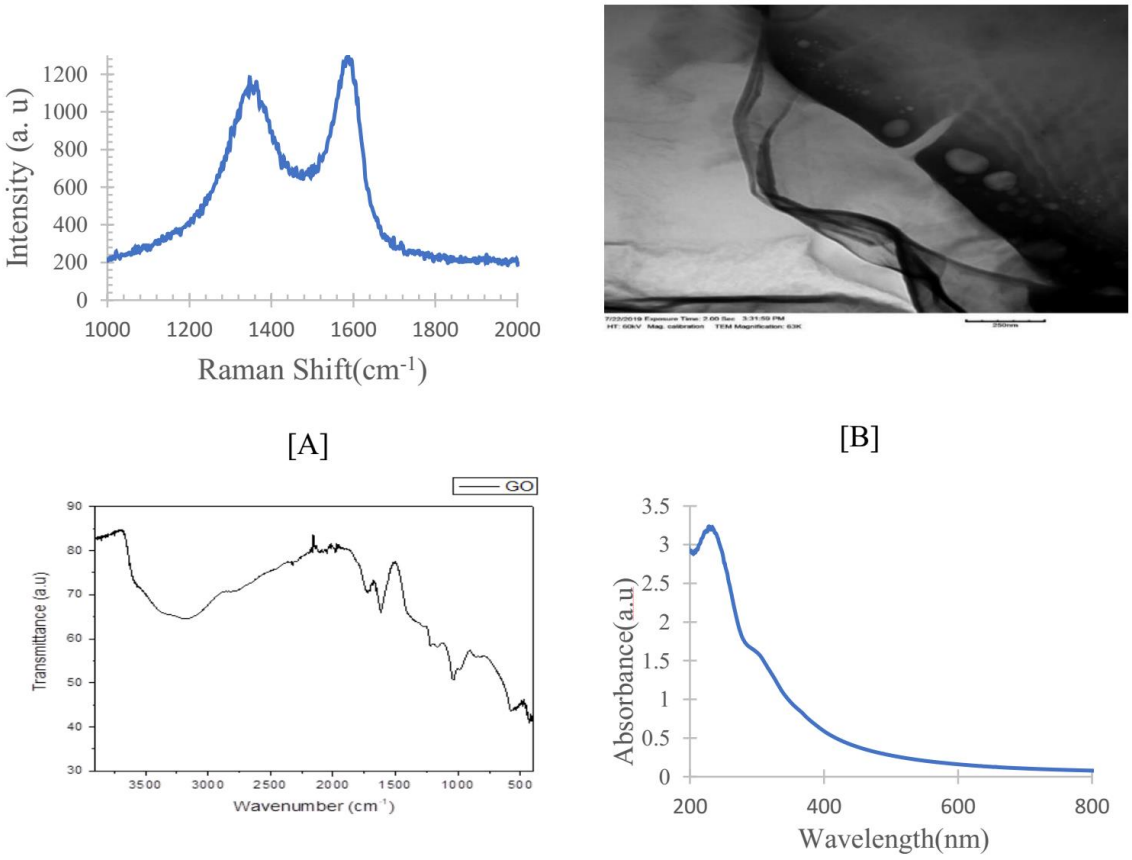

Figure 4.6 Raman spectrum of GO [A]; TEM image of GO [B]; FT-IR spectrum of the as-prepared GO [C] and UV-vis of GO [D]

Characterization of Graphene Oxide The Raman spectrum of GO displays two prominent peaks at 1600 and 1360 cm^{-1}, which correspond to the well-documented G and D bands correspond to sp^2 and sp^3 carbon stretching modes in figure 4.5 [A]. Figure 4.5 [B] shows the TEM images indicating intensity of electrons attenuated by GO platelets of different thickness show a sheet like morphology with different transparencies of the investigated area of about 1.0 × 1.0 µm (scale bar: 250 nm). Dark areas indicate the thick stacking nanostructure of several graphene oxide and/or graphene layers with some amount of oxygen functional groups. The higher transparency areas indicate much thinner films of a few layers graphene oxide resulting from stacking nanostructure exfoliation. Figure 4.5 [C]

shows the FT-IR spectra of graphene oxide. The presence of various types of oxygen functionalities in graphene oxide were confirmed at 3400 cm^{-1} (O–H stretching vibrations), 1720 cm^{-1} (stretching vibrations from C=O), 1600 cm^{-1} (skeletal vibrations from unoxidized graphitic domains), 1220 cm^{-1} (C–OH stretching vibrations), and 1060 cm^{-1} (C–O stretching vibrations). Figure 4.5 D shows the UV-Vis spectrum of yellow-brown GO shows a distinct absorption peak at 230 nm due to the π-π * transition of C=C bonds, which is attributed to the characteristic absorption of GO. The all four features are consistent with a previous report.

4.3 Results and discussion

We designed one simple probe-label-free electrochemical signal enhancement protocols for specific and sensitive detection of thrombin (TB). By gold-sulfur affinity a thiolated modified thrombin binding aptamer (TBA) was self-assembled on a gold electrode. Then based on the strong electrostatic interactions between GO and $Ru(bpy)_3^{2+}$ fabricating GO-Ru composite, where abundant $Ru(bpy)_3^{2+}$ molecules were adsorbed and anchored by GO first. Then the pre-bound ssDNA of the aptamer electrode incubates in GO-$Ru(bpy)_3^{2+}$ composite solution and leading to a strong ECL signal in the absence of target. When TB is present, the formation of an aptamer–TB G-quadruplex structure prohibits π-π stacking interactions between TBA and GO, and consequently draws GO together with plenty of $Ru(bpy)_3^{2+}$ far away from the electrode, resulting in a sharply decreased ECL signal of $Ru(bpy)_3^{2+}$. By monitoring the change of the ECL signal before and after analyte binding the target was detected.

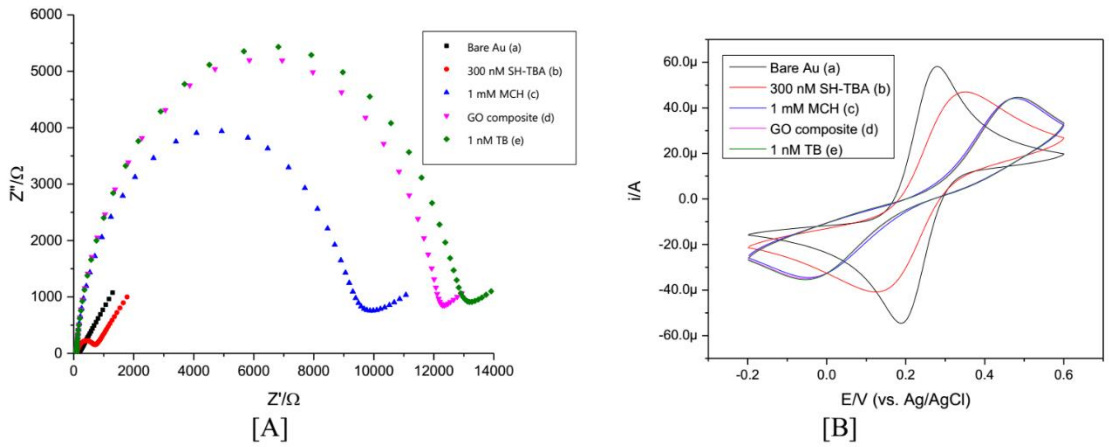

Figure 4.7 EIS (A) and CV (B) of the gold electrode at different stages in 5 mM [Fe $(CN)_6]^{4-/3-}$ in 100 mM PBS-100 mM KCL (pH 7.4).

EIS [A] and CV [B] of the gold electrode at different stages in 5 mM [Fe $(CN)_6]^{4-/3-}$ in 100 mM PBS-100 mM KCL (pH 7.4). Bare gold electrode (a); SH-TBA-aptamer/gold electrode(b); MCH/ SH-TBA-aptamer/gold electrode ©; GO composite/ MCH/ SH-TBA-aptamer/gold electrode (d); and TB/ GO composite/ MCH/ SH-TBA-aptamer/gold electrode (e).

AuE modification	R_{ct} (Ω)	ΔEp (mV)
Bare AuE	107	89.8
300 nM SH-TBA	591	220.8
1 mM MCH	9674	523.2
GO composite	12142	537.6
1 nM TB	13025	537.6

In order to verify ECL aptamer biosensor works as our expected, electrochemical impedance spectra (EIS) and cyclic voltammetry (CV) were investigated at different stages of the ECL aptamer biosensor preparation. EIS was measured in 5 mM [Fe $(CN)_6]^{4-/3-}$ solution in the frequency range of $0.1–10^5$ Hz and Nyquist plots were used to calculate the electron-transfer resistance (R_{et}) for modified electrodes. The corresponding cyclic voltammogram (CV) curves of the electrodes using [Fe $(CN)_6]^{4-/3-}$ as the redox probe were shown in Figure 4.7 [B]. The bare AuE was modified sequentially by SH-TBA, MCH, GO-

Ru(bpy) composite and then challenged with 1 nM TB protein. In EIS shows that the electron-transfer resistance (R_{et}) increases gradually with thioleted-thrombin aptamer and GO modification of the electrode for TB sensor (from lines a=100 Ω to d=12k Ω in EIS figure 4.7 [A]), due to the negative charge of aptemers or GO hindering $[Fe(CN)_6]^{4-/3-}$ from reaching the electrode surface. Meanwhile, the cyclic voltammetric response decreases gradually with the fixing of aptamer and rGO on the electrode, due to the negative charge of aptamer and GO, which hinders the interfacial electron-transfer kinetics of the redox probe. This indicates that aptamer and GO-$Ru(bpy)_3^{2+}$ composite was both successfully immobilized on the electrode in TB sensors. Then the TB sensor, immobilize in 1 nM TB solution for 1 h, the charge transfer resistance in EIS (R_{et}) increases further (from lines d to e in EIS figure 4.7 [A]), indicating that TB molecules successfully interacted with TBA and were tethered on the electrode, and it is the increased steric hindrance that greatly hindered access of electrons for the redox probe of $[Fe(CN)_6]^{4-/3-}$.The successive increase in the R_{et} and the CV curves of the electrodes illustrate the successful modification of the biosensing components onto Au electrode.

Probe density of DNA The surface coverage of the SH-TBA modified AuE was determined by a protocol previously reported by Steel et al[141]. Briefly, the surface coverage of the SH-TBA on modified Au electrode surface was calculated from the number of cationic redox molecules such as, ruthenium hexamine trichloride electrostatically associated with the anionic SH-TBA backbone. The chronocoulometric signals of the modified AuE were followed in the presence and absence of a cationic redox reporter, ruthenium hexamine trichloride, that is electrostatically bound to the negatively charged DNA backbone. After the immobilization of probes on the electrode surface, the probe-

modified electrode was subjected to ruthenium-hexamine. Then, the amount of ruthenium-hexamine was measured by the integrated current, or charge *Q*, as a function of the square root of time ($t^{1/2}$) in a chronocoulometric experiment is given by the integrated the Cottrell equation.

$$Q = \frac{2nFAD_0^{1/2}C_0^*}{\pi^{1/2}} t^{1/2} + Q_{dl} + nFA\Gamma_0$$

Where, *n* represent the number of electrons per molecule for reduction, *F* is the Faraday constant (C/equiv), *A* is the electrode area (cm^2), D_o is the diffusion coefficient (cm^2/s), C_o* is the bulk concentration (mol/cm^2), Q_{dl} is the capacitive charge (C), and $nFA\Gamma_o$ is the charge from the reduction of Γ_o (mol/cm^2) of adsorbed redox marker. The term Γ_o indicates the surface excess and represents the amount of redox marker (RuHex) confined near the electrode surface. The intercept of chronocoulometric at t=0 is the surface excess terms and the sum of the double-layer charging. The surface excess redox marker is calculated from the difference in chronocoulometric intercepts for the identical potential step experiment in the presence and absence of redox marker. DNA surface density was obtained using the following equation:

$$\Gamma_{DNA} = \Gamma_0 \left(\frac{z}{m}\right) N_A$$

Where Γ_{DNA} is the probe surface density in molecules per cm^2, m is the number of bases in probe DNA, z is the charge of ruthenium-hexamine and N_A is the Avogadro's number. The obtained surface density of the probe SH-TBA is equal to (2.0 ± 0.5) *10^{12} molecules per

cm^2. According to the literature, the theoretical surface coverage of hybridized DNA with 100% efficiency was roughly 4×10^{12} molecules/cm^2[132].

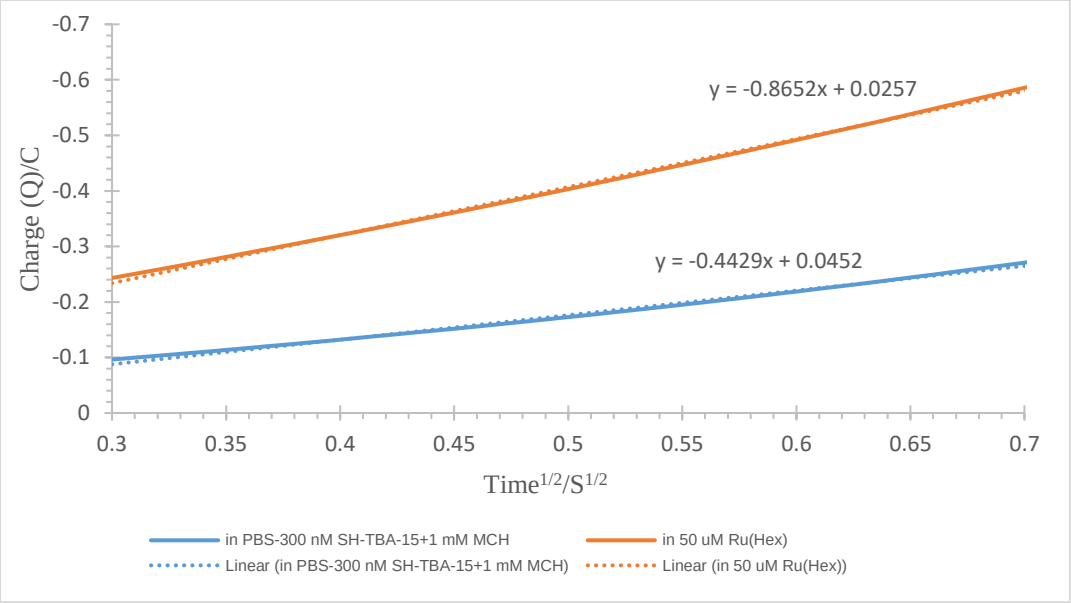

Figure 4.8 Chronocoulometric response curves for SH-TBA/MCH (in PBS; Blue) and SH-TBA/MCH (in 50 μM ruthenium-hexamine ; orange) modified electrodes.

Optimization of pH Several experimental conditions were optimized to achieve the maximum analytical signal. By increasing the amounts of the adsorbed $Ru(bpy)_3^{2+}$ on the aptamer modified electrode, the oxidation signals of $Ru(bpy)_3^{2+}$ should be increased. To overcome the repulsion forces between the negatively charged aptamer and GO in the hybrid structure, the surface charges of the nanohybrid should be controlled by adjusting the pH. To facilitate the interaction of GO-$Ru(bpy)_3^{2+}$ composite with the aromatic hydrophobic rings of DNA bases through π-π stacking, electrostatic repulsion between the DNA and the negatively charged GO surface must be overcome. Therefore, controlling the surface charge of GO by changing the pH of the solution is a key parameter in the response of biosensor. For this purpose, several PBS solutions with different pH over a range of 4.5

to 9.0 were prepared. The adsorption of GO-$Ru(bpy)_3^{2+}$ composite on immobilized DNA strands on electrode surface at different pH were followed by the incubation of the MCH/SH-TBA-15/Au electrode for 1 h at different pH and recording the ECL signal. The maximum ECL signal was observed at pH 8. The GO contains different acidic functional groups in its structure with pK_as over the range of 4.2–4.7[172]. In GO-$Ru(bpy)_3^{2+}$ composite $Ru(bpy)_3^{2+}$ has two positive charges per molecule, for that at higher pH surface are neutralized. Though pH 8 shows higher ECL sensitivity but later we did all experiment at pH 7.4 for maintain physiological pH.

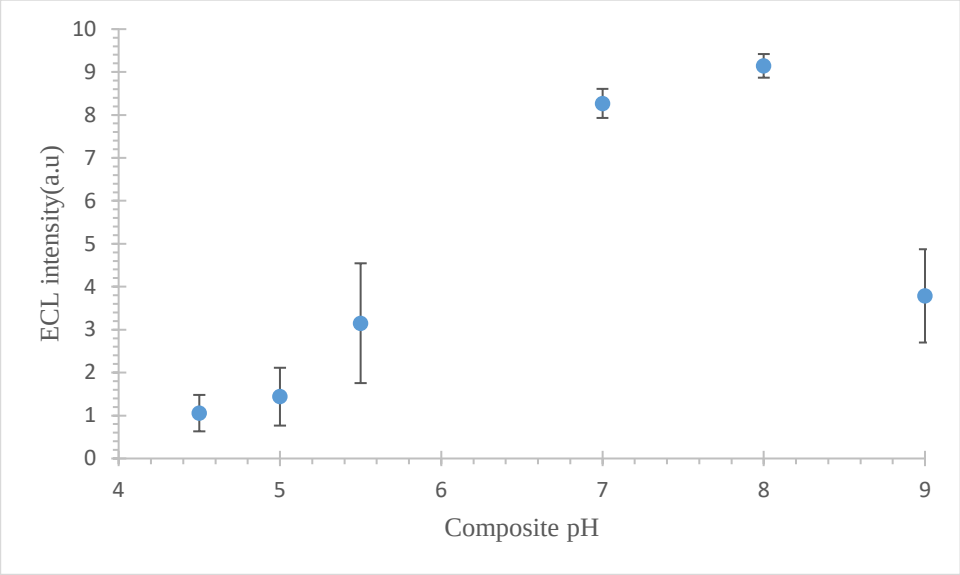

Figure 4.9 ECL intensity (a.u) were measured in 100 mM PBS-100 mM KCl (at different pH) containing 5 uM $[Ru(bpy)_3]^{2+}$-GO composite with 4 mM TPrA.

Optimization of GO concentration Multiple experimental variables were optimized to achieve the maximum analytical signal. By increasing the amounts of the adsorbed $Ru(bpy)_3^{2+}$ on the aptamer modified electrode, the oxidation signals of $Ru(bpy)_3^{2+}$ should be increased. To overcome the aggregation of GO in solution and get higher ECL response should be optimize the GO concentration. Increasing the GO concentration in composite

solution has increase the GO aggregation probability and form larger GO, which will be precipitate in composite solution. So, optimize of GO concentration is important.

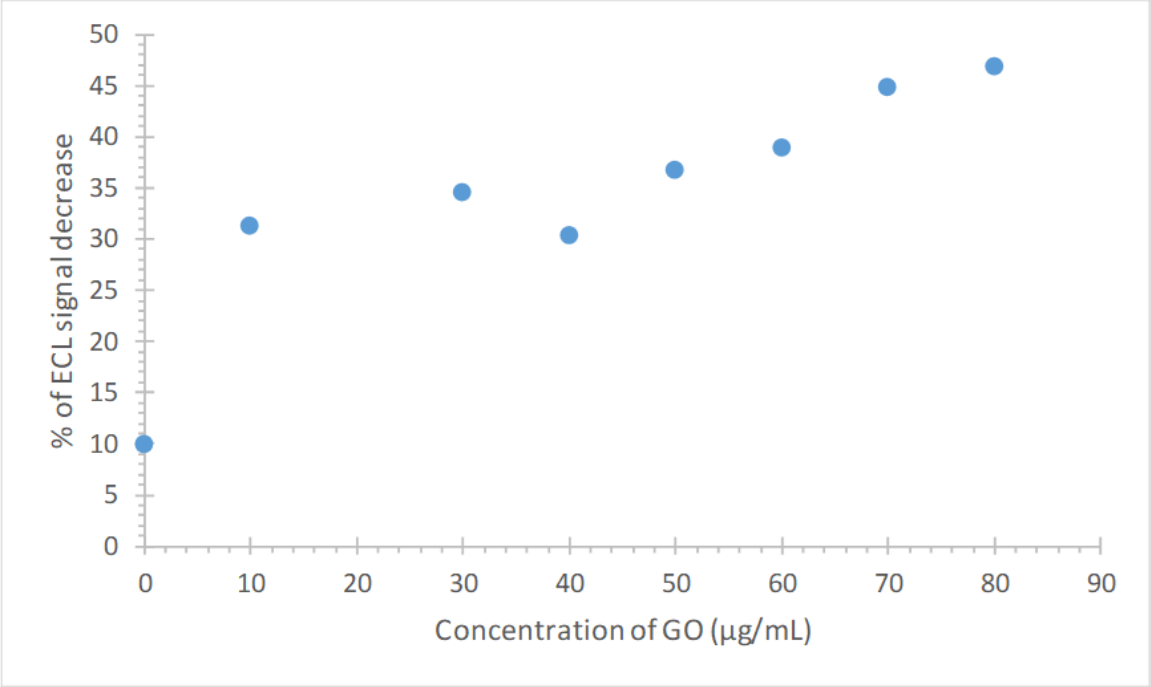

Figure 4.10 % of ECL signal decrease were measured in 100 mM PBS-100 mM KCl (at different GO concentration) containing 5 uM $[Ru(bpy)_3]^{2+}$-GO composite with 4 mM TPrA.

For optimize GO concentration in composite; prepared different concentration of GO in composite solution. The SH-TBA modified AuE incubate in composite solution and check background ECL signal. Followed by that AuE electrode challenged with 16 pM TB protein. Increasing the GO concentration in composite solution, % of ECL signal decrease is maximum at 70 to 80 ug/mL of GO concentration. Finally, all the ECL was done with 70 µg/mL of GO in composite solution.

Table 4.2 Zeta potential of GO and its composite

Composite name	Zeta potential (mV)
GO	-17.0
GO + DNA Loop	-20.2
GO + DNA Loop + $[Ru(bpy)_3]^{2+}$	-18.9

Zeta potential describes the electrical potential in the double layer of ions surrounding a particle at the boundary of the particle surface and the adsorbed ions in the diffuse layer. Graphene oxide potentially form well-dispersed aqueous colloids because its polar and hydrophilic character, appearing by reactive oxygen functional groups like epoxide, hydroxyl and carboxylic acid group[172]. By 70 µg/mL of GO disperse in 930 uL PBS-KCl buffer observed the zeta potential was -17.0 mV due to presence of reactive oxygen functional group. When DNA loop was added with GO solution, observed zeta potential was increasing. DNA has also negative charge, so combination of DNA with GO increases zeta potential. The graphene oxide-DNA-$Ru(bpy)_3^{2+}$ nanocomposites zeta potential was decreasing due to $Ru(bpy)_3^{2+}$ molecules have two positive charge. By electrostatic interaction between GO-DNA and $Ru(bpy)_3^{2+}$ form composite and decrease zeta potential.

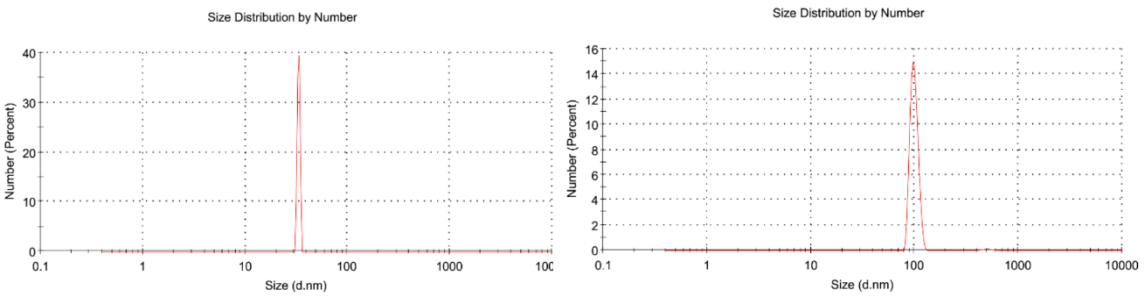

[A] [B]

Figure 4.11 Number based size distribution of GO in PBS-KCl buffer at room temperature.

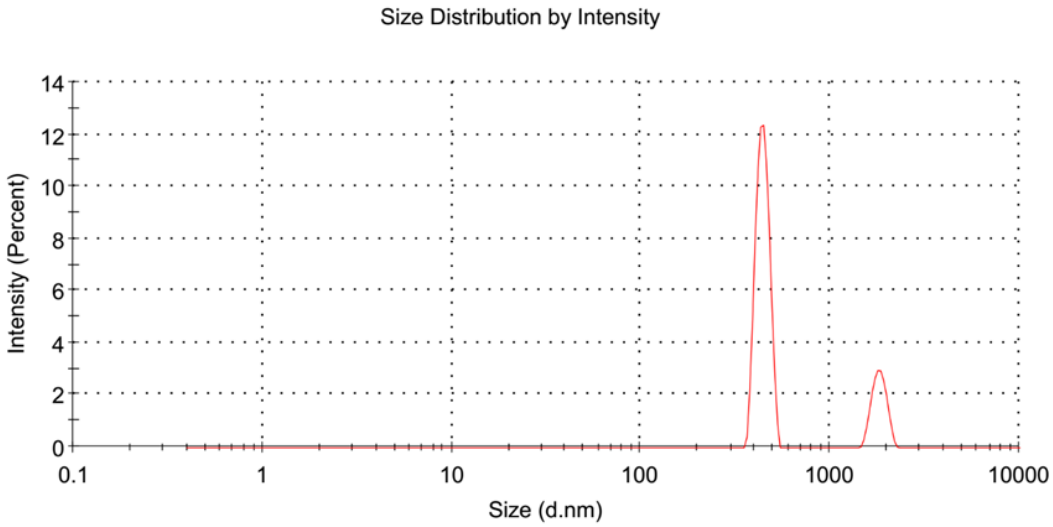

Figure 4.12 Intensity based size distribution of GO in PBS-KCl buffer at room temperature.

The particle size distributions of graphene oxide were investigated at room temperature in PBS buffer. Graphene oxide potentially form well-dispersed aqueous colloids because its polar and hydrophilic character, appearing by reactive oxygen functional groups like epoxide, hydroxyl and carboxylic acid group. The particle size of GO was observed to nm to µm range in the PBS buffer at room temperature. At t = 10 min and nominal concentrations of 70 µg/mL of GO in PBS buffer, one size population was observed in the number-based examinations (Figure 4.11 [A] and [B]) and two size populations were observed in the intensity-based spectra (Figure 4.12 [A]).

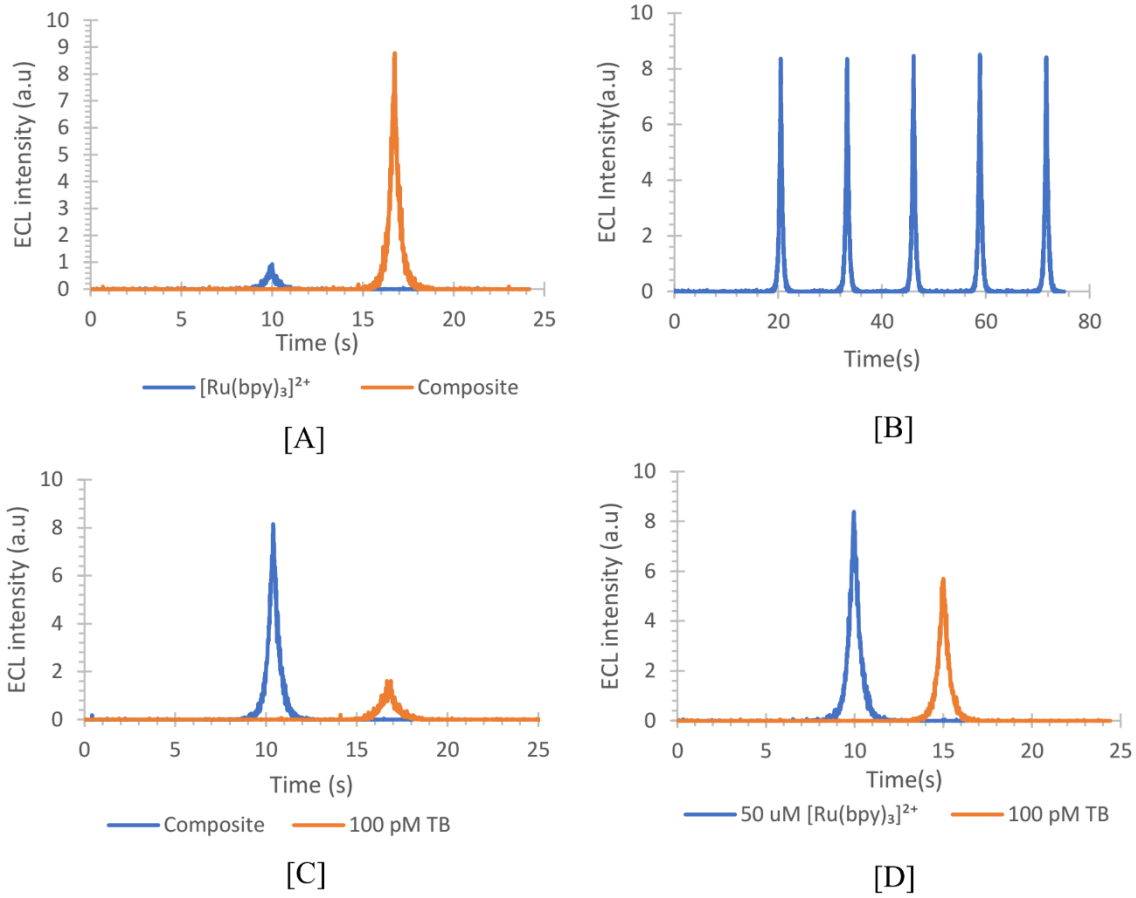

Figure 4.13 Compare ECL intensity between $[Ru(bpy)_3]^{2+}$ and composite [A]; The stability of the ECL aptasensor under consecutive cyclic potential in composite [B]; 100 pM TB in composite (5 uM $[Ru(bpy)_3]^{2+}$ -70 ug GO-DNA, 4 mM TPrA) [C] and 100 pM TB in 50 uM $[Ru(bpy)_3]^{2+}$, 4 mM TPrA [D].

Compare ECL intensity at different condition The corresponding ECL intensity-potential curves of the electrodes are presented in Figure 4.13. To better understand the role of GO in the aptasensor, ECL responses of GO-bound and no GO bound sensors were studied under the same conditions. As illustrated in Figure 4.13 [A] the ECL intensity (without target) of the GO-bound sensors (yellow line) are apparently larger than those of the no GO-bound sensors (blue line). This can be ascribed to the free bases of aptamers on the electrode, which could bind lots of GO molecules on themselves in the absence of target, therefore leading to large numbers of $Ru(bpy)_3^{2+}$ molecules anchored on the GO

nanoplatform. This indicate that the ECL aptasensor working very promisingly. The stability of the ECL aptasensor was also studied, and the results are presented in figure 4.13 [B], even after continuous potential scanning the electrodes can give an unchanged ECL intensity without the obvious loss of $Ru(bpy)_3^{2+}$ from the electrode surface. In Figure 4.13 [A] we observed that the background signal is very low without GO in same concentration of $Ru(bpy)_3^{2+}$. In figure 4.13 [D] only $Ru(bpy)_3^{2+}$ concentration increasing 10 times for comparing background ECL signal. Followed by challenged both aptasensor by same amount TB. That illustrate % of ECL signal decreasing 2.5 times more between Figure 4.13 [C] and [D].

Table 4.3 Comparison of % of ECL signal decrease

Composition	300 nM SH-TBA (ECL intensity (a.u))	100 pM TB (ECL intensity (a.u))	% of ECL signal decrease
5 uM $[Ru(bpy)_3]^{2+}$-GO-DNA, 4 mM TPrA	8.12	1.60	80
50 uM $[Ru(bpy)_3]^{2+}$, 4 mM TPrA	8.38	5.67	32

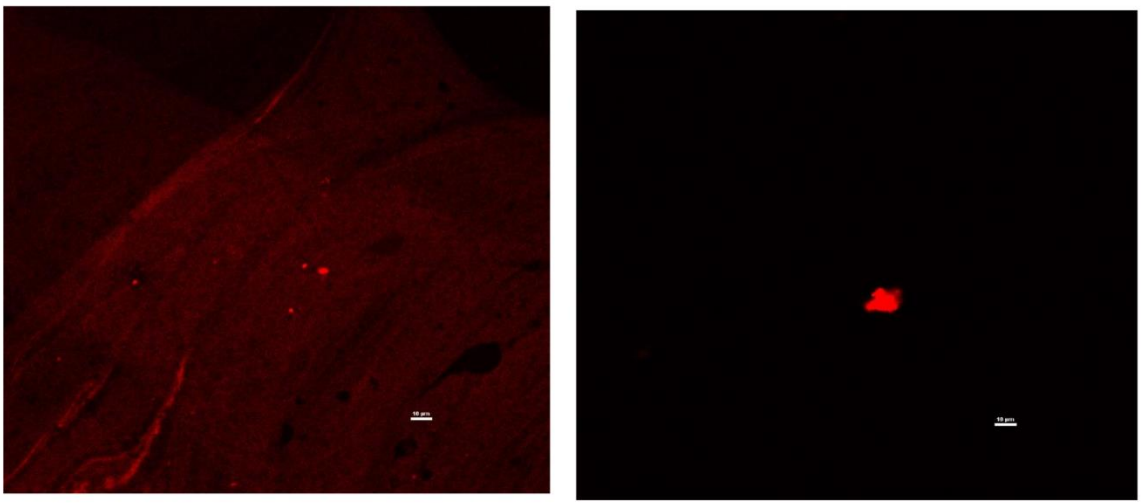

[A] [B]

Figure 4.14 Confocal fluorescence images (A) incubate in $[Ru(bpy)_3]^{2+}$-GO composite and (B) sensor incubate in 1 nM TB; Other experimental conditions are the same as calibration curve.

Table 4.4Comparisn of fluorescence intensity without and with TB.

Composition	Area	Fluorescence
5 uM $[Ru(bpy)_3]^{2+}$-GO-DNA, 4 mM TPrA	1E+06	3.225
5 uM $[Ru(bpy)_3]^{2+}$-GO-DNA, 4 mM TPrA & 1 nM TB	1E+06	2.67

Fluorescence image of GO-Ru(bpy)$_3^{2+}$ composite Fluorescence images (Figure 4. 14) were acquired on a Nikon A1+/MP confocal scanning laser microscope (Nikon Instruments, Inc., Melville, NY) with 10x objectives. This is the fluorescence image of GO-Ru(bpy)$_3^{2+}$ composite on semi-transparent gold-coated glass slides. The red image indicates that Ru(bpy)$_3^{2+}$ molecule on the Au surface. Followed by this Au glass slide was challenged with 1 nM TB and we observed here fluorescence intensity was decreasing.

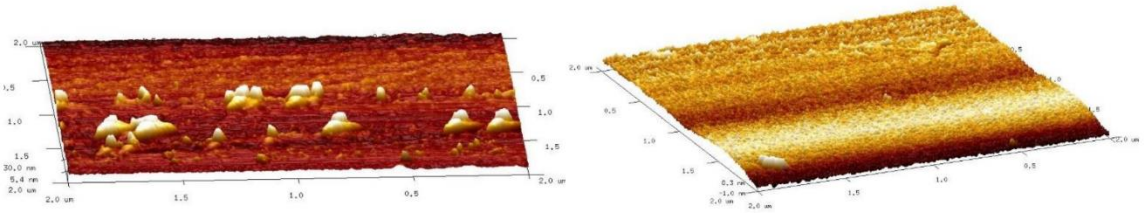

[A] [B]

Figure 4.15 AFM of sensor (A) incubate in $[Ru(bpy)_3]^{2+}$-GO composite and (B) sensor incubate in 1 nM TB; Other experimental conditions are the same as calibration curve.

AFM image of GO-Ru(bpy)$_3^{2+}$ composite AFM characterization of graphene Oxide (GO)-Ru(bpy)$_3^{2+}$ composite was carried out using a Bruker MultiMode 8 atomic force microscope (Bruker, USA) in air and at room temperature. Thus, the modified Au slides were thoroughly rinsed with PBS buffer and then dried under N_2 flow before AFM scanning. The semitransparent gold-coated microscope slides were used to formed SH-TBA SAMs first and that modified glass slide incubate in GO-Ru(bpy)$_3^{2+}$ composite solution as described above. Followed by that biosensor challenge by 1 nM Thrombin. In

Figure 4.15 [A] in AFM image shows the composite, which relative size is around 40 nm. In Figure 4.15 [B], we challenged the modified Au slide with 1 nM TB; the GO-Ru(bpy) leave the surface due to form G- quadruplex structure between SH-TBA and TB interaction.

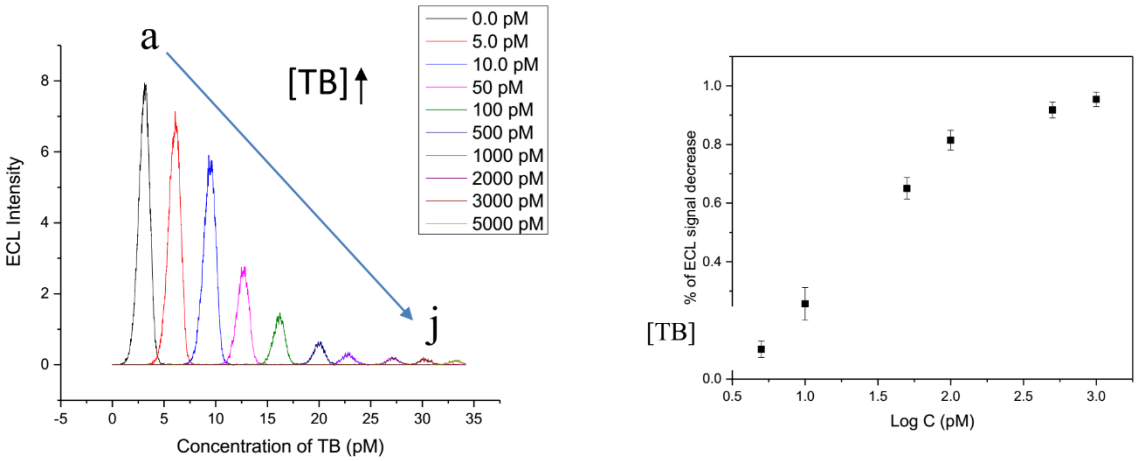

Figure 4.16 ECL intensity vs time curves for different SH-TBA-thrombin complex electrode.

[A] The concentration of thrombin were 0.0 M (a); 5 pM (b); 10 pM ©; 50 pM (d); 100 pM (e); 500 pM (f); 1 nM (g); 2 nM (h); 3 nM (i); and 5 nM (j), respectively. Thrombin detection limit of 5 pM was achieved, with a dynamic range up to 1 nM. [B] the calibration curve of thrombin detection. ECL curves were measured in 100 mM PBS-100 mM KCl (pH 7.4) containing 5 uM $[Ru(bpy)_3]^{2+}$-GO composite with 4 mM TPrA.

Calibration curve To evaluate the sensitivity of the this methods, the as prepared sensing interfaces were immersed in a series of target solutions of different concentrations for 30 min at room temperature, with the same electrode (TB ranging from 0 to 5 nM), and then a series of ECL signals were observed. The results are given in Figure 4.16 [A]. ECL intensity (a.u) decreased gradually with increasing concentration of TB (a–j in Figure 4.16 [A]). However, when the concentration of TB reached 1nM, the ECL signals no longer

decreased because of the saturation effect. For the TB sensor, the linear relationship between the % of ECL signal decrease and the logarithm of TB concentration (log C_{TB}) over a range of 5pM–1 nM is shown in the Figure 4.16 [B]. This strategy was capable to detect TB with a dynamic range of 5 pM to 1 nM. For the TB sensor, we can see the ECL signal quickly decreased due to, firstly a complex of quadruplex–TB attached on the electrode after TB binding, which weakened the interaction of GO and aptamer significantly, and consequently resulted in plenty of Ru anchored GO far away from TBA strands and the electrode. Secondly, the bulky G-quadruplex structure tethered on the electrode would be a larger barrier for electrons and would inhibit the electron transfer greatly. And it is the steric hindrance that would block the binding of the large molecule TB with the aptamer further.

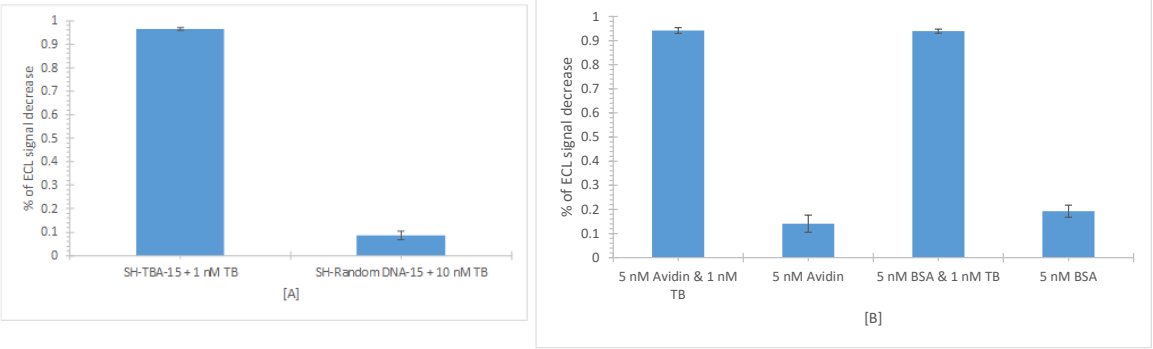

Figure 4.17 The selectivity of TB aptasensor; Other experimental conditions are the same as calibration curve.

Selectivity of TB aptasensor To demonstrate specificity, the aptamer-based ECL was challenged with nonspecific proteins including Avidin, BSA and random DNA-15. In figure 4.17 [A] Au electrode was modified with SH-Random-DNA-15 and challenged by 10 nM TB; this figure 4.17 [A] shows that essentially no response was observed in the presence of 10 nM TB. Control experiments were carried out to detect the selectivity of the proposed aptasensors, by 30 min immersion in target or two other interfering agents like

avidin and BSA, with the SH-TBA modified electrode. In figure 4.17 B, TB show sharp decrease of % of ECL signal, while the others had almost negligible. This means that the developed strategies had an enough specificity to TB against the other three interfering agents and possessed high selectivity.

4.4 Conclusions

In this work, we have presented a new assay design and have developed ECL aptasensor for the detection of thrombin by using GO-DNA-$[Ru(bpy)_3]^{2+}$ composite. Notably, we demonstrate that presence of GO is indeed a very important factor for enhancing ECL emission. $[Ru(bpy)_3]^{2+}$ adsorbs on GO by electrostatic interaction, this composite amplifies the ECL signal by increasing the local concentration of $[Ru(bpy)_3]^{2+}$. By contrast, we show here that, when modified AuE was challenged with TB solutions, the interaction of TB with TBA causes the adsorbed composite to desorb from the surface, leading to a decrease in the observed ECL intensity in direct proportion to the concentration of TB. Ease of fabrication and operation of this ECL aptamer biosensor, makes it a promising alternative to conventional thrombin detection method. Incorporating the assay's flexibility and simplicity with high selectivity of ECL readout, this assay is encouraging for future application of aptasensor to biological samples, which helps to design other biomarker detection and point-of-care settings.

CHAPTER 5

Conclusions and Future Directions

The primary objective of this dissertation work is to develop new platforms by applying versatile recognition elements for electrochemical sensors. We have successfully demonstrated the incorporation of biomolecules like aptamers, DNA with transducer (like Au or GCE) surface to construct electrochemical sensors for different applications including protein quantitation, DNA loop as target of ECPA model detection, and measurement. In DNA loop ECPA model relies on two affinity probes and proximity effect to move a redox-active molecule, MB, close to a transducer like carbon or gold surface in the presence of a target. Because of its intrinsic flexibility, ECPA should be useful in quantifying any protein with a pair of aptamers.

To further improve this system, some efforts can be implemented in its fabrication and modification. A biosensor is a device that integrates a biologically active layer as the identification element and transforms of the biological interaction physical parameters into a measurable analytical signal. Even though many methods have been proposed based on PCR, fluorescence, radioactivity, etc., the large-scale, routine clinic screening based on gene diagnostics is limited by the currently available technologies. Compared to other techniques, electrochemical biosensors relying on the conversion of a recognition event into a useful electrical signal is highly sensitive, inexpensive, easy-to-use, portable, and compatible with microfabrication technologies. Thus, they seem to be excellent candidates for rapid and inexpensive diagnosis[173].

Another aspect address is amplifying the electrochemical response concerning the case of probe-target recognition. In all the recognition events, the DNA hybridization is commonly developed via an increase in the current signal of an electroactive indicator (either be attached to the target DNA or binds to the single/double-stranded DNA, or from other hybridization-induced changes in electrochemical parameters. In order to reduce the background and maximally amplify the signal in the presence of the analyte, the sequence of T-DNA as the capture probe (on the gold electrode) and the signaling probe (MB-DNA for example) need to be carefully designed in addition to minimizing the chance of cross hybridization.

The capture probe immobilized on the surface should have as few G numbers as possible. In contrast, the signaling probe, which could be hybridized sufficiently in the presence target under the proximity effect, should have as many Gs as possible for MB intercalation. It would be the primary principle of the DNA sequence design. Besides, due to either two antibody arms or two aptamers hybridizing with the capture and signaling probe, the sequences of them also need to be considered. First, the antibody arm or aptamer (Apt 1 or Ab 1) that hybridizes with the capture DNA should have few Gs in order to suppress the background, while Apt 2 or Ab 2, which binds with the signaling probe is expected to have more Gs. Besides, MB has a weak intercalation affinity to the G on ds-DNA compared to ss-DNA. If G must be present to avoid cross-hybridization, it is preferred to code inside the base regions that hybridize between the probes and antibody arms (or aptamers).

In the ECPA, attention should also be given to direct, label-free electrochemical detection, which is not accepted by the ECL system due to most of the time, no faradaic

reaction is involved. Instead of the electrochemical signal from reduction or oxidation, other electrical parameter changes induced by the DNA conformation change could be monitored without the use of an indicator which is often toxic or carcinogenic compounds. The first indicator-free method was introduced by Wang et al. by the decrease of the guanine peak from the immobilized probe upon the addition of complementary target[174]. Then it was improved by using the inosine-modified (guanine-free) probe, which forms a specific base-pair with the cytosine residue[175]. The duplex formation was thus detected through the appearance of the guanine oxidation peak of the target sequence. A different label-free approach, based on doping nucleic-acid probes within conducting polymer films, was also proposed by Wang. Distinct transient hybridization current peaks, with opposite directions in the presence of complementary and non-complementary DNA sequences, were obtained as a result of the changed conductivity of the host PPy network.

However, the label-free technique based on guanine oxidation will suffer from a high background if there is nonspecific adsorption of guanine containing sequences to the sensor surface[176]. Magnetic bead capture could be used to eliminate nonspecific adsorption effects based on stripping potentiometric measurements of the targeted guanine at graphite electrodes256. Zhou constructed a graphite electrode sensor coated with DNA films[177]. The DNA damage by toxic metabolites such as styrene oxide was evaluated by the oxidation peaks from known covalent adducts with guanine and adenine in DNA with genetic consequences[178].

The achievement of high selectivity and sensitivity requires the maximization of hybridization efficiency and the minimization of nonspecific adsorption, respectively. Control of the surface chemistry and coverage are essential for assuring the high reactivity,

orientation, accessibility, and stability of the surface-confined probe as well as minimizing nonspecific adsorption events. The ECPA sensor needs to be tested directly with unprocessed samples in the next step, such as human blood or urine. By further engineering and miniaturizing, ECPA could be easily integrated with portable electronic devices and applied in point-of-care settings.

We also introduced a new ECL aptasensor for the detection of thrombin by using GO-DNA-$[Ru(bpy)_3]^{2+}$ composite, which exploits by ECL signal off strategy. Judging from the successful fabrication of ECL aptasensor, it is reasonable to assume that the ECL aptasensor platform should perform well in quantifying any other protein with an available aptamer. Fabrication ECL aptasensor integrate with the bipolar electrochemical system and optimize the operational condition of this ECL aptamer biosensor, and it will make a promising alternative to conventional thrombin detection method. Combining the assay's flexibility and high sensitivity with the simplicity of ECL signal off readout, this biosensing platform should be useful in a variety of settings in the future, including medical diagnostics, biological research, and point-of-care testing.

REFERENCES

[1] M. Labib, E. H. Sargent, and S. O. Kelley, "Electrochemical Methods for the Analysis of Clinically Relevant Biomolecules," *Chemical Reviews,* vol. 116, pp. 9001-9090, 2016/08/24 2016.

[2] A. Csordas, A. E. Gerdon, J. D. Adams, J. Qian, S. S. Oh, Y. Xiao, *et al.*, "Detection of Proteins in Serum by Micromagnetic Aptamer PCR (MAP) Technology," *Angewandte Chemie International Edition,* vol. 49, pp. 355-358, 2010/01/08 2010.

[3] M. Urdea, L. A. Penny, S. S. Olmsted, M. Y. Giovanni, P. Kaspar, A. Shepherd, *et al.*, "Requirements for high impact diagnostics in the developing world," *Nature,* vol. 444, pp. 73-79, 2006/11/01 2006.

[4] J. F. Rusling, C. V. Kumar, J. S. Gutkind, and V. Patel, "Measurement of biomarker proteins for point-of-care early detection and monitoring of cancer," *Analyst,* vol. 135, pp. 2496-2511, 2010.

[5] D. Grieshaber, R. MacKenzie, J. Vörös, and E. Reimhult, "Electrochemical Biosensors - Sensor Principles and Architectures," *Sensors,* vol. 8, 2008.

[6] D. W. Kimmel, G. LeBlanc, M. E. Meschievitz, and D. E. Cliffel, "Electrochemical Sensors and Biosensors," *Analytical Chemistry,* vol. 84, pp. 685-707, 2012/01/17 2012.

[7] C. R. Lowe, "Biosensors," *Trends in Biotechnology,* vol. 2, pp. 59-65, 1984/05/01/ 1984.

[8] D. R. Thévenot, K. Toth, R. A. Durst, and G. S. Wilson, "ELECTROCHEMICAL BIOSENSORS: RECOMMENDED DEFINITIONS AND CLASSIFICATION*," *Analytical Letters,* vol. 34, pp. 635-659, 2001/03/31 2001.

[9] D. A. Giljohann and C. A. Mirkin, "Drivers of biodiagnostic development," *Nature,* vol. 462, pp. 461-464, 2009/11/01 2009.

[10] N. J. Ronkainen, H. B. Halsall, and W. R. Heineman, "Electrochemical biosensors," *Chemical Society Reviews,* vol. 39, pp. 1747-1763, 2010.

[11] D. A. Skoog, F. J. Holler, and S. R. Crouch, *Principles of instrumental analysis*, 6th ed. / ed.: Belmont (Calif.) : Thomson, 2007.

[12] B. Corry, J. Uilk, and C. Crawley, "Probing direct binding affinity in electrochemical antibody-based sensors," *Analytica Chimica Acta,* vol. 496, pp. 103-116, 2003/10/31/ 2003.

[13] J. Lei and H. Ju, "Signal amplification using functional nanomaterials for biosensing," *Chemical Society Reviews,* vol. 41, pp. 2122-2134, 2012.

[14] E. Heyduk, B. Dummit, Y.-H. Chang, and T. Heyduk, "Molecular Pincers: Antibody-Based Homogeneous Protein Sensors," *Analytical Chemistry*, vol. 80, pp. 5152-5159, 2008/07/01 2008.

[15] D. Kim, W. L. Daniel, and C. A. Mirkin, "Microarray-Based Multiplexed Scanometric Immunoassay for Protein Cancer Markers Using Gold Nanoparticle Probes," *Analytical Chemistry,* vol. 81, pp. 9183-9187, 2009/11/01 2009.

[16] T. Konry, R. B. Hayman, and D. R. Walt, "Microsphere-Based Rolling Circle Amplification Microarray for the Detection of DNA and Proteins in a Single Assay," *Analytical Chemistry,* vol. 81, pp. 5777-5782, 2009/07/15 2009.

[17] S. Fredriksson, M. Gullberg, J. Jarvius, C. Olsson, K. Pietras, S. M. Gústafsdóttir, *et al.*, "Protein detection using proximity-dependent DNA ligation assays," *Nature Biotechnology,* vol. 20, pp. 473-477, 2002/05/01 2002.

[18] M. Gullberg, S. M. Gústafsdóttir, E. Schallmeiner, J. Jarvius, M. Bjarnegård, C. Betsholtz, *et al.*, "Cytokine detection by antibody-based proximity ligation," *Proceedings of the National Academy of Sciences of the United States of America*, vol. 101, p. 8420, 2004.

[19] J. Hu, Y. Yu, J. C. Brooks, L. A. Godwin, S. Somasundaram, F. Torabinejad, *et al.*, "A Reusable Electrochemical Proximity Assay for Highly Selective, Real-Time Protein Quantitation in Biological Matrices," *Journal of the American Chemical Society*, vol. 136, pp. 8467-8474, 2014/06/11 2014.

[20] K. Ren, J. Wu, F. Yan, and H. Ju, "Ratiometric electrochemical proximity assay for sensitive one-step protein detection," *Scientific Reports*, vol. 4, p. 4360, 2014/03/12 2014.

[21] Y.-L. Zhang, Y. Huang, J.-H. Jiang, G.-L. Shen, and R.-Q. Yu, "Electrochemical Aptasensor Based on Proximity-Dependent Surface Hybridization Assay for Single-Step, Reusable, Sensitive Protein Detection," *Journal of the American Chemical Society*, vol. 129, pp. 15448-15449, 2007/12/01 2007.

[22] Y.-L. Zhang, P.-F. Pang, J.-H. Jiang, G.-L. Shen, and R.-Q. Yu, "Electrochemical Aptasensor Based on Proximity-Dependent Surface Hybridization Assay for Protein Detection," *Electroanalysis*, vol. 21, pp. 1327-1333, 2009/06/01 2009.

[23] T. Hianik and J. Wang, "Electrochemical Aptasensors – Recent Achievements and Perspectives," *Electroanalysis*, vol. 21, pp. 1223-1235, 2009/06/01 2009.

[24] A. Sassolas, L. J. Blum, and B. D. Leca-Bouvier, "Electrochemical Aptasensors," *Electroanalysis*, vol. 21, pp. 1237-1250, 2009/06/01 2009.

[25] S. Chen, R. Yuan, Y. Chai, Y. Xu, L. Min, and N. Li, "A new antibody immobilization technique based on organic polymers protected Prussian blue nanoparticles and gold colloidal nanoparticles for amperometric immunosensors," *Sensors and Actuators B: Chemical,* vol. 135, pp. 236-244, 2008/12/10/ 2008.

[26] I. Palchetti and M. Mascini, "Electrochemical nanomaterial-based nucleic acid aptasensors," *Analytical and Bioanalytical Chemistry,* vol. 402, pp. 3103-3114, 2012/04/01 2012.

[27] S. Dulay, P. Lozano-Sánchez, E. Iwuoha, I. Katakis, and C. K. O'Sullivan, "Electrochemical detection of celiac disease-related anti-tissue transglutaminase antibodies using thiol based surface chemistry," *Biosensors and Bioelectronics,* vol. 26, pp. 3852-3856, 2011/05/15/ 2011.

[28] E. B. Bahadır and M. K. Sezgintürk, "Applications of commercial biosensors in clinical, food, environmental, and biothreat/biowarfare analyses," *Analytical Biochemistry,* vol. 478, pp. 107-120, 2015/06/01/ 2015.

[29] K. Itaya and A. J. Bard, "Chemically modified polymer electrodes: synthetic approach employing poly(methacryl chloride) anchors," *Analytical Chemistry,* vol. 50, pp. 1487-1489, 1978/09/01 1978.

[30] P. R. Moses, L. Wier, and R. W. Murray, "Chemically modified tin oxide electrode," *Analytical Chemistry,* vol. 47, pp. 1882-1886, 1975/10/01 1975.

[31] B. F. Watkins, J. R. Behling, E. Kariv, and L. L. Miller, "Chiral electrode," *Journal of the American Chemical Society,* vol. 97, pp. 3549-3550, 1975/06/01 1975.

[32] D. K. Pattadar and F. P. Zamborini, "Size Stability Study of Catalytically Active Sub-2 nm Diameter Gold Nanoparticles Synthesized with Weak Stabilizers,"

Journal of the American Chemical Society, vol. 140, pp. 14126-14133, 2018/10/31 2018.

[33] C. Liu, F. Li, L.-P. Ma, and H.-M. Cheng, "Advanced Materials for Energy Storage," *Advanced Materials,* vol. 22, pp. E28-E62, 2010/02/23 2010.

[34] D. K. Pattadar, J. N. Sharma, B. P. Mainali, and F. P. Zamborini, "Impact of the Assembly Method on the Surface Area-to-Volume Ratio and Electrochemical Oxidation Potential of Metal Nanospheres," *The Journal of Physical Chemistry C,* vol. 123, pp. 24304-24312, 2019/10/03 2019.

[35] R. R. Pethig and S. Smith, *Introductory Bioelectronics: For Engineers and Physical Scientists*: Wiley, 2012.

[36] D. K. Pattadar, J. N. Sharma, B. P. Mainali, and F. P. Zamborini, "Anodic stripping electrochemical analysis of metal nanoparticles," *Current Opinion in Electrochemistry,* vol. 13, pp. 147-156, 2019/02/01/ 2019.

[37] D. K. Pattadar and F. P. Zamborini, "Halide-Dependent Dealloying of Cux/Auy Core/Shell Nanoparticles for Composition Analysis by Anodic Stripping Voltammetry," *The Journal of Physical Chemistry C,* vol. 123, pp. 9496-9505, 2019/04/11 2019.

[38] A. T. Sage, J. D. Besant, B. Lam, E. H. Sargent, and S. O. Kelley, "Ultrasensitive Electrochemical Biomolecular Detection Using Nanostructured Microelectrodes," *Accounts of Chemical Research,* vol. 47, pp. 2417-2425, 2014/08/19 2014.

[39] C. G. Zoski, *Handbook of Electrochemistry*: Elsevier Science, 2007.

[40] A. J. Bard and L. R. Faulkner, *Electrochemical Methods: Fundamentals and Applications, 2nd Edition*: Wiley Textbooks, 2000.

[41] V. Mirceski, D. Guziejewski, and K. Lisichkov, "Electrode kinetic measurements with square-wave voltammetry at a constant scan rate," *Electrochimica Acta,* vol. 114, pp. 667-673, 2013/12/30/ 2013.

[42] L. Ramaley and M. S. Krause, "Theory of square wave voltammetry," *Analytical Chemistry,* vol. 41, pp. 1362-1365, 1969/09/01 1969.

[43] J. Das and S. O. Kelley, "Tuning the Bacterial Detection Sensitivity of Nanostructured Microelectrodes," *Analytical Chemistry,* vol. 85, pp. 7333-7338, 2013/08/06 2013.

[44] Y. Lu, N. Zhu, P. Yu, and L. Mao, "Aptamer-based electrochemical sensors that are not based on the target binding-induced conformational change of aptamers," *Analyst,* vol. 133, pp. 1256-1260, 2008.

[45] J. Das and S. O. Kelley, "Protein Detection Using Arrayed Microsensor Chips: Tuning Sensor Footprint to Achieve Ultrasensitive Readout of CA-125 in Serum and Whole Blood," *Analytical Chemistry,* vol. 83, pp. 1167-1172, 2011/02/15 2011.

[46] S. S. Mahshid, S. Camiré, F. Ricci, and A. Vallée-Bélisle, "A Highly Selective Electrochemical DNA-Based Sensor That Employs Steric Hindrance Effects to Detect Proteins Directly in Whole Blood," *Journal of the American Chemical Society,* vol. 137, pp. 15596-15599, 2015/12/23 2015.

[47] J. Hu, T. Wang, J. Kim, C. Shannon, and C. J. Easley, "Quantitation of Femtomolar Protein Levels via Direct Readout with the Electrochemical Proximity Assay," *Journal of the American Chemical Society,* vol. 134, pp. 7066-7072, 2012/04/25 2012.

[48] A. K. H. Cheng, B. Ge, and H.-Z. Yu, "Aptamer-Based Biosensors for Label-Free Voltammetric Detection of Lysozyme," *Analytical Chemistry,* vol. 79, pp. 5158-5164, 2007/07/01 2007.

[49] J. D. Besant, J. Das, E. H. Sargent, and S. O. Kelley, "Proximal Bacterial Lysis and Detection in Nanoliter Wells Using Electrochemistry," *ACS Nano,* vol. 7, pp. 8183-8189, 2013/09/24 2013.

[50] J. Das, I. Ivanov, E. H. Sargent, and S. O. Kelley, "DNA Clutch Probes for Circulating Tumor DNA Analysis," *Journal of the American Chemical Society,* vol. 138, pp. 11009-11016, 2016/08/31 2016.

[51] Z. Fang, L. Soleymani, G. Pampalakis, M. Yoshimoto, J. A. Squire, E. H. Sargent, *et al.*, "Direct Profiling of Cancer Biomarkers in Tumor Tissue Using a Multiplexed Nanostructured Microelectrode Integrated Circuit," *ACS Nano,* vol. 3, pp. 3207-3213, 2009/10/27 2009.

[52] R. J. White, N. Phares, A. A. Lubin, Y. Xiao, and K. W. Plaxco, "Optimization of Electrochemical Aptamer-Based Sensors via Optimization of Probe Packing Density and Surface Chemistry," *Langmuir,* vol. 24, pp. 10513-10518, 2008/09/16 2008.

[53] S. S. Mahshid, F. Ricci, S. O. Kelley, and A. Vallée-Bélisle, "Electrochemical DNA-Based Immunoassay That Employs Steric Hindrance To Detect Small Molecules Directly in Whole Blood," *ACS Sensors,* vol. 2, pp. 718-723, 2017/06/23 2017.

[54] S. S. Mahshid, A. Vallée-Bélisle, and S. O. Kelley, "Biomolecular Steric Hindrance Effects Are Enhanced on Nanostructured Microelectrodes," *Analytical Chemistry*, vol. 89, pp. 9751-9757, 2017/09/19 2017.

[55] W. Zhou, S. S. Mahshid, W. Wang, A. Vallée-Bélisle, P. W. Zandstra, E. H. Sargent, *et al.*, "Steric Hindrance Assay for Secreted Factors in Stem Cell Culture," *ACS Sensors*, vol. 2, pp. 495-500, 2017/04/28 2017.

[56] D. K. Pattadar, B. P. Mainali, J. B. Jasinski, and F. P. Zamborini, "Electrooxidation, Size Stability, and Electrocatalytic Activity of 0.9 nm Diameter Gold Nanoclusters Coated with a Weak Stabilizer," *ChemElectroChem*, vol. 7, pp. 800-809, 2020/02/03 2020.

[57] N. T. Flynn, T. N. T. Tran, M. J. Cima, and R. Langer, "Long-Term Stability of Self-Assembled Monolayers in Biological Media," *Langmuir*, vol. 19, pp. 10909-10915, 2003/12/01 2003.

[58] M. Labib, N. Khan, and M. V. Berezovski, "Protein Electrocatalysis for Direct Sensing of Circulating MicroRNAs," *Analytical Chemistry*, vol. 87, pp. 1395-1403, 2015/01/20 2015.

[59] D. H. Johnston, C.-C. Cheng, K. J. Campbell, and H. H. Thorp, "Trans-Dioxorhenium(V)-Mediated Electrocatalytic Oxidation of DNA at Indium Tin-Oxide Electrodes: Voltammetric Detection of DNA Cleavage in Solution," *Inorganic Chemistry*, vol. 33, pp. 6388-6390, 1994/12/01 1994.

[60] D. H. Johnston, K. C. Glasgow, and H. H. Thorp, "Electrochemical Measurement of the Solvent Accessibility of Nucleobases Using Electron Transfer between DNA

and Metal Complexes," *Journal of the American Chemical Society*, vol. 117, pp. 8933-8938, 1995/09/01 1995.

[61] P. M. Armistead and H. H. Thorp, "Modification of Indium Tin Oxide Electrodes with Nucleic Acids: Detection of Attomole Quantities of Immobilized DNA by Electrocatalysis," *Analytical Chemistry*, vol. 72, pp. 3764-3770, 2000/08/01 2000.

[62] R. C. Holmberg and H. H. Thorp, "Digital Simulation of Catalytic Cyclic Voltammograms for Oxidation of DNA by a Heterobimetallic Dimer: Effects of DNA Binding and Mass Transport," *Analytical Chemistry*, vol. 75, pp. 1851-1860, 2003/04/01 2003.

[63] S. O. Kelley, E. M. Boon, J. K. Barton, N. M. Jackson, and M. G. Hill, "Single-base mismatch detection based on charge transduction through DNA," *Nucleic Acids Research*, vol. 27, pp. 4830-4837, 1999.

[64] A. L. Furst, M. G. Hill, and J. K. Barton, "Electrocatalysis in DNA sensors," *Polyhedron*, vol. 84, pp. 150-159, 2014/12/14/ 2014.

[65] M. A. Lapierre-Devlin, C. L. Asher, B. J. Taft, R. Gasparac, M. A. Roberts, and S. O. Kelley, "Amplified Electrocatalysis at DNA-Modified Nanowires," *Nano Letters*, vol. 5, pp. 1051-1055, 2005/06/01 2005.

[66] Z. Fang and S. O. Kelley, "Direct Electrocatalytic mRNA Detection Using PNA-Nanowire Sensors," *Analytical Chemistry*, vol. 81, pp. 612-617, 2009/01/15 2009.

[67] M. Rizwan, N. F. Mohd-Naim, and M. U. Ahmed, "Trends and Advances in Electrochemiluminescence Nanobiosensors," *Sensors*, vol. 18, 2018.

[68] W. Jing and G. Min, "Microfluidic sensing: state of the art fabrication and detection techniques," *Journal of Biomedical Optics*, vol. 16, pp. 1-13, 8/1 2011.

[69] K. N. Han, C. A. Li, and G. H. Seong, "Microfluidic Chips for Immunoassays," *Annual Review of Analytical Chemistry,* vol. 6, pp. 119-141, 2013/06/12 2013.

[70] M. Mirasoli, M. Guardigli, E. Michelini, and A. Roda, "Recent advancements in chemical luminescence-based lab-on-chip and microfluidic platforms for bioanalysis," *Journal of Pharmaceutical and Biomedical Analysis,* vol. 87, pp. 36-52, 2014/01/18/ 2014.

[71] W. Miao, "Electrogenerated Chemiluminescence and Its Biorelated Applications," *Chemical Reviews,* vol. 108, pp. 2506-2553, 2008/07/01 2008.

[72] M. M. Richter, "Electrochemiluminescence (ECL)," *Chemical Reviews,* vol. 104, pp. 3003-3036, 2004/06/01 2004.

[73] R. J. Forster, P. Bertoncello, and T. E. Keyes, "Electrogenerated Chemiluminescence," *Annual Review of Analytical Chemistry,* vol. 2, pp. 359-385, 2009/07/19 2009.

[74] W. Cao, J. P. Ferrance, J. Demas, and J. P. Landers, "Quenching of the Electrochemiluminescence of Tris(2,2‘-bipyridine)ruthenium(II) by Ferrocene and Its Potential Application to Quantitative DNA Detection," *Journal of the American Chemical Society,* vol. 128, pp. 7572-7578, 2006/06/01 2006.

[75] H. Wei and E. Wang, "Electrochemiluminescence of tris(2,2′-bipyridyl)ruthenium and its applications in bioanalysis: a review," *Luminescence,* vol. 26, pp. 77-85, 2011.

[76] W. Miao, J.-P. Choi, and A. J. Bard, "Electrogenerated Chemiluminescence 69: The Tris(2,2‘-bipyridine)ruthenium(II), (Ru(bpy)32+)/Tri-n-propylamine (TPrA)

System RevisitedA New Route Involving TPrA•+ Cation Radicals," *Journal of the American Chemical Society*, vol. 124, pp. 14478-14485, 2002/12/01 2002.

[77] H. Zheng and Y. Zu, "Emission of Tris(2,2‘-bipyridine)ruthenium(II) by Coreactant Electrogenerated Chemiluminescence: From O2-Insensitive to Highly O2-Sensitive," *The Journal of Physical Chemistry B*, vol. 109, pp. 12049-12053, 2005/06/01 2005.

[78] K.-F. Chow, F. Mavré, and R. M. Crooks, "Wireless Electrochemical DNA Microarray Sensor," *Journal of the American Chemical Society*, vol. 130, pp. 7544-7545, 2008/06/18 2008.

[79] F. Mavré, R. K. Anand, D. R. Laws, K.-F. Chow, B.-Y. Chang, J. A. Crooks, *et al.*, "Bipolar Electrodes: A Useful Tool for Concentration, Separation, and Detection of Analytes in Microelectrochemical Systems," *Analytical Chemistry*, vol. 82, pp. 8766-8774, 2010/11/01 2010.

[80] X. Wang, P. Dong, W. Yun, Y. Xu, P. He, and Y. Fang, "A solid-state electrochemiluminescence biosensing switch for detection of thrombin based on ferrocene-labeled molecular beacon aptamer," *Biosensors and Bioelectronics*, vol. 24, pp. 3288-3292, 2009/07/15/ 2009.

[81] J. McCall, C. Alexander, and M. M. Richter, "Quenching of Electrogenerated Chemiluminescence by Phenols, Hydroquinones, Catechols, and Benzoquinones," *Analytical Chemistry*, vol. 71, pp. 2523-2527, 1999/07/01 1999.

[82] B. Geißer and R. Alsfasser, "A peptide approach to covalently linked [Ru(bipy)3]2+–ferrocene and [Ru(bipy)3]2+–tyrosine conjugates," *Inorganica Chimica Acta*, vol. 344, pp. 102-108, 2003/02/20/ 2003.

[83] D. K. Liu, B. S. Brunschwig, C. Creutz, and N. Sutin, "Formation of electronically excited products in electron-transfer reactions: reaction of polypyridine complexes of cobalt(I) and ruthenium(III) in acetonitrile," *Journal of the American Chemical Society*, vol. 108, pp. 1749-1755, 1986/04/01 1986.

[84] R. Ramamoorthy, P. K. Dutta, and S. A. Akbar, "Oxygen sensors: Materials, methods, designs and applications," *Journal of Materials Science*, vol. 38, pp. 4271-4282, 2003/11/01 2003.

[85] A. W. Martinez, S. T. Phillips, G. M. Whitesides, and E. Carrilho, "Diagnostics for the Developing World: Microfluidic Paper-Based Analytical Devices," *Analytical Chemistry*, vol. 82, pp. 3-10, 2010/01/01 2010.

[86] L. Hood, J. R. Heath, M. E. Phelps, and B. Lin, "Systems Biology and New Technologies Enable Predictive and Preventative Medicine," *Science*, vol. 306, p. 640, 2004.

[87] J.-M. Nam, C. S. Thaxton, and C. A. Mirkin, "Nanoparticle-Based Bio-Bar Codes for the Ultrasensitive Detection of Proteins," *Science*, vol. 301, p. 1884, 2003.

[88] D. M. Rissin, C. W. Kan, T. G. Campbell, S. C. Howes, D. R. Fournier, L. Song, *et al.*, "Single-molecule enzyme-linked immunosorbent assay detects serum proteins at subfemtomolar concentrations," *Nature Biotechnology*, vol. 28, pp. 595-599, 2010/06/01 2010.

[89] T. Heyduk, "Practical biophysics: Sensors for rapid detection of biological targets utilizing target-induced oligonucleotide annealing," *Biophysical Chemistry*, vol. 151, pp. 91-95, 2010/10/01/ 2010.

[90] F. Li, H. Zhang, Z. Wang, X. Li, X.-F. Li, and X. C. Le, "Dynamic DNA Assemblies Mediated by Binding-Induced DNA Strand Displacement," *Journal of the American Chemical Society,* vol. 135, pp. 2443-2446, 2013/02/20 2013.

[91] H. Zhang, X.-F. Li, and X. C. Le, "Binding-Induced DNA Assembly and Its Application to Yoctomole Detection of Proteins," *Analytical Chemistry,* vol. 84, pp. 877-884, 2012/01/17 2012.

[92] H. Zhang, F. Li, B. Dever, C. Wang, X.-F. Li, and X. C. Le, "Assembling DNA through Affinity Binding to Achieve Ultrasensitive Protein Detection," *Angewandte Chemie International Edition,* vol. 52, pp. 10698-10705, 2013/10/04 2013.

[93] J. J. Gooding, F. Mearns, W. Yang, and J. Liu, "Self-Assembled Monolayers into the 21st Century: Recent Advances and Applications," *Electroanalysis,* vol. 15, pp. 81-96, 2003/02/01 2003.

[94] N. K. Chaki and K. Vijayamohanan, "Self-assembled monolayers as a tunable platform for biosensor applications," *Biosensors and Bioelectronics,* vol. 17, pp. 1-12, 2002/01/01/ 2002.

[95] J. Liu, L. Cheng, B. Liu, and S. Dong, "Covalent Modification of a Glassy Carbon Surface by 4-Aminobenzoic Acid and Its Application in Fabrication of a Polyoxometalates-Consisting Monolayer and Multilayer Films," *Langmuir,* vol. 16, pp. 7471-7476, 2000/09/01 2000.

[96] H. F. Teh, H. Gong, X.-D. Dong, X. Zeng, A. Lai Kuan Tan, X. Yang, *et al.*, "Electrochemical biosensing of DNA with capture probe covalently immobilized

onto glassy carbon surface," *Analytica Chimica Acta,* vol. 551, pp. 23-29, 2005/10/17/ 2005.

[97] L. Kashefi-Kheyrabadi and M. A. Mehrgardi, "Design and construction of a label free aptasensor for electrochemical detection of sodium diclofenac," *Biosensors and Bioelectronics,* vol. 33, pp. 184-189, 2012/03/15/ 2012.

[98] D. Kang, X. Zuo, R. Yang, F. Xia, K. W. Plaxco, and R. J. White, "Comparing the Properties of Electrochemical-Based DNA Sensors Employing Different Redox Tags," *Analytical Chemistry,* vol. 81, pp. 9109-9113, 2009/11/01 2009.

[99] E. E. Ferapontova, E. M. Olsen, and K. V. Gothelf, "An RNA Aptamer-Based Electrochemical Biosensor for Detection of Theophylline in Serum," *Journal of the American Chemical Society,* vol. 130, pp. 4256-4258, 2008/04/01 2008.

[100] K. Jung, J. Zachow, M. Lein, B. Brux, P. Sinha, S. Lenk, *et al.*, "Rapid detection of elevated prostate-specific antigen levels in blood: performance of various membrane strip tests compared11This study includes parts of the doctoral thesis of Jürgen Zachow," *Urology,* vol. 53, pp. 155-160, 1999/01/01/ 1999.

[101] L. S. Gómez and G. Rojas, "A simple visual immunoassay (VIA) for rapid identification of high lipoprotein(a) blood levels," *Clinica Chimica Acta,* vol. 260, pp. 65-71, 1997/04/04/ 1997.

[102] R. C. Engstrom and V. A. Strasser, "Characterization of electrochemically pretreated glassy carbon electrodes," *Analytical Chemistry,* vol. 56, pp. 136-141, 1984/02/01 1984.

[103] M. A. Mehrgardi and R. Daneshtalab, "Electrochemical detection of different types of single-base mismatches in DNA using copper-phthalocyanine tetrasulfonic

acid," *Journal of Electroanalytical Chemistry*, vol. 650, pp. 214-218, 2011/01/01/ 2011.

[104] M.-S. Wu, D.-J. Yuan, J.-J. Xu, and H.-Y. Chen, "Electrochemiluminescence on bipolar electrodes for visual bioanalysis," *Chemical Science*, vol. 4, pp. 1182-1188, 2013.

[105] M.-S. Wu, Z. Liu, H.-W. Shi, H.-Y. Chen, and J.-J. Xu, "Visual Electrochemiluminescence Detection of Cancer Biomarkers on a Closed Bipolar Electrode Array Chip," *Analytical Chemistry*, vol. 87, pp. 530-537, 2015/01/06 2015.

[106] J. C. Hoogvliet, M. Dijksma, B. Kamp, and W. P. van Bennekom, "Electrochemical Pretreatment of Polycrystalline Gold Electrodes To Produce a Reproducible Surface Roughness for Self-Assembly: A Study in Phosphate Buffer pH 7.4," *Analytical Chemistry*, vol. 72, pp. 2016-2021, 2000/05/01 2000.

[107] Q. Cheng and A. Brajter-Toth, "Selectivity and sensitivity of self-assembled thioctic acid electrodes," *Analytical Chemistry*, vol. 64, pp. 1998-2000, 1992/09/01 1992.

[108] M. Dijksma, B. Kamp, J. C. Hoogvliet, and W. P. van Bennekom, "Formation and Electrochemical Characterization of Self-Assembled Monolayers of Thioctic Acid on Polycrystalline Gold Electrodes in Phosphate Buffer pH 7.4," *Langmuir*, vol. 16, pp. 3852-3857, 2000/04/01 2000.

[109] M. Akram, M. C. Stuart, and D. K. Y. Wong, "Direct application strategy to immobilise a thioctic acid self-assembled monolayer on a gold electrode," *Analytica Chimica Acta*, vol. 504, pp. 243-251, 2004/02/23/ 2004.

[110] M. Dijksma, B. A. Boukamp, B. Kamp, and W. P. van Bennekom, "Effect of Hexacyanoferrate(II/III) on Self-Assembled Monolayers of Thioctic Acid and 11-Mercaptoundecanoic Acid on Gold," *Langmuir,* vol. 18, pp. 3105-3112, 2002/04/01 2002.

[111] J. M. Abad, S. F. L. Mertens, M. Pita, V. M. Fernández, and D. J. Schiffrin, "Functionalization of Thioctic Acid-Capped Gold Nanoparticles for Specific Immobilization of Histidine-Tagged Proteins," *Journal of the American Chemical Society,* vol. 127, pp. 5689-5694, 2005/04/01 2005.

[112] W. Limbut, P. Kanatharana, B. Mattiasson, P. Asawatreratanakul, and P. Thavarungkul, "A comparative study of capacitive immunosensors based on self-assembled monolayers formed from thiourea, thioctic acid, and 3-mercaptopropionic acid," *Biosensors and Bioelectronics,* vol. 22, pp. 233-240, 2006/08/15/ 2006.

[113] R. L. McCreery, "Advanced Carbon Electrode Materials for Molecular Electrochemistry," *Chemical Reviews,* vol. 108, pp. 2646-2687, 2008/07/01 2008.

[114] W. Yang, M. Ozsoz, D. B. Hibbert, and J. J. Gooding, "Evidence for the Direct Interaction Between Methylene Blue and Guanine Bases Using DNA-Modified Carbon Paste Electrodes," *Electroanalysis,* vol. 14, pp. 1299-1302, 2002/10/01 2002.

[115] A. Tani, A. J. Thomson, and J. N. Butt, "Methylene blue as an electrochemical discriminator of single- and double-stranded oligonucleotides immobilised on gold substrates," *Analyst,* vol. 126, pp. 1756-1759, 2001.

[116] M. D. Holtan, S. Somasundaram, N. Khuda, and C. J. Easley, "Nonfaradaic Current Suppression in DNA-Based Electrochemical Assays with a Differential Potentiostat," *Analytical Chemistry,* vol. 91, pp. 15833-15839, 2019/12/17 2019.

[117] J. Liu, "Adsorption of DNA onto gold nanoparticles and graphene oxide: surface science and applications," *Physical Chemistry Chemical Physics,* vol. 14, pp. 10485-10496, 2012.

[118] A. W. Peterson, R. J. Heaton, and R. M. Georgiadis, "The effect of surface probe density on DNA hybridization," *Nucleic Acids Research,* vol. 29, pp. 5163-5168, 2001.

[119] D. C. Hay Burgess, J. Wasserman, and C. A. Dahl, "Global health diagnostics," *Nature,* vol. 444, pp. 1-2, 2006/11/01 2006.

[120] P. Yager, G. J. Domingo, and J. Gerdes, "Point-of-Care Diagnostics for Global Health," *Annual Review of Biomedical Engineering,* vol. 10, pp. 107-144, 2008/08/01 2008.

[121] M. Kroll, "Tietz Textbook of Clinical Chemistry, Third Edition. Carl A. Burtis and Edward R. Ashwood, eds. Philadelphia, PA: WB Saunders, 1998, 1917 pp., $195.00. ISBN 0-7216-5610-2," *Clinical Chemistry,* vol. 45, pp. 913-914, 1999.

[122] J. Wang, "Electrochemical biosensors: Towards point-of-care cancer diagnostics," *Biosensors and Bioelectronics,* vol. 21, pp. 1887-1892, 2006/04/15/ 2006.

[123] Z. Shen, H. O. Sintim, and S. Semancik, "Rapid nucleic acid melting analyses using a microfabricated electrochemical platform," *Analytica Chimica Acta,* vol. 853, pp. 265-270, 2015/01/01/ 2015.

[124] G.-U. Flechsig, J. Peter, G. Hartwich, J. Wang, and P. Gründler, "DNA Hybridization Detection at Heated Electrodes," *Langmuir,* vol. 21, pp. 7848-7853, 2005/08/01 2005.

[125] C. Fan, K. W. Plaxco, and A. J. Heeger, "Electrochemical interrogation of conformational changes as a reagentless method for the sequence-specific detection of DNA," *Proceedings of the National Academy of Sciences,* vol. 100, p. 9134, 2003.

[126] A. Idili, A. Amodio, M. Vidonis, J. Feinberg-Somerson, M. Castronovo, and F. Ricci, "Folding-Upon-Binding and Signal-On Electrochemical DNA Sensor with High Affinity and Specificity," *Analytical Chemistry,* vol. 86, pp. 9013-9019, 2014/09/16 2014.

[127] R. Y. Lai, E. T. Lagally, S.-H. Lee, H. T. Soh, K. W. Plaxco, and A. J. Heeger, "Rapid, sequence-specific detection of unpurified PCR amplicons via a reusable, electrochemical sensor," *Proceedings of the National Academy of Sciences of the United States of America,* vol. 103, p. 4017, 2006.

[128] R. Y. Lai, "Chapter Eight - Folding- and Dynamics-Based Electrochemical DNA Sensors," in *Methods in Enzymology*. vol. 589, R. B. Thompson and C. A. Fierke, Eds., ed: Academic Press, 2017, pp. 221-252.

[129] A. Patterson, F. Caprio, A. Vallée-Bélisle, D. Moscone, K. W. Plaxco, G. Palleschi, *et al.*, "Using Triplex-Forming Oligonucleotide Probes for the Reagentless, Electrochemical Detection of Double-Stranded DNA," *Analytical Chemistry,* vol. 82, pp. 9109-9115, 2010/11/01 2010.

[130] K. A. Peterlinz, R. M. Georgiadis, T. M. Herne, and M. J. Tarlov, "Observation of Hybridization and Dehybridization of Thiol-Tethered DNA Using Two-Color Surface Plasmon Resonance Spectroscopy," *Journal of the American Chemical Society*, vol. 119, pp. 3401-3402, 1997/04/01 1997.

[131] Z. Shen, S. Nakayama, S. Semancik, and H. O. Sintim, "Signal-on electrochemical Y or junction probe detection of nucleic acid," *Chemical Communications*, vol. 48, pp. 7580-7582, 2012.

[132] J. Das, I. Ivanov, L. Montermini, J. Rak, E. H. Sargent, and S. O. Kelley, "An electrochemical clamp assay for direct, rapid analysis of circulating nucleic acids in serum," *Nature Chemistry*, vol. 7, pp. 569-575, 2015/07/01 2015.

[133] K. W. Plaxco and H. T. Soh, "Switch-based biosensors: a new approach towards real-time, in vivo molecular detection," *Trends in Biotechnology*, vol. 29, pp. 1-5, 2011/01/01/ 2011.

[134] S. Cagnin, M. Caraballo, C. Guiducci, P. Martini, M. Ross, M. SantaAna, *et al.*, "Overview of Electrochemical DNA Biosensors: New Approaches to Detect the Expression of Life," *Sensors*, vol. 9, 2009.

[135] F. Xia, R. J. White, X. Zuo, A. Patterson, Y. Xiao, D. Kang, *et al.*, "An Electrochemical Supersandwich Assay for Sensitive and Selective DNA Detection in Complex Matrices," *Journal of the American Chemical Society*, vol. 132, pp. 14346-14348, 2010/10/20 2010.

[136] X. Zuo, Y. Xiao, and K. W. Plaxco, "High Specificity, Electrochemical Sandwich Assays Based on Single Aptamer Sequences and Suitable for the Direct Detection

of Small-Molecule Targets in Blood and Other Complex Matrices," *Journal of the American Chemical Society*, vol. 131, pp. 6944-6945, 2009/05/27 2009.

[137] B. R. Baker, R. Y. Lai, M. S. Wood, E. H. Doctor, A. J. Heeger, and K. W. Plaxco, "An Electronic, Aptamer-Based Small-Molecule Sensor for the Rapid, Label-Free Detection of Cocaine in Adulterated Samples and Biological Fluids," *Journal of the American Chemical Society*, vol. 128, pp. 3138-3139, 2006/03/01 2006.

[138] Y. Xiao, A. A. Lubin, B. R. Baker, K. W. Plaxco, and A. J. Heeger, "Single-step electronic detection of femtomolar DNA by target-induced strand displacement in an electrode-bound duplex," *Proceedings of the National Academy of Sciences*, vol. 103, p. 16677, 2006.

[139] Y. Liu, N. Tuleouva, E. Ramanculov, and A. Revzin, "Aptamer-Based Electrochemical Biosensor for Interferon Gamma Detection," *Analytical Chemistry*, vol. 82, pp. 8131-8136, 2010/10/01 2010.

[140] A.-E. Radi, J. L. Acero Sánchez, E. Baldrich, and C. K. O'Sullivan, "Reusable Impedimetric Aptasensor," *Analytical Chemistry*, vol. 77, pp. 6320-6323, 2005/10/01 2005.

[141] A. B. Steel, T. M. Herne, and M. J. Tarlov, "Electrochemical Quantitation of DNA Immobilized on Gold," *Analytical Chemistry*, vol. 70, pp. 4670-4677, 1998/11/01 1998.

[142] J. Kim, J. Hu, R. S. Sollie, and C. J. Easley, "Improvement of Sensitivity and Dynamic Range in Proximity Ligation Assays by Asymmetric Connector Hybridization," *Analytical Chemistry*, vol. 82, pp. 6976-6982, 2010/08/15 2010.

[143] F. P. Zamborini and R. M. Crooks, "In-Situ Electrochemical Scanning Tunneling Microscopy (ECSTM) Study of Cyanide-Induced Corrosion of Naked and Hexadecyl Mercaptan-Passivated Au(111)," *Langmuir,* vol. 13, pp. 122-126, 1997/01/01 1997.

[144] A. Bogomolova, E. Komarova, K. Reber, T. Gerasimov, O. Yavuz, S. Bhatt, *et al.*, "Challenges of Electrochemical Impedance Spectroscopy in Protein Biosensing," *Analytical Chemistry,* vol. 81, pp. 3944-3949, 2009/05/15 2009.

[145] J. Lazar, C. Schnelting, E. Slavcheva, and U. Schnakenberg, "Hampering of the Stability of Gold Electrodes by Ferri-/Ferrocyanide Redox Couple Electrolytes during Electrochemical Impedance Spectroscopy," *Analytical Chemistry,* vol. 88, pp. 682-687, 2016/01/05 2016.

[146] S. Vogt, Q. Su, C. Gutiérrez-Sánchez, and G. Nöll, "Critical View on Electrochemical Impedance Spectroscopy Using the Ferri/Ferrocyanide Redox Couple at Gold Electrodes," *Analytical Chemistry,* vol. 88, pp. 4383-4390, 2016/04/19 2016.

[147] R. J. White and K. W. Plaxco, "Exploiting Binding-Induced Changes in Probe Flexibility for the Optimization of Electrochemical Biosensors," *Analytical Chemistry,* vol. 82, pp. 73-76, 2010/01/01 2010.

[148] S. E. K. Kirschbaum and A. J. Baeumner, "A review of electrochemiluminescence (ECL) in and for microfluidic analytical devices," *Analytical and Bioanalytical Chemistry,* vol. 407, pp. 3911-3926, 2015/05/01 2015.

[149] Z. Wang, Z. Yan, F. Wang, J. Cai, L. Guo, J. Su, *et al.*, "Highly sensitive photoelectrochemical biosensor for kinase activity detection and inhibition based

on the surface defect recognition and multiple signal amplification of metal-organic frameworks," *Biosensors and Bioelectronics,* vol. 97, pp. 107-114, 2017/11/15/ 2017.

[150] K.-J. Huang, Y.-J. Liu, and Q.-F. Zhai, "Ultrasensitive biosensing platform based on layered vanadium disulfide–graphene composites coupling with tetrahedron-structured DNA probes and exonuclease III assisted signal amplification," *Journal of Materials Chemistry B,* vol. 3, pp. 8180-8187, 2015.

[151] P. Bertoncello, A. J. Stewart, and L. Dennany, "Analytical applications of nanomaterials in electrogenerated chemiluminescence," *Analytical and Bioanalytical Chemistry,* vol. 406, pp. 5573-5587, 2014/09/01 2014.

[152] M. Rizwan, N. F. Mohd-Naim, N. A. Keasberry, and M. U. Ahmed, "A highly sensitive and label-free electrochemiluminescence immunosensor for beta 2-microglobulin," *Analytical Methods,* vol. 9, pp. 2570-2577, 2017.

[153] Y.-S. Borghei, M. Hosseini, M. Dadmehr, S. Hosseinkhani, M. R. Ganjali, and R. Sheikhnejad, "Visual detection of cancer cells by colorimetric aptasensor based on aggregation of gold nanoparticles induced by DNA hybridization," *Analytica Chimica Acta,* vol. 904, pp. 92-97, 2016/01/21/ 2016.

[154] H. A. Kermani, M. Hosseini, M. Dadmehr, and M. R. Ganjali, "Rapid restriction enzyme free detection of DNA methyltransferase activity based on DNA-templated silver nanoclusters," *Analytical and Bioanalytical Chemistry,* vol. 408, pp. 4311-4318, 2016/06/01 2016.

[155] B. Zhou, M. Zhu, Y. Hao, and P. Yang, "Potential-Resolved Electrochemiluminescence for Simultaneous Determination of Triple Latent

Tuberculosis Infection Markers," *ACS Applied Materials & Interfaces,* vol. 9, pp. 30536-30542, 2017/09/13 2017.

[156] X. Zhu, Q. Zhai, W. Gu, J. Li, and E. Wang, "High-Sensitivity Electrochemiluminescence Probe with Molybdenum Carbides as Nanocarriers for α-Fetoprotein Sensing," *Analytical Chemistry,* vol. 89, pp. 12108-12114, 2017/11/21 2017.

[157] L. Yang, Y. Li, Y. Zhang, D. Fan, X. Pang, Q. Wei, *et al.*, "3D Nanostructured Palladium-Functionalized Graphene-Aerogel-Supported Fe3O4 for Enhanced Ru(bpy)32+-Based Electrochemiluminescent Immunosensing of Prostate Specific Antigen," *ACS Applied Materials & Interfaces,* vol. 9, pp. 35260-35267, 2017/10/11 2017.

[158] M. Zhao, A.-Y. Chen, D. Huang, Y.-Q. Chai, Y. Zhuo, and R. Yuan, "MoS2 Quantum Dots as New Electrochemiluminescence Emitters for Ultrasensitive Bioanalysis of Lipopolysaccharide," *Analytical Chemistry,* vol. 89, pp. 8335-8342, 2017/08/15 2017.

[159] D. K. Pattadar and F. P. Zamborini, "Effect of Size, Coverage, and Dispersity on the Potential-Controlled Ostwald Ripening of Metal Nanoparticles," *Langmuir,* vol. 35, pp. 16416-16426, 2019/12/17 2019.

[160] J. N. Sharma, D. K. Pattadar, B. P. Mainali, and F. P. Zamborini, "Size Determination of Metal Nanoparticles Based on Electrochemically Measured Surface-Area-to-Volume Ratios," *Analytical Chemistry,* vol. 90, pp. 9308-9314, 2018/08/07 2018.

[161] Y. Lin, H. Dai, G. Xu, T. Yang, C. Yang, Y. Tong, *et al.*, "Enhanced luminol electrochemiluminescence triggered by an electrode functionalized with dendrimers modified with titanate nanotubes," *Microchimica Acta,* vol. 180, pp. 563-572, 2013/06/01 2013.

[162] Y. Kim and J. Kim, "Modification of Indium Tin Oxide with Dendrimer-Encapsulated Nanoparticles To Provide Enhanced Stable Electrochemiluminescence of Ru(bpy)32+/Tripropylamine While Preserving Optical Transparency of Indium Tin Oxide for Sensitive Electrochemiluminescence-Based Analyses," *Analytical Chemistry,* vol. 86, pp. 1654-1660, 2014/02/04 2014.

[163] K. S. Novoselov, A. K. Geim, S. V. Morozov, D. Jiang, Y. Zhang, S. V. Dubonos, *et al.*, "Electric Field Effect in Atomically Thin Carbon Films," *Science,* vol. 306, p. 666, 2004.

[164] M. Pumera, "Graphene-based nanomaterials and their electrochemistry," *Chemical Society Reviews,* vol. 39, pp. 4146-4157, 2010.

[165] M. Hosseini, N. Mirzanasiri, M. Rezapour, M. H. Sheikhha, F. Faridbod, P. Norouzi, *et al.*, "Sensitive determination of carbidopa through the electrochemiluminescence of luminol at graphene-modified electrodes," *Luminescence,* vol. 30, pp. 376-381, 2015/06/01 2015.

[166] S. Peng, G. Zou, and X. Zhang, "Nanocomposite of electrochemically reduced graphene oxide and gold nanoparticles enhanced electrochemilunescence of peroxydisulfate and its immunosensing abililty towards human IgG," *Journal of Electroanalytical Chemistry,* vol. 686, pp. 25-31, 2012/10/15/ 2012.

[167] K. Zhou, Y. Zhu, X. Yang, and C. Li, "Preparation and Application of Mediator-Free H2O2 Biosensors of Graphene-Fe3O4 Composites," *Electroanalysis*, vol. 23, pp. 862-869, 2011.

[168] Y. Xu, H. Bai, G. Lu, C. Li, and G. Shi, "Flexible Graphene Films via the Filtration of Water-Soluble Noncovalent Functionalized Graphene Sheets," *Journal of the American Chemical Society*, vol. 130, pp. 5856-5857, 2008/05/01 2008.

[169] D. Voiry, J. Yang, J. Kupferberg, R. Fullon, C. Lee, H. Y. Jeong, *et al.*, "High-quality graphene via microwave reduction of solution-exfoliated graphene oxide," *Science*, vol. 353, p. 1413, 2016.

[170] Y. Xiao, R. Y. Lai, and K. W. Plaxco, "Preparation of electrode-immobilized, redox-modified oligonucleotides for electrochemical DNA and aptamer-based sensing," *Nature Protocols*, vol. 2, pp. 2875-2880, 2007/11/01 2007.

[171] M. R. Esfahani, H. A. Stretz, and M. J. M. Wells, "Abiotic reversible self-assembly of fulvic and humic acid aggregates in low electrolytic conductivity solutions by dynamic light scattering and zeta potential investigation," *Science of The Total Environment*, vol. 537, pp. 81-92, 2015/12/15/ 2015.

[172] H. Park, S.-J. Hwang, and K. Kim, "An electrochemical detection of Hg2+ ion using graphene oxide as an electrochemically active indicator," *Electrochemistry Communications*, vol. 24, pp. 100-103, 2012/10/01/ 2012.

[173] F. Lucarelli, G. Marrazza, A. P. F. Turner, and M. Mascini, "Carbon and gold electrodes as electrochemical transducers for DNA hybridisation sensors," *Biosensors and Bioelectronics*, vol. 19, pp. 515-530, 2004/01/15/ 2004.

[174] J. Wang, X. Cai, B. Tian, and H. Shiraishi, "Microfabricated thick-film electrochemical sensor for nucleic acid determination," *Analyst,* vol. 121, pp. 965-969, 1996.

[175] J. Wang, A.-N. Kawde, A. Erdem, and M. Salazar, "Magnetic bead-based label-free electrochemical detection of DNA hybridization," *Analyst,* vol. 126, pp. 2020-2024, 2001.

[176] D. O. Ariksoysal, H. Karadeniz, A. Erdem, A. Sengonul, A. A. Sayiner, and M. Ozsoz, "Label-Free Electrochemical Hybridization Genosensor for the Detection of Hepatitis B Virus Genotype on the Development of Lamivudine Resistance," *Analytical Chemistry,* vol. 77, pp. 4908-4917, 2005/08/01 2005.

[177] J. Mbindyo, L. Zhou, Z. Zhang, J. D. Stuart, and J. F. Rusling, "Detection of Chemically Induced DNA Damage by Derivative Square Wave Voltammetry," *Analytical Chemistry,* vol. 72, pp. 2059-2065, 2000/05/01 2000.

[178] G. J. Latham and R. S. Lloyd, "Deoxynucleotide polymerization by HIV-1 reverse transcriptase is terminated by site-specific styrene oxide adducts after translesion synthesis," *The Journal of biological chemistry,* vol. 269, pp. 28527-28530, 1994/11// 1994.